DOCTOR OF PHILOSOPHY

Optimal resource allocation for unmanned aerial vehicle- assisted wireless communications

Nguyen, Thi Minh Hien

Award date:
2024

Awarding institution:
Queen's University Belfast

Optimal Resource Allocation for Unmanned Aerial Vehicle-Assisted Wireless Communications

Thi Minh Hien Nguyen

School of Electronics, Electrical Engineering and Computer Science

Queen's University Belfast

A thesis submitted for the degree of

Doctor of Philosophy

January 8, 2024

Abstract

Unmanned aerial vehicles (UAVs) have had an impressive number of real-world applications and will continue to play a significant role in the future. Yet, UAV-assisted communication is constrained by scarce resources - a common issue in wireless communication. Optimal resource allocation is thus of critical importance for UAVs to operate and fulfil their missions. Although resource allocation in UAV-assisted communication is not a new topic, many challenges exist. Resource allocation is a non-trivial task due to the constraints of UAVs (such as flight time, deployment strategy, cache storage) and the many constraints of the wireless network supported by UAVs (such as power of the base station, quality-of-service), amid the presence of numerous users and devices. Moreover, optimisation problems in this context are often highly non-convex and difficult to solve.

Inspired by the aforementioned discussion, this thesis proposes optimal resource allocation strategies in UAV-assisted wireless communication, taking into account resources such as spectrum, power, and cache in specific UAV use cases. In particular, Chapter 3 looks at a spectrum-sharing cognitive radio network where the UAVs are deployed as flying base stations to provide network coverage to the secondary network in a disaster area. A learning-aided optimisation

scheme is designed to allocate radio resources under the constraints of maximum tolerable interference. Chapter 4 considers integrating reconfigurable intelligent surfaces onboard the UAVs to extend network coverage in a massive multiple-input multiple-output system. The joint problem of optimal power allocation and phase-shift is solved, subject to deployment strategy and minimum data throughput. Finally, in Chapter 5, the UAVs assist in content caching in an integrated terrestrial-non terrestrial network. The joint optimisation problem of user clustering, cache placement, and power allocation is solved efficiently by using a distributed approach. In all these cases, low-complexity algorithms are proposed and their usefulness is confirmed through simulation.

Acknowledgements

This thesis would have been impossible without the help and support of many people, to whom I am deeply indebted.

My special thanks go to my supervisor, Dr. Francisco Emiliano Garcia-Palacios, whose has generously shared his knowledge and expertise, providing valuable feedback and advice during my study.

I also would like to thank my co-authors for many fruitful discussions and collaboration over the last three years.

Finally, I am very much grateful to my parents, my husband, and my children for their understanding and continued support.

To my family,

for their unconditional support

Author's publications

Journal papers:

[J1] **M.-H. T. Nguyen**, Tinh T. Bui, Long D. Nguyen, E. Garcia-Palacios, Hans-Jürgen Zepernick, Hyundong Shin and Trung Q. Duong, "Real-time optimised clustering and caching for 6G satellite-UAV-terrestrial networks," *IEEE Trans. Intell. Transp. Syst.*, Jun. 2023.

[J2] **M.-H. T. Nguyen**, Garcia-Palacios, T. Do-Duy, O. A. Dobre and T. Q. Duong, "UAV-aided aerial reconfigurable intelligent surface communications with massive MIMO system," *IEEE Trans. Cogn. Communs. Netw.*, vol. 8, no. 4, pp. 1828-1838, Dec. 2022.

[J3] **M.-H. T. Nguyen**, E. Garcia-Palacios, T. Do-Duy, L. D. Nguyen, S. T. Mai and T. Q. Duong, "Spectrum-sharing UAV-assisted mission-critical communication: Learning-aided real-time optimisation," *IEEE Access*, vol. 9, pp. 11622-11632, 2021.

Conference papers:

[C1] **M.-H. T. Nguyen**, T. T. Bui, L. D. Nguyen, E. Garcia-Palacios, H.-J. Zepernick, and T. Q. Duong, "Real-time large-scale 6G satellite-UAV networks," in Proc. *22nd IEEE Statistical Signal Process. Workshop (SSP)*,

Hanoi, Vietnam, Jul. 2023.

[C2] **M. -H. T. Nguyen** and E. Garcia-Palacios, "Optimal resource allocation in aerial reconfigurable intelligent surface-aided communications for beyond 5G," in Proc. *2021 IEEE Int. Symp. Dynamic Spectrum Access Networks (DySPAN)*, Los Angeles, CA, Dec. 2021, pp. 237-241.

Table of Contents

List of Tables

List of Figures

List of Notations

$\boldsymbol{X}$ and $\boldsymbol{x}$	Matrix $\boldsymbol{X}$ and vector $\boldsymbol{x}$
$\langle \boldsymbol{x}, \boldsymbol{y} \rangle = \boldsymbol{x}^H \boldsymbol{y}$	The inner product between vectors $\boldsymbol{x}$ and $\boldsymbol{y}$
$M : N$	$M, M+1, \cdots, N$
$\boldsymbol{X^2} = \boldsymbol{X}\boldsymbol{X^H}$	for a matrix X
$\boldsymbol{X}^T$, $\boldsymbol{X}^*$ and $\boldsymbol{X}^H$	The transpose, complex conjugate and conjugate-transpose of matrix $\boldsymbol{X}$
$tr(.)$	The trace operator
$\boldsymbol{I}_M$ and $\boldsymbol{0}_M$	The identity and zero matrices of size $M \times M$
$\mathsf{diag}(\boldsymbol{X})$	The vector of diagonal elements of $\boldsymbol{X}$
$\|\|\boldsymbol{x}\|\|$	The Euclidean norm of a vector $\boldsymbol{x}$
$x \sim \mathcal{CN}(0, \sigma_x^2)$	Complex-valued Gaussian random scalar with mean zero and covariance σ_x^2

Abbreviations

ATG	air-to-ground
BCD	block coordinate descent
BS	base station
CSI	channel state information
CRN	cognitive radio network
DNN	deep neural network
GA	genetic algorithm
GT	game theory
GU	ground user
IoT	Internet-of-Things
LoS	line-of-sight
MBS	macro base station
MIMO	multiple-input multiple-output
mMIMO	massive multiple-input multiple-output
MES	mobile edge server
ML	machine learning
NLoS	non line-of-sight
NOMA	non-orthogonal multiple access

QoS	quality-of-service
PA	power allocation
PU	primary user
RIS	reconfigurable intelligent surface
SU	secondary user
SUTN	satellite-UAV-terrestrial network
UAV	unmanned aerial vehicle
UE	user equipment

Chapter 1

Introduction and overview

1.1 UAV-assisted wireless communication

Wireless communications is being advanced in the way that more capacity is added, together with an increasingly higher data rate, yet at ultra-low latency and extremely high reliability of data transmission. These are the challenges to be met by the evolving wireless technologies, amongst which are unmanned aerial vehicles (UAVs). Not long ago since UAVs first found their way into the real world applications, they have rapidly emerged to become an important component of wireless technologies. In the UK, it is estimated that by 2030, UAVs could contribute up to 45 billion pounds to the UK economy, with 920,000 UAVs being in use [1].

UAVs' main advantages of flexible mobility and cost-effectiveness have enabled their application in a plethora of use cases and scenarios, from search and

rescue to coverage, data collection, monitoring, and delivery, each with its own communication requirements regarding connectivity, traffic demands and adaptability in a fluid environment [2]. For instance, in disaster relief, since a quick network recovery is a priority and crucial to rescue missions, UAVs' fast deployment makes them particularly suitable for establishing a temporary network that aids rescue efforts.

From the communication perspective, UAVs' roles are categorised into three main types: UAVs acting as relays, UAVs acting as flying base stations to provide ubiquitous coverage, and UAVs assisting in information dissemination and data collection [3]. UAVs operate at a high altitude above the ground, making it possible to establish line-of-sight (LoS) connections with both the base station and ground users, avoiding obstructions and blockages (e.g., high buildings, trees etc.) in between, and improve quality-of-service for users. In remote areas or when the terrestrial networks are underdeveloped, UAVs are a quick and efficient solution by flying above and providing network connection within a wide region. Furthermore, UAVs can be tasked with data collection from wireless sensor nodes [4], assist in improving data transmission in vehicular ad hoc networks [5], or support in content delivery [6].

UAV-assisted communication is characterised by four features. *First of all*, UAV-assisted communication has LoS connections for the air-to-air, air-to-ground and ground-to-air links. In particular, the air-to-air links undergo free space propagation since the UAVs operate at a high altitude and without obstructions in between. The latter two types of links are more complex due to propagation blockage, and must depend on the environment and the elevation angle of the UAVs [7]. *Secondly*, a UAV-assisted wireless network has three-dimensional topology as a

result of the UAVs' high altitude that extends the network topology vertically. *Thirdly*, the network topology may change quickly due to the movements of UAVs and users. *Last but not least*, UAVs' operation is limited by their energy capacity, which is also their major drawback. The battery is drained out after only half an hour to a few hours, depending on the complexity and requirements of the missions they undertake. This further exacerbates the challenge of resource allocation and management in wireless networks supported by UAVs. The deployment of UAVs entails decision making on their three-dimensional locations, trajectory, hover time, on-board power, UAV clustering and user association. This is a challenging task, having to consider effects from a number of parameters/factors such as UAV channel gain, channel models communication between UAVs in a fleet, and the environment in which they are deployed [8].

UAVs are not a stand-alone technology and combining UAVs and other wireless technologies can bring about advantages and opportunities. At the same time, by integrating resource-constrained UAVs into wireless networks that currently have scarce resources, new related problems arise. The next section will detail the research challenges in resource allocation in UAV-assisted wireless communication.

1.2 Research challenges in resource allocation for UAV-assisted wireless communication

UAVs' short operational time and their high mobility in a dynamic environment with many constraints pose the need for optimisation of their operation [9]. When

we take into account UAVs' unique features and the intertwine between stringent constraints on energy and flight time [10], resource allocation in UAV-assisted communication should follow optimisation objectives while satisfying certain constraints such as the deployment of UAVs, power budget, and UAVs' cache storage.

In this thesis, the resource allocation problems to be considered in UAV-assisted wireless communication are related to power, spectrum, clustering, and cache. Resource allocation problems in UAV-assisted wireless communication are often optimisation problems of high complexity, non-convex and combinatorial nature. Solving these problems is often very challenging and takes up a lot of compute resources. In addition, most of the research on resource allocation has not considered solving time of optimisation problems. In what follows, we will look at these challenges in more detail.

1.2.1 Resource allocation with spectrum sharing in UAV-assisted networks

UAVs are currently sharing unlicensed spectrum bands with other wireless, terrestrial technologies and devices. These bands will soon become overcrowded due to the tens of billions of Internet-of-Things devices that are operating within the bands, coupled with the growing number of UAVs themselves. On the other hand, licensed spectrum offers the access to adequate channel capacities, which is particularly suitable for the deployment of real-time applications in UAV-assisted communications [11]. Therefore, spectrum sharing serves as an option to increase the radio resources available to UAVs. In particular, cognitive radio networks (CRN) offer secondary users (unlicensed users, i.e., UAVs) the capability of shar-

ing bandwidth with primary users (licensed users) provided that the interference imposed on the latter is kept below a certain threshold.

Spectrum sharing for UAV-assisted networks has received tremendous attention from the research community. There has been research to improve spectrum sensing performance [12], to jointly optimise trajectory and power allocation for UAV-CRN to maximise achievable rate of UAV-SU link [13], or to jointly optimise location and spectrum sensing duration of the UAVs to maximise network throughput [14].

Most of the studies have only considered a simple system set-up (e.g., one single UAV), and a long computation time has been required to solve the optimisation problems. In addition, the dominance of LoS links in UAV communication may cause severe intra- and inter-cell interference that should be managed, especially in the case of spectrum sharing [15].

1.2.2 Power allocation in UAV-reconfigurable intelligent surface- assisted networks

The advances in meta-materials have brought a new technology to wireless communication, that is reconfigurable intelligent surface (RIS). A RIS is a planar structure comprised of hundreds or thousands of reflecting units that reflect incoming signals without amplifying (passive RIS) or with amplifying the signals (active RIS). This thesis only considers passive RISs.

RISs have many advantages, such as:

- Throughput enhancement by forming LoS links between base stations and users, especially when there are blockages and obstacles in between.

- Low power consumption: RISs reflect signals without the need for a power amplifier. Even so, since the phase shifts of the RIS elements can be changed by the RIS controller, they will require a very small amount of power for running the controller and reconfiguring the RIS elements [16, 17].
- Low implementation complexity: There are many options for the installation location of RIS panels, such as on building facades, indoor walls, rooftops, street intersections, or onboard UAVs.

RISs have been considered a great deal in the literature, but in these studies, they were mainly installed at fixed locations. By contrast, when a RIS panel is mounted onboard a UAV to form an aerial RIS, the UAV coverage and communication quality can be improved [17]. To this end, the location of the aerial RISs and phase shift of the RISs should be carefully selected.

As an exciting topic, integrating RISs and UAVs has continued to draw the attention of the research community. Nonetheless, most of the studies were of an exploration nature, relying on simple system models with a single aerial RIS assisting the network, or having a single end user to support. This is in fact a limitation of state-of-the-art research since the number of devices is growing rapidly and one RIS can hardly make sufficient impact to a system in reality. It is only practical to use multiple aerial RISs to efficiently support numerous users.

1.2.3 User clustering and cache placement in UAV-aided content caching

UAVs are connected to the core network via backhaul links from a macro base station or satellite that may be congested during peak hours. In order to al-

leviate this problem, the UAVs can cache popular content in advance (during off-peak hours), and deliver to ground users when requested. Hence, caching at the UAVs during off-peak hours will avoid the use of congested backhaul links and reduce energy consumption at the UAVs during operation while improving transmission rate for users [18]. However, the content popularity may change over time, requiring a frequent update in the caches. In addition, due to the limit in cache capacity, cache placement at UAVs should be optimised to improve the performance of UAV-assisted networks.

Caching enabled by UAVs has been examined in conjunction with UAV deployment, trajectory, and power allocation. In [6], multiple UAVs cooperate in providing content services to multiple users. The authors maximised the minimum throughput amongst the users served by these UAVs, by jointly considering cache placement, UAV trajectory and transmission power. User clustering was not considered, and the UAVs were not able to exchange cached data. This can increase transmission time to users. In [19], for an integrated satellite-terrestrial network support by cache-enabling UAVs, a UAV would have to request the content directly from a satellite if it does not have this content in its cache. Given the long distances from the satellite, transmission time is longer, compared with the case the content is sent by a neighbour UAV having the files.

While satellite communication has begun to regain its popularity, there is a lack of research on UAVs supporting satellite and caching in satellite-terrestrial networks [6]. Additionally, inter-UAV communication also merits more investigation, especially in content caching.

1.2.4 Challenges in solving complex optimisation problems in UAV-assisted communications

In the literature, most optimisation problems considered in UAV-assisted communication have been solved efficiently [20]. However, the increasing number of devices in wireless networks (e.g., IoT devices, sensors) will result in an exponential increase in optimisation problems' complexity. In UAV-assisted wireless networks, it is even more challenging due to the dynamic network topology, e.g., the 3D locations and the number of UAVs impose more stringent constraints on the optimisation problem.

In addition, reducing execution time (e.g, for time-critical applications such as in disaster management) when solving optimisation problems in UAV deployment and radio resource allocation is a challenging but an interesting research direction. Real-time optimisation has attracted attention from research communities in 5G networks and beyond and will become a promising research trend in wireless communications. Yet, for meeting the requirement of solving optimisation problems within strict time-frame to inform real-time choices in UAV communications, the current research literature is not sufficient [21].

Real-time optimisation in the context of UAV-assisted communication is not yet a mature technology, and thus, its potential lies ahead. Particularly, the application of real-time convex optimisation into solving challenges associated with UAVs is still limited. Few studies have attempted to evaluate the solving time of their proposed techniques, or provided an optimal solution to the deployment and resource allocation problems in real-time.

Further to this, machine learning (ML) methods have been widely adopted

in UAV research, with a range of methods employed in solving various problems (e.g., UAV path planning, trajectory design, resource allocation, energy efficiency maximisation) [22]. Distributed methods are also able to solve optimisation problems efficiently.

This thesis adopts optimisation methods, ML methods and distributed approach where appropriate to alleviate the aforementioned challenges. Convex optimisation has many advantages as will be discussed in Chapter 2, while ML methods and distributed approach work well in solving optimisation problems and reducing execution time.

1.3 Thesis's focus

Inspired by the aforementioned discussion, this thesis aims to provide optimal resource allocation strategies in UAV-assisted communication. In particular, the thesis involves the study of optimal strategies for the allocation of power resources in accordance with spectrum resources and/or caching resources in UAV-assisted wireless networks under different scenarios. The main methodology in this thesis is mathematical modelling and simulation using Matlab where the effectiveness of the proposed algorithms is demonstrated. Convex optimisation, together with ML methods and game theory, is the approach to solving optimisation problems of resource allocation.

The focus of this thesis is on resource allocation in UAV-assisted communications with resource constraints that are specific to the use cases being taken into account. This thesis looks at several scenarios of UAV-assisted and communication, such as when the UAVs act as flying base stations or relays to support

in providing network coverage, or when the UAVs assist in content caching. By aiming at optimal deployment strategies and resource allocation, this thesis proposes optimisation algorithms that are useful to the research and application of UAVs in the aforementioned cases, and potentially have a positive impact. For instance, the efficient deployment of UAVs in search and rescue missions will reduce the security and safety risks, operation costs and human lives [2], while UAVs carrying RISs are beneficial to users suffering from obstruction or blockage in urban areas.

1.4 Thesis's contributions

The thesis proposes optimal strategies for resource allocation in UAV-assisted communication. Optimisation problems taking into consideration different resources in UAV-assisted wireless networks are jointly optimised. Unlike most studies in the literature, the studies in this thesis are formed from a more practical viewpoint, with numerous devices (satellites, UAVs, RISs, user equipments) co-existing in the system. This large number of devices entails a large number of variables and constraints, making the optimisation problems difficult to solve. Nonetheless, low-complexity optimisation algorithms that are capable of solving UAVs' resource allocation problems in specific contexts are proposed and proven to outperform other benchmark schemes.

To this end, convex optimisation is the main approach to solving optimisation problems in resource allocation, and is supplemented by ML methods (e.g., deep neural networks, clustering methods, genetic algorithm) and game theory (e.g., non-cooperative game) in order to solve the optimisation problems that are too

complex or difficult. Another reason behind the use of the aforementioned methods is to speed up the process of yielding an optimal solution where appropriate, i.e., making a scheme work faster is crucial, for example, in scenarios where real-time optimisation is necessary, as will be seen in parts of this thesis. It is shown that the proposed algorithms are efficient in handling UAV's resource allocation problems.

The thesis has the following contributions:

- A new, real-time power allocation scheme is proposed for UAV-assisted communications with spectrum-sharing, where the UAVs can serve as relays to connect users that require mission-critical services (e.g., in the event of natural disasters). The optimal resource allocation scheme is designed in terms of the number of UAVs used and the power allocated in the primary and secondary networks. Execution time and throughput maximisation are jointly considered, via the deployment of the UAVs and resource (UAV's power) allocation under stringent constraints. In addition, unlike most other studies that did not consider relevant wireless network challenges [8], we consider the interference impinged on the ground users. Chapter 3 will present the proposed scheme in detail.

- A UAV's quick deployment strategy supported by machine learning (a deep neural network in this instance) is proposed. In the literature, an approach to UAV's deployment considers UAV's trajectory location, speed, and acceleration, as in [3, 21, 23]. By contrast, this thesis considers the UAV's deployment problem as a UAV positioning optimisation problem to provide a best-effort transmission service (as in Chapter 3 and Chapter 4).

- A framework for maximising the total network throughput when multiple aerial RISs are used to extend network coverage, is proposed. The UAV-mounted RISs are passive reflectors in this scenario. The UAVs' power allocation is optimised jointly with the RISs' phase shift in a highly non-convex optimisation problem. Not all users will equally receive the benefits of throughput improvement, as such, we also consider users with lowest throughput (i.e, users at the edge of the coverage area) to reveal the impact of our proposed scheme. Chapter 4 provides the details of how this optimisation problem is solved and the proposed scheme evaluated.

- A real-time, jointly optimal scheme of ground user clustering, UAV cache placement and resource allocation is designed for minimising total latency in an integrated satellite-UAV-terrestrial network. Due to the extremely complex nature of the original problem, it is decomposed into three sub-problems as mentioned above. Since we aim to solve the problem/sub-problems and solve them quickly, a distributed method consisting of game theory, genetic algorithm, and quick estimation technique, is proposed, allowing the original optimisation problem to be solved in real-time. As a benchmark, convex optimisation methods (first-order approximation) applied to the sub-problem of power allocation is presented. Moreover, inter-UAV communication is taken into account when we attempt to reduce network latency. Finally, the UAVs' power divided between inter-UAV communication and UAV-ground user communication is explored. The details are given in Chapter 5.

1.5 Thesis's organisation

The thesis is comprised of 6 chapters and organised as follows. Chapter 1 has just established the context for resource allocation in UAV-assisted wireless communications, the motivation, and contribution of this thesis.

Chapter 2 presents the many methods used in solving resource allocation problems in UAV-assisted wireless networks and provides background information for understanding the studies in the subsequent chapters. Chapter 2 is based on references [J1-3] in the Author's publication list.

In Chapter 3, we look into UAVs in disaster scenarios. When a disaster strikes, utility networks and other infrastructure can get disrupted. Telecommunications base stations in the disaster areas can be out of order, making mobile and network communication within their coverage impossible. This affects (i) users in the disaster areas who need to connect to their family or emergency and rescue services, and (ii) the rescue teams who need to communicate with others in the safe area, for example with the hospitals. To provide urgent network connection in the disaster areas, multiple UAVs can be sent to set up temporary network coverage. Chapter 3 analyses the problem of spectrum sharing in a UAV-enabled wireless network where the UAVs can gain access to both licensed and unlicensed spectrum. Real-time optimisation algorithms of low-complexity are proposed for the primary and secondary networks, aiming at optimising the total throughput in the primary and secondary networks under the constraints of strict tolerable interference imposed on the primary users. A deep neural network plays an important role in reducing the execution time in UAV deployment optimisation problems, making it suitable as a real-time solution. Chapter 3 is published as

[J3] in the Author's publication list.

Chapter 4 considers using UAVs to extend and improve network coverage by integrating a RIS panel on-board multiple UAVs. RIS is a suitable candidate that complements the current state-of-the-art network and communication technologies by providing spectrum/energy efficiency in a cost-efficient manner. The integration of RISs and UAVs that combines the benefit of UAVs and RISs as smart reflection units (UAV-RISs) has been proven to expand reliable wireless network operation and improve network performance. Employing multiple UAV-RISs (aerial RISs), we solve the problem of total network throughput maximisation by optimising the RIS phase shifts and UAVs' power allocation. Chapter 4 is published as [J2] and based on [C2] in the Author's publication list.

In Chapter 5, the roles of UAVs are seen in two aspects: they are used as relays to improve network coverage, and they also assist in content caching. We consider a satellite-UAV-user network where several low Earth orbit satellites, many UAVs and a lot of ground users are operating. Since high latency often incurs in satellite communication due to long distance transmission, the main aim of the study in this chapter is to minimise the total network latency, subject to ground user clustering, cache placement at the UAVs, and power allocation at the satellites and UAVs. A distributed approach is proposed to solve the problem in real-time. A more centralised approach is also presented - the purpose is to have a benchmark as to how well the quick estimation technique works. In addition, the impact of inter-UAV communication on the network latency is evaluated. Chapter 5 is published as [J1] and based on [C1] in the Author's publication list.

Finally, Chapter 6 summarises the key findings in the thesis and discusses research directions for future investigation.

Chapter 2

Background and literature review

2.1 Approaches to solving resource allocation optimisation problems in UAV-assisted communication

2.1.1 Convex optimisation approach

A general convex optimisation problem takes the form of minimising a convex function (or maximising a concave function) subject to linear constraints. From this definition, convex optimisation comes in different classes [24]: linear programs, quadratic programs, geometric programs, convex optimisation problems with generalised inequality constraints (conic programs, semi-definite programs), and vector optimisation programs [1].

Convex optimisation has many advantages. An important feature of convex optimisation that has gained it the widespread adoption is that any locally op-

[1] This chapter is based on references [J1-3] in the Author's publication list.

timal solution is also globally optimal [24]. In addition, there are methods and algorithms that can solve convex optimisation problems efficiently [25], such as Newton's method and interior-point methods.

Many optimisation problems in wireless communication can be formulated as or transformed into convex optimisation problems: downlink beamforming problems can be formulated as semi-definite and second-order cone programming (e.g., [26–28]), sensor network localisation problems can be relaxed to a semi-definite programming (e.g., [29]), the problem of energy-efficiency in UAV communications and networks has been generally formulated as a fractional maximisation problem (e.g., [3, 21]), to name but a few.

When the problems become complex or the number of variables increases, it will take considerably longer to solve those problems, especially in large-scale scenarios. An optimisation algorithm often falls within the categories of iterative algorithms, indicating that a (large) number of iterations will have to be made in order to reach optimal solutions. The running of such a procedure is often costly, requiring both computation resources and time, thus restricts the algorithm's suitability for time-sensitive tasks. Let us take the mixed-integer programming as an example. Mixed-integer optimisation problems are those with integer decision variables. In special cases, these are binary problems where the decision variable is 0 or 1. Mix-integer programming is difficult to solve, and the solution time may increase exponentially with the problem size.

Practical problems in UAV networks and communications are usually nonlinear programming and involve a large numbers of variables [21]. The optimisation of UAV deployment [20, 30] or resource allocation [31, 32] in a UAV-assisted wireless network may result in mixed-integer nonlinear programming problems.

Fortunately, CVXPY embedded in Python can solve this class of problem, by using an appropriate solver (e.g., ECOS_BB). In other cases, the formulated optimisation problems are non-convex due to the non-convexity nature of the objective functions (such as maximising a convex function as in [3]) or the non-convexity of the constraints (as in [20]). Compared with convex optimisation problems, non-convex optimisation problems are more difficult to solve. There is no general method of solving non-convex problems whilst there are many local optima. An approach to this situation is to transform the non-convex problems into convex ones that are easier to handle.

Alternatively, there are solving approaches that can reduce computational complexity of optimisation problems, as detailed in the next subsections.

2.1.2 Machine learning methods

A great number of ML methods have been adopted to improve the performance of UAV-assisted communication or reduce solving time [33]: supervised learning methods (such as support vector machines, neural networks), unsupervised learning (such as K-means), reinforcement learning, self-learning (such as federated learning, transfer learning) [22], and nature-inspired algorithms (such as genetic algorithms, particle swarm optimisation algorithms). Many ML algorithms, e.g., evolutionary or genetic algorithms, can reduce the computational complexity of combinatorial problems, and are suitable for solving complex, large-scale optimisation problems.

Learning-based approaches have been used in solving clustering optimisation in UAV-user association. In [23], a constrained K-means clustering method was

proposed for grouping ground sensors and estimating the minimum of UAVs needed in collecting data from these ground sensors. The K-means method has been shown to significantly reduce solving time in comparison with peer-to-peer UAV-ground sensor scheme. In another study, the use of a deep neural network with several layers can estimate the behaviour of the optimisation algorithm, reduce the error of solution and with that, computation time [31].

The deployment of UAVs as relays can improve network connectivity, energy and spectral efficiency when their clustering strategies are optimised [8]. For example, in [30], a clustering model based on constrained K-means procedure was designed to group users in a disaster scenario. Other approaches see reinforcement learning and deep reinforcement learning being applied to optimise UAV's trajectory. In [34], given the lack of prior and full knowledge of the system, reinforcement learning was used to solve UAVs' trajectory design with the aim to minimise energy consumption while maximising network throughput. In [35], a UAV was used as a relay in an emergency situation. The authors designed the UAV trajectory by using double deep Q network, whereas transfer learning was integrated to reduce training time.

2.1.3 Centralised optimisation approach versus distributed optimisation approach

Compared with a distributed approach, a centralised approach often produces better optimal solutions. On the other hand, the distributed approach can ensure faster running time, yet cannot yield as good an optimal solution as the centralised approach. This thesis relies on both the centralised and distributed approaches.

Particularly for distributed methods, the thesis adopts a non-cooperative game (game theory) and a genetic algorithm (ML method).

In Chapter 5, game theory is applied to solve the problem of ground user clustering/association in a satellite-UAV-terrestrial network, which is formulated as a binary programming. The suitability of a game theory method is based on the following reasons: *(i) Fairness:* In conventional optimisation, optimising network latency for all the users in the considered network may result in very low latency for some users while very high latency for some other. By contrast, the non-cooperative game proposed in the chapter will allow the ground users to choose their best responses, given the actions of the others. In other words, each and every user can choose the cluster that gives them the lowest latency, given the clustering of the other users. *(ii) Discrete programming:* The clustering variable is binary with two possible values of 0 and 1 for all the users. Hence, it is possible to model the clustering problem as a game in which the users choose their actions from a set of possible actions (i.e., to be associated with this UAV or not). *(iii) Parallel computing:* The game theory-based algorithm can solve the sub-problems of optimising the users' response in a parallel manner, on multiple processors. This reduces the time for finding the optimal solution.

Similarly, a genetic algorithm is applied to solve the problem of cache placement at the multiple UAVs in Chapter 5. The reasons are as follows: *(i) Discrete programming:* The indicator of cache placement for a file is a binary variable with possible values of 0 and 1. In their simplest form, the chromosomes in a genetic algorithm are also modelled as binary strings. Thus, the chromosomes can represent the cache placement well. *(ii) Parallel computing:* Cache placement of each UAV cluster can be solved in parallel, thereby reducing running time. *(iii)*

Applicability: Genetic algorithms can be applied to solve various complex problems. However, genetic algorithms also have some drawbacks, for example the difficulties in choosing parameters such as crossover/mutation probability. This issue is also discussed.

A comparison of the centralised and distributed methods used for solving the joint optimisation of user clustering, cache placement and resource allocation in SUINs is given in Chapter 5.

2.2 Resource allocation in UAV-cognitive radio networks in mission-critical communication

In mission-critical communication, such as in the event of a natural disaster, unmanned aerial vehicles (UAVs) play a significant role. The UAVs have to stay airborne above the affected area to aid first responders in search and rescue mission and assessing the gravity of the disaster as promptly as possible [9].

The UAVs' operation is conventionally mandated in the unlicensed spectrum bands shared with other wireless technologies including the IEEE S-Band, IEEE L-Band, and ISM-Band. These bands are becoming more crowded due to the escalating proliferation of Internet-of-Things devices and device-to-device communications. Hence, supporting the UAVs' operation in a cognitive radio network (CRN) becomes a promising technique of increasing the UAVs' available radio resources in addition to the unlicensed band. The integration of UAVs into spectrum-sharing networks has attracted substantial interest from the research community [12,36,37]. In [12], the authors enhanced the spectrum sensing perfor-

mance, by arranging for a UAV to perform spectrum sensing by circularly flying over the primary user (PU) in order to sense and access the idle spectrum. By contrast, the UAV can also operate concurrently with the PU [36], where it acts as a relay to forward the messages from both the PU and SU to the designated receivers.

While combining a UAV with CRNs is capable of improving the spectral efficiency, there are several technical problems associated with UAV-assisted communication. One of the most important issues is the UAV's energy consumption, which represents the main drawback of UAVs' applications [13, 38]. To address this issue, joint trajectory and power allocation optimisation has been conceived for UAV-CRNs in [13]. Given this transmission strategy, the average achievable rate of the UAV to SU link can be optimised subject to the UAV's speed, location and transmit power. Although the aforementioned contributions have shed light on the UAVs' application, especially on their suitability in disaster relief efforts, UAV-assisted communication is still facing limitations that should be addressed for ensuring the success of search and rescue missions. In particular, a prompt action is required of network controllers in support of UAV communications due to the dynamically changing environment [9], which is one of the most critical constraints in UAV applications. In all the UAV-assisted optimisation scenarios found in the open literature [12, 13, 36–38] and the references therein, solving a convex optimisation problem can only be achieved after a long period of time, which is not particularly suitable for mission-critical services. Therefore, maximising the performance of UAV communication networks is vital.

In [39], the authors utilised UAVs as a solution to enhance the average secrecy rate in the cognitive communication networks, by optimising UAVs' robust

trajectory and transmit power allocation. In [40], considering the downlink transmission of UAV-enabled networks in coexistence with device-to-device communication, the authors proposed a joint design of device-to-device assignment and resource allocation for maximising ground terminals throughput. In addition, in [14], the authors have formulated and solved the throughput maximisation problem, by jointly combining optimal location and spectrum sensing duration of the UAVs. However, the cognitive UAV network considered in [14] only consists of a single (primary) receiver, which is generally different from our model. Moreover, aiming at maximising a SU's throughput, the work in [41] studied the joint optimisation problem of the UAV placement and power allocation. However, the authors in [41] considered only a cognitive/secondary UAV transmitter communicating with the ground SU. Very recently, the energy efficiency of UAV-CRNs in disaster recover scenarios have been investigated in [20, 23, 42].

In summary, most of the previous studies have only considered a simple system set-up and involved a long solving time of optimisation problems. Additionally, the interference caused by the dominance of LoS links in UAV-assisted communications has not been well addressed.

2.3 Resource allocation in aerial-reconfigurable intelligent surface (UAV-RIS)- assisted wireless communication for coverage extension

Reconfigurable intelligent surface (RIS) is considered as a key technology for beyond 5G communications [43]. Being significantly advantageous in terms of spec-

trum/energy efficiency and cost-effectiveness, RIS has been shown to be a suitable candidate that complements the current state-of-the-art network and communication technologies. In massive multiple-input multiple-output (MIMO) systems, the use of RISs can serve as an approach to overcome the major challenges of energy consumption and hardware costs in network coverage extension.

A typical RIS is a programmable two-dimensional structure comprised of a large number of elements that reflect signals towards the receivers without amplifying them. The RIS elements can be finely adjusted to control the radio propagation for numerous purposes. In fact, in wireless communications, the RIS phase shifts have often been optimised in association with other factors such as beamforming design, transmit power, and RIS placement. Particularly, the problem of maximising the weighted sum-rate of all the users in a RIS-aided multiuser multiple-input single-output system was considered in [44], by jointly optimising the beamforming design at the access point and phase vectors of the RIS's reflecting elements. To this end, the authors proposed a method based on the block coordinate descent (BCD) when perfect channel state information (CSI) of the channels between the access point-RIS and RIS-user is known, and a procedure based on successive convex approximation in the case of imperfect CSI. Considering the problem of weighted sum-rate maximisation within the uplink from vehicles to the base station (BS), the authors in [45] proposed an alternating algorithm that yields the jointly optimal power control, receive filtering and RIS phase. In [46], an aerial RIS-assisted cell-free massive MIMO system where a number of access points serve several users that are obstructed by tall buildings or distributed in a fairly remote location, was studied. The authors examined the single-user case and optimised the user's achievable rate subject to the trans-

mit power allocation, the access point's precoding vector, RIS phase shift and its placement with respect to horizontal coordinate and height.

Recently, the integration of RISs and unmanned aerial vehicles (UAVs) has been explored in a number of studies to further improve network performance. The benefits of RIS and UAV integration include but are not limited to: improvements in the performance of the air-to-ground network by line-of-sight (LoS) connections thanks to the altitude of the UAVs and any RIS mounted on the UAV(s); the ability to overcome blockage effects when users are obstructed from the BS signals by obstacles such as buildings; and the potential to enhance communication for as many users as possible with the optimised deployment of the UAVs and RISs.

In [47], a caching-enabling UAV was exploited as a two-way relay to assist information transmission to multiple terrestrial user pairs. In [48], the authors proposed a novel prediction model to avoid service interruption caused by the movement of mobile users in wireless networks with the support of multiple UAVs. However, the works in [47] and [48] do not consider the combination of RISs and UAVs. In [49], the authors introduced a RIS to assist a UAV-enabled orthogonal frequency division multiple access communication network, aiming at maximising the system sum-rate by a joint design of the UAV's trajectory, RIS scheduling, and resource allocation. In [50], the authors considered using a RIS mounted on a high-rise building to assist a UAV in providing wireless service. The problem of minimising the UAV's energy consumption via deciding its trajectory design, the RIS' phase shift, power allocation policy, and decoding order, was solved by applying a decaying deep Q-network. In [51], a terrestrial RIS panel was used to provide secure communication between a UAV and a ground user, in

the presence of an eavesdropper. The authors maximised the average worst-case secrecy rate with respect to the UAV's trajectory, RIS beamforming, and legitimate transmitters' power, by using alternating optimisation. In [52], a UAV was deployed to support terahertz (THz) communication, in the presence of a RIS that assists the transmission. The authors proposed to jointly optimise the UAV's trajectory, RIS phase shifts, THz sub-band allocation, and the power control, in order to maximise the minimum average rate amongst all user equipments (UEs). In [53], the authors considered UAVs as aerial users and deployed a RIS on a building wall to reflect signals towards the UAVs from a BS with down-tilt antennas, the aim being to increase the UAVs' received signal. Their results indicated that a small RIS can significantly improve the signal gain for the UAVs.

As mentioned in [54], there are two possible UAV/RIS configurations, namely (i) airborne UAV - terrestrial RIS (e.g., the RIS is mounted on a facade of a building), and (ii) aerial RIS (e.g., the RIS is carried by an airborne UAV). There are studies that support aerial RISs over terrestrial RISs in terms of average data rate and LoS probability achievable for downlink between the RIS and users [55]. The former also have 360° full-angle reflections, stronger channels, and reduced signal power loss as the result of reduced number of reflections [56]. In [55], the authors considered a MISO system and deployed a UAV-RIS to maximise the downlink transmission capacity in order to serve a NLoS user. Particularly, a reinforcement learning approach was proposed to optimise the location and reflection coefficient of the UAV-RIS. In [57], the energy efficiency maximisation problem was studied for a UAV-RIS assisted communication system. Maximum-ratio transmission was applied for the design of beamforming vector at the multi-antenna base station and an alternating optimisation technique was proposed to jointly optimise

the power allocation and RIS phase shifts. In [56], an aerial RIS was deployed to assist a BS in extending network coverage, the objective being to maximise the worst-case signal-to-noise ratio by jointly optimising the transmit beamforming, the aerial RIS's placement, and its three-dimensional passive beamforming. In [58], the authors could enhance the secure energy efficiency of an aerial RIS-assisted system by up to 38%, by jointly optimising the UAV's trajectory, RIS phase shifts, user association, and transmit power. Successive convex approximation and alternating methods were used as the solving approach. In [59], the authors analysed the performance of an aerial RIS system in three modes: (i) only the UAV performs relaying, (ii) only the RIS performs reflecting, and (iii) the UAV performs relaying and the RIS performs reflecting, while the receivers use selection combining. An analytic criterion was derived, allowing the optimal selection of different modes that maximise the ergodic capacity and energy efficiency of the system. In [60], an aerial RIS is deployed to passively relay data from a number of Internet-of-Things devices to the BS. The authors aimed to optimise the aerial RIS's altitude, RIS phase shifts, and communication schedule, to minimise the elapsed time between when data is sampled until an update of receipt is generated at the BS (i.e., to minimise the age-of-information). A deep reinforcement learning algorithm based on proximal policy optimisation was proposed and shown to significantly minimise the sum age-of-information.

Chapter 4 is focused on aerial RIS systems by combining the benefit of UAVs (flexibility) and RISs (low profile and light weight) [44] as smart reflection units (UAV-RISs) to expand reliable wireless network operation and to serve many users at high quality-of-service (QoS). The considered system not only leverages the benefits of both the UAVs and RISs but also alleviates their drawbacks.

Specifically, a low-cost UAV is limited in terms of battery and bandwidth, making it impractical as a small-cell flying BS. Now, implementing a RIS panel onboard the UAV can significantly reduce the energy consumption. Instead of having to regularly reposition the UAV according to the updated network topology (due to UEs' mobility), we can tune the phase shifts of the RIS to form new LoS links that can avoid the need for the UAV's constant movement.

At the time of writing, to our knowledge, only a few papers have addressed the scenarios of aerial RISs. In [54], the authors proposed the integration of RIS and UAV for future beyond 5G and 6G wireless networks. Promising use cases and new communication design issues such as UAV trajectory optimisation, RIS beamforming, channel estimation were discussed to show the benefits of both terrestrial and aerial RIS deployment in enhancing the network performance. In [61], the authors studied a UAV-assisted multiple-RIS symbiotic system, aiming to minimise the weighted sum bit error rate. To this end, they proposed a relaxation-based method to solve the problem, subject to the UAV's optimal trajectory, RIS phase shift and scheduling. In [62], a RIS panel was mounted on a UAV to assist in transmission between a BS and a ground user. The authors derived the analytic expressions for the achievable symbol error rate, ergodic capacity and outage probability, and showed that RIS-assisted UAV communication systems can offer up to 10 times higher capacity compared to UAV communications.

Furthermore, most of the previous work was developed based on a simplified set-up with one UAV-RIS (e.g., [55, 57]), or a single ground end user (e.g., [62]). Very few attempts have been made with multiple UAV-RIS set-up. In [63], the authors proposed an iterative algorithm that updates the BS's power coefficients and block length in an alternating manner. Multiple UAV-RISs were proposed

to support ultra-reliable low-latency communication. The authors solved the problem of minimising the decoding error probability at the users' end subject to blocklength constraint at the BS, power allocation, latency requirements and UAV-RIS clustering constraints. In [64], several aerial RISs were employed for energy efficiency in a heterogeneous network. The joint optimisation of UAVs' trajectory/velocity, subcarrier allocations, RIS phase shifts, and active beamformers at the base stations was decomposed into two sub-problems which were solved by applying dueling deep Q-network learning approach and successive convex approximation method. It is important to note that the ability of multiple UAV-RISs to support ground users in practice has been confirmed [65], but not yet investigated thoroughly.

In summary, the previous studies in integrating RISs and UAVs were relying on simple system models with a single aerial RIS or a single end user, and thus limiting the application of UAV-RISs in practice.

2.4 Resource allocation in integrated satellite-UAV-terrestrial networks

Among other expected features, the sixth generation (6G) wireless networks will be capable of providing ubiquitous connectivity [66]. This will address the issue of inadequate network coverage in many areas. In fact, 80% of the Earth's surface is now not connected to terrestrial networks [67], mainly due to under-developed infrastructure or the lack thereof. To wirelessly connect these areas, the integration of satellite and terrestrial networks in 6G is a favourable approach.

Satellites have been only commercialised in broadcasting services such as television, audio broadcasting, or location positioning, which do not require real-time connections or high data-rate transmission. One of the main reasons was the prohibitive cost of constructing, launching, and maintaining satellites compared to terrestrial networks. The recent advances in technology have now noticeably diminished the cost of satellite communication deployment. At the same time, the development of terrestrial networks has gradually saturated, whilst there are still many uncovered areas. For these reasons, satellite communication is re-gaining its popularity to become an attractive component in 6G communications [68].

Although satellite communication with ubiquitous coverage has the ability to outweigh other approaches in providing global coverage, it still exhibits major limitations as a result of high path-loss and long latency [69]. [2] To confront high attenuation by long distances, direct signal transmission between satellites and ground users would require mobile devices of bulky size to accommodate both high-capacity batteries and high-gain antennas. This makes it hard for satellite communication to reach lightweight handheld devices, especially Internet-of-Things (IoT) devices distributed everywhere over the Earth. In this context, using unmanned aerial vehicles (UAVs) as flying relay stations to improve the quality of signals between satellites and ground users plays a key role.

UAVs have recently been a research hot-spot in wireless communications. Important UAV applications include data collection, localisation, tracking [71,72], and fast network deployment such as in emergency situations [73]. With the rapid

[2]Propagation delay accounts for long latency in satellite communication. Although low Earth orbit satellites have the lowest latency compared with the other two types of satellites (i.e., medium Earth orbit and geostationary equatorial orbit satellites), their one-way propagation delay is 4 ms [70] - this is higher than the end-to-end latency of 1 ms required in 5G.

development of UAV manufacturing technology, future UAVs are expected to have the characteristics of high energy efficiency usage, high-capacity batteries, long flight time, and low cost. Nevertheless, users' fast movements and jitters caused by winds pose a challenge since the channels can change quickly over time [72]. Thus, the requirements of real-time optimisation and real-time computing are indispensable in UAV-assisted networks in order to quickly respond to changes in channels [74].

The integration of satellites and UAV-assisted networks has only just begun to attract researchers' interest. Thanks to high mobility and flexibility, UAVs as relay base stations can be easily integrated into satellite-terrestrial networks with many important roles, such as signal delivery [75], data collection in IoT networks [76], supplementary for terrestrial small base stations [77], and the support for uplink communication [78]. In addtion, in [79], a hybrid satellite-UAV relay network with non-orthogonal multiple access (NOMA) and coordinated multi-point was studied with respect to two problems of relay selection and power allocation (PA). In [80], the PA problem was solved to maximise the ergodic sum-rate of a NOMA-based satellite-UAV-terrestrial network for maritime on-demand services. In [81], machine learning methods were applied in the form of a graph neural network and reinforcement learning, to solve the problems of link selection and UAV trajectory in a UAV-aided hybrid satellite-terrestrial network. In spite of some noticeable improvements in performance, cache placement in UAVs, which plays an important role in mitigating backhaul congestion for satellites, has still not been considered [79,81]. In terms of a cache-assisted UAV, the work in [19] considered aerial networks consisting of a satellite and an UAV, and achieved the total throughput improvement compared to benchmarks. Ad-

ditionally, in [82], the authors proposed a cache-enabled integrated satellite-UAV network to provide connectivity for vehicle users, resulting in an enhancement of energy consumption for both the satellite and UAVs. However, in [19, 82], the system models with only one satellite and/or one UAV do not reflect realistic scenarios where several satellites and multiple UAVs will have to co-exist. To improve the content pushing phase in cache placement, the NOMA scheme proposed in [83] can be used to leverage efficiently the limited spectrum resource to push multiple common files to content servers. In addition, using inter-UAV communication for exchanging cached data between the UAVs can reduce file transmission time to users compared with sending by satellites from long distances. However, to the best of our knowledge, there is a lack of work considering inter-UAV communication to support integrated satellite-terrestrial networks.

In summary, UAVs supporting satellites and caching in satellite-terrestrial networks merit more investigation. Further to this, there are still many research gaps in UAV-enabled caching. For example, previous studies did not consider user clustering and the cooperation between UAVs in content delivery.

Chapter 3

Spectrum-sharing UAV-assisted mission-critical communication: Learning-aided real-time optimisation

This chapter [3] proposes a UAV communications scheme with spectrum-sharing mechanism to provide mission-critical services such as in disaster recovery and public safety. Specifically, the UAVs can serve as flying base stations to provide extended network coverage for the affected area under spectrum-sharing cognitive radio networks (CRNs). To cope with the effects of network destruction caused by a disaster, we propose a real-time optimisation framework for resource allocation (e.g., power and number of UAVs) for CRNs assisted by UAV relays. The proposed optimisation scheme aims at optimising the network throughput

[3]This chapter is published as [J3] in the Author's publication list.

of primary and secondary networks under the stringent constraint of maximum tolerable interference impinged on the primary users. We also propose a deep neural network (DNN) model to significantly reduce the execution time under real-time solution of mixed-integer UAV deployment problems. For both primary and secondary networks, our real-time optimisation algorithms impose low computational complexity, hence, have a low execution time in solving throughput optimisation problems, which demonstrates the benefit of our approach proposed for spectrum-sharing UAV-assisted mission-critical services.

3.1 Introduction

We extend the work in [20] by conceiving advanced optimisation techniques and training deep neural networks (DNNs). We propose a practical optimisation technique for enabling cognitive UAV communications to restore reliable network coverage in disaster-relief missions. Explicitly, joint execution time and throughput optimisation is conceived, which involves the deployment of UAVs under the control of mix-integer optimisation programming and robust resource allocation under throughput maximisation. The numerical results demonstrate the benefits of our approaches proposed for UAV-CRNs.

The main contributions are as follows:

- We consider CRNs assisted by UAVs acting as relays, to cope with the network destruction in the event of a natural disaster. We then propose optimal resource allocation algorithms to maximise the throughput of primary and secondary networks under the rapid UAVs' deployment. Our model considers real-time optimisation in embedded UAV-CRN communication invoked

for recovering wireless communication services.

- For the UAV deployment, an amalgamated optimisation and machine learning method relying on a DNN model is proposed that leads to a significant reduction in the execution time for real-time solution of mixed-integer UAV deployment problems. This technique results in a learning-based optimisation programming.

- For the throughput maximisation of primary and secondary networks, we propose real-time optimisation algorithms to maximise the total throughput and guarantee the QoS fairness, i.e., maximise the worst-case scenario (PU or UAV) in the networks.

- All proposed optimal resource allocation algorithms have low-complexity for solving the non-convex throughput maximisation problem with rapid UAV deployment under both power budget and quality-of-service (QoS) constraints for dealing with the challenges of limited spectral and power resources in UAV systems. Our solutions become capable of supporting real-time applications in disaster recovery scenarios with low execution time in solving practical optimisation problems.

3.2 UAV-CRN system and channel model

3.2.1 System model

We consider multiple UAVs acting as relays in a CRN in disaster relief efforts. The macro base station (BS) is equipped with a massive multiple-input multiple-

output (MIMO) array, in which the N transmit antennas are utilised to serve K_P primary users (PUs) located in the primary network (safety area). Meanwhile, in the secondary network (disaster area), the UAVs are deployed as small-cell flying base stations that are connected to the cellular networks via the BS; the aim is to restore reliable wireless network(s) operation in the disaster area and to serve as many SUs as possible in the disaster area.

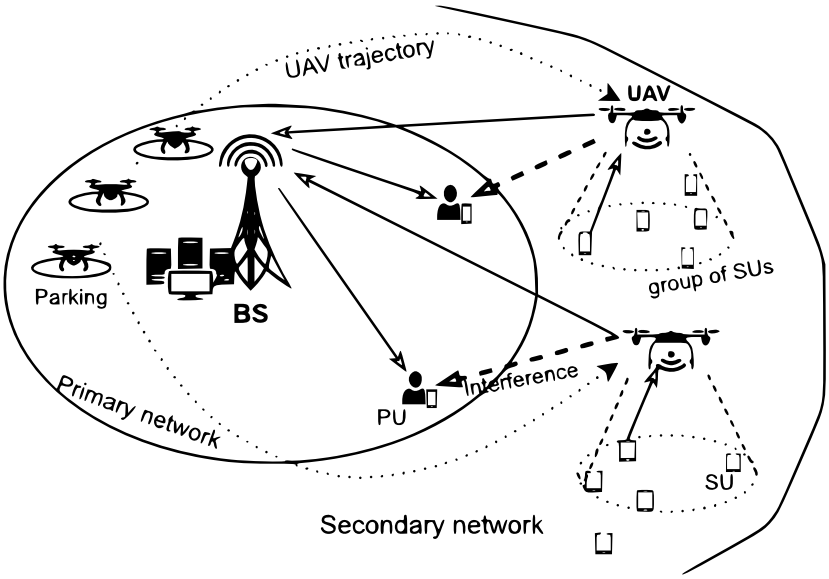

Figure 3.1: A model of UAV-enabled cognitive small-cell network in disaster relief.

All the SUs that are served are represented by M groups given by the set of $\mathcal{K}_S = \{\mathcal{K}_1, ..., \mathcal{K}_M\}$, supported by the set of UAVs $\mathcal{M} = \{1, ..., M\}$ required for restoring reliable network operation. We set the number of PUs and SUs to $\mathcal{K}_P = \{1, ..., K_P\}$ and $\mathcal{K}_S = \{1, ..., K_S\}$, respectively. Both the PUs and SUs are randomly distributed in the primary and secondary networks constituted by the set of $\mathcal{K} = \{\mathcal{K}_P, \mathcal{K}_S\}$. The deployment and trajectory design of the UAVs is controlled by the terrestrial BS as shown in Fig. 3.1. Apart from the BS, all other terminals are single-antenna equipped.

3.2.2 Channel model

We define the three-dimensional location of the BS, the UAVs and of all the users (PUs and SUs) as (x_0, y_0, H_0), (x_m, y_m, H_m), $m \in \mathcal{M}$ and $(x_k, y_k, 0)$, $k \in \mathcal{K}$, respectively. The antenna heights of the BS and a UAV m are respectively denoted as H_0 and H_m. We assume a UAV's antenna altitude is also the UAV's altitude. These locations are determined by using the Global Positioning System (GPS) and stored at the ground station.

Due to the line-of-sight (LoS) propagation and the three-dimensional nature of UAV-enabled communications, we can exploit the air-to-air link to enhance the BS-UAV links, as LoS propagation is highly likely to occur in the air-to-air links. Hence, the path loss between the BS and the m-th UAV follows the free-space path loss model as [42, 84]

$$\beta_{0,m} = \frac{\beta_0}{d_{0,m}^2 + (H_0 - H_m)^2}, \ m = 1 : M, \tag{3.1}$$

where β_0 is the channel's power gain at reference distance d_0, and the horizontal distance between the BS and the m-th UAV is $d_{0,m} = \sqrt{(x_0 - x_m)^2 + (y_0 - y_m)^2}$.

By contrast, the air-to-ground (ATG) channels are more complex due to the effects of propagation blockage such as shadowing, blockage geometry and disaster paraphernalia. The path-loss expression between the m-th UAV and the k-th user is denoted as [7]

$$\beta_{m,k} = PL_{m,k} + \eta_{LoS} P_{m,k}^{LoS} + \eta_{NLoS} P_{m,k}^{NLoS}, \tag{3.2}$$

where η_{LoS} and η_{NLoS} are the average additional losses for the LoS and NLoS

paths, respectively. Here, the distance-related path loss is given by

$$PL_{m,k} = 10 \log \left(\frac{4\pi f_c R_{m,k}}{c} \right)^{\alpha}, \tag{3.3}$$

where f_c is the carrier frequency (Hz), c is the speed of light (m/s), and $\alpha \geq 2$ is the path loss exponent. The probability of LoS is given by [85]

$$P_{m,k}^{LoS} = \frac{1}{1 + a \exp\left[-b \left(\arctan\left(\frac{H_m}{d_{m,k}} \right) - a \right) \right]}, \tag{3.4}$$

where a and b are constants, depending on the environment. Then, we have $P_{m,k}^{NLoS} = 1 - P_{m,k}^{LoS}$.

Finally, we can rewrite (3.2) as

$$\beta_{m,k} = 10\alpha \log(R_{m,k}) + A \times P_{m,k}^{LoS} + B, \tag{3.5}$$

where $A = \eta_{LoS} - \eta_{NLoS}$, $B = PL_{m,k} + \eta_{NLoS}$, and $R_{m,k}$ denotes the distance between the m-th UAV and the k-th user, formulated as

$$R_{m,k} = \sqrt{d_{m,k}^2 + H_m^2}, k \in \mathcal{K}, \tag{3.6}$$

where $d_{m,k} = \sqrt{(x_m - x_k)^2 + (y_m - y_k)^2}$ is the Euclidean distance between the m-th UAV and the k-th user.

3.2.3 Transmission scheme

3.2.3.1 Primary network

Let us consider the transmission in the primary network where the BS transmits its signal to the PUs. The signal received at the k-th PU ($k \in \mathcal{K}_P$) is given by

$$y_{0,k} = \underbrace{\sqrt{P_0}\boldsymbol{g}_{0,k}^T \boldsymbol{f}_{0,k} s_{0,k}}_{\text{desired signal}} + \underbrace{\sum_{k' \in \mathcal{K}_P \setminus \{k\}} \sqrt{P_0}\boldsymbol{g}_{0,k}^T \boldsymbol{f}_{0,k'} s_{0,k'}}_{\text{co-tier interference}} + \underbrace{\sum_{l=1}^{M} g_{l,k}\sqrt{P_l} s_{l,0}}_{\text{inter-cell interference}} + n_k, \tag{3.7}$$

where P_0 is the transmit power of the BS; $\boldsymbol{g}_{0,k} \in \mathbb{C}^N$ is the channel coefficients between the BS and k-th PU; $\boldsymbol{f}_{0,k} \in \mathbb{C}^N$ and $s_{0,k} \in \mathbb{C}$ are the beamforming vector and the information transmitted from the BS with $|s_{0,k}|^2 \leq 1$.

Here, we utilise the structure of the air-to-air links by including both large-scale and small-scale fading effects as $\boldsymbol{g}_{0,k} = \sqrt{\beta_{0,k}}\boldsymbol{h}_{0,k}$, where $\boldsymbol{h}_{0,k}$ is the small-scale fading coefficients for channels from BS to k-th PU. Moreover, P_l is the transmit power of the l-th UAV; $n_k \sim \mathcal{CN}(0, \sigma_k^2)$ is the additive white Gaussian noise. To elaborate the right-hand side of (3.7), the first term is the desired signal designated for the kth PU, the second term is the co-tier interference from the remaining PUs, and the last term is the inter-cell interference from the UAVs in the secondary network.[4]

In this chapter, we employ efficient maximal ratio transmission criterion in beamforming design for the massive MIMO array at the BS, which is formulated as [86]: $\boldsymbol{f}_{0,k} = \sqrt{p_{0,k}}\frac{\boldsymbol{g}_{0,k}^*}{\|\boldsymbol{g}_{0,k}\|}$, where $p_{0,k}$ is the power control coefficient.

[4]We assume that the SUs in the disaster area are located far from the PUs, hence their interference imposed on the PUs is negligible.

Then, we introduce $\rho_{0,k,j} = \boldsymbol{g}_{0,k}^T \boldsymbol{g}_{0,j}^* / \|\boldsymbol{g}_{0,j}\|$.

For the power control coefficients $\boldsymbol{p}_0 = [p_{0,k}]_{k\in\mathcal{K}_P}$ and $\boldsymbol{p}_M = [P_m]_{m\in\mathcal{M}}$, the network interference imposed on the primary network is characterised by the co-tier interference formulated as

$$\mathcal{I}_k^{\mathsf{intra}}(\boldsymbol{p}_0) = P_0 \sum_{k'\in\mathcal{K}_P\setminus\{k\}} p_{0,k'} |\rho_{0,k,k'}|^2, k \in \mathcal{K}_P, \tag{3.8}$$

and the inter-cell interference inflicted by the secondary network[5]

$$\mathcal{I}_k^{\mathsf{inter}}(\boldsymbol{p}_M) = \sum_{m\in\mathcal{M}} P_m |\beta_{m,k}^{atg}|^2, k \in \mathcal{K}_P. \tag{3.9}$$

The information throughput of the k-th PU (in nats) is given by

$$R_{0,k}(\boldsymbol{p}_0, \boldsymbol{p}_M) = \ln\left(1 + \frac{P_0 p_{0,k} |\rho_{0,k,k'}|^2}{\mathcal{I}_k^{\mathsf{intra}}(\boldsymbol{p}_0) + \sigma_k^2}\right). \tag{3.10}$$

To ensure the quality-of-service (QoS) of the primary network, the QoS constraints have to be investigated in the face of inter-cell interference

$$\mathcal{I}_k^{\mathsf{inter}}(\boldsymbol{p}_M) \leq I_{th}^{PU}, \tag{3.11}$$

where I_{th}^{PU} is the maximum tolerable interference still capable of ensuring the

[5]Since it is very hard to estimate the air-to-ground channel, i.e., small-scale fading, between the UAVs and PUs, the inter-cell interference from the secondary network can only be approximated with respect to large-scale fading, as determined in (3.9).

QoS of the PUs. Thus, the total throughput of the primary network is

$$R_{pri}(\boldsymbol{p}_0, \boldsymbol{p}_M) = \sum_{k \in \mathcal{K}_P} R_{0,k}(\boldsymbol{p}_0, \boldsymbol{p}_M). \tag{3.12}$$

3.2.3.2 Secondary network

Simultaneously, we consider the transmission in the secondary network where the UAVs also forward the signals from the SUs to the BS. The signal received at the BS from the m-th UAV is written as

$$y_{m,0} = \underbrace{\boldsymbol{g}_{m,0}^T \boldsymbol{f}_{m,0} \sqrt{P_m} s_{m,0}}_{\text{desired signal}} + \underbrace{\sum_{l=1, l \neq m}^{M} \boldsymbol{g}_{m,0}^T \boldsymbol{f}_{l,0} \sqrt{P_l} s_{l,0}}_{\text{inter-cell interference}} + n_0 \tag{3.13}$$

where P_m is the m-th UAV's transmit power; $\boldsymbol{g}_{m,0}$ is the channel coefficients between the m-th UAV and BS; $\boldsymbol{f}_{m,0}$ is transmit beamforming vector and $s_{m,0}$ is information transmitted by the m-th UAV; and $|s_{m,0}|^2 \leq 1$, $n_0 \sim \mathcal{CN}(0, \sigma_0^2)$ is the additive white Gaussian noise. The inter-cell interference imposed on the BS is caused by the other UAVs transmitting signals from their SUs to the BS.

We apply maximal ratio transmission for the transmission of the secondary network and we also introduce $\rho_{m,0,l} = \boldsymbol{g}_{m,0}^T \boldsymbol{g}_{l,0}^* / \|\boldsymbol{g}_{l,0}\|$.

The information throughput of the BS (in nats) received by the m-th UAV can be written as

$$R_{m,0}(\boldsymbol{p}_M) = \ln\left(1 + \frac{P_m |\rho_{m,0,m}|^2}{\mathcal{I}_m^{\mathsf{BS}}(\boldsymbol{p}_M) + \sigma_0^2}\right), \tag{3.14}$$

where $\mathcal{I}_m^{\mathsf{BS}}(\boldsymbol{p}_M) = \sum_{l \in \mathcal{M}, l \neq m} P_l |\rho_{m,0,l}|^2$ represents the inter-cell interference im-

posed on the BS. Thus, the total throughput of the secondary network is expressed as the total throughput of all UAVs, i.e.,

$$R_{sec}(\boldsymbol{p}_M) = \sum_{m \in \mathcal{M}} R_{m,0}(\boldsymbol{p}_M). \tag{3.15}$$

3.3 Problem formulation

Our main target is to maximise the network throughput of either the primary or secondary network by using BS association and power allocation optimisation for CRNs assisted by UAVs. Hence, we define two optimisation problems: the maximisation of the primary network throughput (MaxPRI) and the maximisation of the secondary network throughput (MaxSEC). The corresponding optimisation problems are respectively formulated as

$$\text{Problem I}: \quad \max_{\boldsymbol{p}_0, \boldsymbol{p}_M, (m,k)} R_{pri}(\boldsymbol{p}_0, \boldsymbol{p}_M) \tag{3.16a}$$

$$\text{s.t.} \quad \sum_{k \in \mathcal{K}_P} p_{0,k} \leq 1, P_m \leq P_m^{\mathsf{max}}, m \in \mathcal{M}, \tag{3.16b}$$

$$R_{m,0}(\boldsymbol{p}_M) \geq \bar{r}_{m,0}, \ m \in \mathcal{M}, \tag{3.16c}$$

$$R_{0,k}(\boldsymbol{p}_0, \boldsymbol{p}_M) \geq \bar{r}_{0,k}, \ k \in \mathcal{K}_P, \tag{3.16d}$$

$$(m,k) \in \mathcal{K}_m, m \in \mathcal{M}, \ k \in \mathcal{K}_m, \tag{3.16e}$$

$$\text{Problem II}: \quad \max_{\boldsymbol{p}_0, \boldsymbol{p}_M, (m,k)} R_{sec}(\boldsymbol{p}_M) \tag{3.17a}$$

$$\text{s.t.} \quad (3.16\text{b}) - (3.16\text{e}), \tag{3.17b}$$

where the constraint (3.16b) represents the power requirements at the UAVs and the BS, while the constraints (3.16c) and (3.16d) formulate the QoS requirement of the UAV-BS and BS-PU links, respectively. The constraint (3.16e) corresponds to the deployment of the UAVs at the beginning. We set $\mathcal{K}_m = \{1, ..., K_m\}$ and $\sum_{m \in \mathcal{M}} K_m = K_S$.

The problems in (3.16)-(3.17) are non-convex problems with the non-convexity of objective functions (3.16a) and (3.17a), and constraint functions (3.16c)-(3.16e). Moreover, when large-scale scenarios are considered, the problems become very complex due to the large number of UAVs (M) and users in the deployment area. For efficiently solving the non-convex problems (3.16)-(3.17), we separate the two problems into two sub-problems. Firstly, the user association with UAV clustering will be proposed that will satisfy constraint (3.16e) under the deployment of UAVs. Then, a DNN is applied for constructing the optimisation strategy of UAV deployment for the real-time context considered. Finally, the optimal power is assigned for maximising the network throughput given QoS requirements.

3.4 Learning optimisation for a real-time scenario of UAV deployment

3.4.1 Conventional optimisation approach for UAV deployment

In order to guarantee the QoS of ATG links between UAVs and users, we consider the coverage region by defining a circular disc of radius D_{cov}, which is related to

the altitude of UAV m as follows:

$$H_m = D_{m,cov} \tan(\theta), \forall m, \tag{3.18}$$

where θ is set to 42.44° [87]. Therefore, a SU can be served by a UAV m in its coverage area $(m,k) \in \mathcal{K}_m$ if the Euclidean distance between the UAV and the SU is less than the coverage distance $D_{m,cov}$, which is formulated as

$$d_{m,k} \leq D_{m,cov}^{max} \ , k \in \mathcal{K}_S, \tag{3.19}$$

where $D_{m,cov}^{max} = H_m^{max} / \tan(\theta)$.

Let us define a binary variable $u_{m,k}$ such that:

$$u_{m,k} = \begin{cases} 1, & \text{if UAV } m \text{ serves SU } k \\ 0, & \text{otherwise.} \end{cases} \tag{3.20}$$

Given the limited operational range of the UAV, we formulate a UAV positioning optimisation problem to provide a best-effort transmission service for the secondary network in each group

$$\max_{\boldsymbol{q}_m, u_{m,k}} \sum_{m=1}^{M} \sum_{k=1}^{K_m} u_{m,k} \tag{3.21a}$$

$$\text{s.t. } d_{m,k}^2 \leq (D_{m,cov}^{max})^2 + \lambda_m (1 - u_{m,k}), \tag{3.21b}$$

$$\boldsymbol{q}_m \in [\boldsymbol{q}_m^{\mathsf{min}}, \boldsymbol{q}_m^{max}], \tag{3.21c}$$

$$u_{m,k} \in \{0, 1\}, \tag{3.21d}$$

$$m \in \mathcal{M}, \ k \in \mathcal{K}_m,$$

where $\boldsymbol{q}_m = [x_m, y_m, H_m^{max}]^T$, λ_m is chosen as a specific value corresponding to the maximum network coverage area of the m-th UAV (i.e., $\lambda_m > (D_{m,cov}^{max})^2$), while (x_{min}, x_{max}) and (y_{min}, y_{max}) represent the lower and upper bounds of the horizontal and vertical range of UAVs, respectively. The binary variable $u_{m,k}$ takes the value of 1 when UAV m serves SU k, and takes the value of 0 otherwise. Notice that the problem in (3.21) is a mixed-integer (binary) quadratically constrained programming problem, which is a non-convex one. Solving the above problem, which belongs to combinatorial (or discrete) optimisation, is often very difficult. Fortunately, the Python-embedded optimisation program CVXPY [88] is capable of solving problem (3.21) using an appropriate solver.

Although conventional optimisation for UAV deployment relying on the CVXPY platform for example can solve problem (3.21), the execution time imposed by solving the related mixed-integer program is excessive, when the networking scenario becomes more complex or the number of integer variables ($u_{m,k}$) increases. The problem (3.21) is one of the most complex problem with the worst-case complexity order of up to $\mathcal{O}(2^{mk})$ where m and k are the number of UAVs and SUs, respectively. There are approaches to reducing the computational complexity of combinatorial algorithms for solving this kind of problems such as exhaustive search, evolution algorithm or genetic algorithms. As a result, we will propose a new optimisation algorithm for UAVs deployment using a DNN for learning optimisation in the next sub-section.

3.4.2 Deep neural network for learning optimisation of UAV deployment

While existing optimisation algorithms might be infeasible, the collaboration of machine learning and optimisation offers simple and efficient techniques in dealing with NP-problems [31,89,90], and complex and large-scale optimisation problems in real-time applications. In this regard, DNN [91, 92] is an efficient machine learning approach that can be applied in real-time optimisation methods.

In particular, to tackle the aforementioned problem, we apply a new optimisation technique eminently suitable for real-time applications by amalgamating DNN and optimisation algorithms. This technique results in learning-based optimisation programming [31].

Following the system setup in [31], we configure the network structure for our DNN model as follows:

- The input of the network is the location of the UAVs and SUs $(\boldsymbol{q}_m, \boldsymbol{q}_k^{SU})$, while the output of the network is the optimal value of $\boldsymbol{q}_m^*$. We use "linear function" as the activation function at the output layer, and "sigmoid" $f(x) = \frac{1}{1+e^{-x}}$ as the activation function at the other layers. The DNN is a dense, feed-forward, network that has 3 hidden layers with 200, 80, and 80 nodes.

- In the training stage, we use a large training data set $(\boldsymbol{q}_m, \boldsymbol{q}_k^{SU})$ for optimising and learning the weights of the DNN model. The cost function is the mean squared error (MSE) and the mini-batch stochastic gradient descent (SGD) optimisation algorithm is used [31].

- In the testing stage, we also generate the structure based on the same distribution during the training stage. Each distributed location experiment is passed through the trained network and then we collect the resultant optimal location of the UAVs.

The optimisation algorithms will be trained for learning the input/output relationship by using a DNN model during the training stage. Several network layers will approximate a training set of resource management algorithms by using a DNN model, which requires simple operations to implement a finite training sample set. With the aid of sufficient training data set, their optimisation technique is capable of completely replacing the conventional optimisation processes during the testing stage. If the learning-based optimisation algorithm learns the updated formula, it can learn a new algorithm that is modelled as a neural network. Learning the weights of the neural network and parameterising the updated formula of the algorithm can provide useful function approximators, model any updated formula with sufficient capacity, allow for efficient search and easily perform training process with backpropagation. The appropriate optimiser would simply memorise the optimum, and after learning with sufficient training set, the optimiser then converges to the optimum within a few steps regardless of initialisation in the future.

3.5 Maximising network throughput via robust power allocation

After solving the UAV deployment problem, in this section, we conceive efficient resource allocation for solving the network throughput maximisation problems (3.16)-(3.17) in the absence of non-convex user association constraints ($u_{m,k}$). On the other hand, the problems (3.16)-(3.17) are still non-convex since the objective functions are non-concave. Hence, we consider the modified problems as

$$\text{Problem I} - \text{B}: \quad \max_{\boldsymbol{p}_0, \boldsymbol{p}_M} \; R_{pri}(\boldsymbol{p}_0, \boldsymbol{p}_M) \tag{3.22a}$$

$$\text{s.t.} \quad (3.16\text{b}) - (3.16\text{d}). \tag{3.22b}$$

$$\text{Problem II} - \text{B}: \quad \max_{\boldsymbol{p}_0, \boldsymbol{p}_M} \; R_{sec}(\boldsymbol{p}_M) \tag{3.23a}$$

$$\text{s.t.} \quad (3.16\text{b}) - (3.16\text{d}). \tag{3.23b}$$

To solve problems (3.22)-(3.23), we use some efficient approximation and logarithm inequalities [93] (see Appendix A for detailed proofs).

Hence, at the i-th iteration, the following convex problems are solved to gen-

erate the feasible points:

$$\text{Problem I} - \text{C}: \quad \max_{\boldsymbol{p}_0, \boldsymbol{p}_M} \hat{R}^{(i)}_{pri}(\boldsymbol{p}_0, \boldsymbol{p}_M) \tag{3.24a}$$

$$\text{s.t.} \quad \sum_{k \in \mathcal{K}_P} p_{0,k} \leq 1, P_m \leq P_m^{\mathsf{max}}, m \in \mathcal{M}, \tag{3.24b}$$

$$\hat{R}^{(i)}_{m,0}(\boldsymbol{p}_M) \geq \bar{r}_{m,0}, \ m \in \mathcal{M}, \tag{3.24c}$$

$$\hat{R}^{(i)}_{0,k}(\boldsymbol{p}_0, \boldsymbol{p}_M) \geq \bar{r}_{0,k}, \ k \in \mathcal{K}_P, \tag{3.24d}$$

$$\text{Problem II} - \text{C}: \quad \max_{\boldsymbol{p}_0, \boldsymbol{p}_M} \hat{R}^{(i)}_{sec}(\boldsymbol{p}_M) \tag{3.25a}$$

$$\text{s.t.} \quad (3.24\text{b}) - (3.24\text{d}), \tag{3.25b}$$

where $\hat{R}^{(i)}_{pri}(\boldsymbol{p}_0, \boldsymbol{p}_M) = \sum_{k \in \mathcal{K}_P} \hat{R}^{(i)}_{0,k}(\boldsymbol{p}_0, \boldsymbol{p}_M)$;

$\hat{R}^{(i)}_{sec}(\boldsymbol{p}_M) = \sum_{m \in \mathcal{M}} \hat{R}^{(i)}_{m,0}(\boldsymbol{p}_M)$.

The form of $\hat{R}^{(i)}_{m,0}(\boldsymbol{p}_M)$ and $\hat{R}^{(i)}_{0,k}(\boldsymbol{p}_0, \boldsymbol{p}_M)$ are defined by (A.6) and (A.4), respectively.

We now proceed by proposing an algorithm to solve the proposed throughput maximisation problems. In Algorithm 1, we propose a power allocation procedure for solving problem (3.24). The initial point $(\boldsymbol{p}_0^{(0)}, \boldsymbol{p}_M^{(0)})$ for (3.24) may be found by random search for a point satisfying the constraints (3.24b)-(3.24d). The power allocation procedure for solving problem (3.25) is similar to Algorithm 1.

Algorithm 1 : Power allocation procedure for solving problem (3.24)

Input:

Set M, K_m, K_p, P_0, P_m.

Set the tolerance $\varepsilon = 10^{-2}$ or the maximum number of iterations $I_{max} = 20$ to stop the algorithm.

Set $i = 0$ and a feasible point.

Repeat

Solve problem (3.24) for the optimal solution $(\boldsymbol{p}_0^{(i+1)}, \boldsymbol{p}_M^{(i+1)})$

Set $i := i + 1$

Until Convergence of the objective function in (3.24) or $i > I_{max}$.

Output: Optimal power control coefficients $(\boldsymbol{p}_0, \boldsymbol{p}_M)$

3.6 Simulation results

In this section, the performance of the considered system is evaluated by using embedded optimisation programming, such as for example the CVXPY version 1.0.21 in Python [88]. The computational platform includes a PC having a AMD Ryzen 7 2700X, CPU @3.7GHz and 32GB memory. Our DNN model was implemented in Python 3.6 associated with Keras 2.2.4 using TensorFlow 1.13.1.

3.6.1 Simulation settings

We set the system parameters for our simulations as follows:

- The safety area is a circle coverage with a radius of 500m, the disaster area is extended from the safety area with a radius up to 2000m.

- The location of the BS is assumed at $(0, 0, 30)$ while PUs and SUs are randomly distributed in the primary network and secondary network, respectively. The limited altitude of the UAVs (H^{min}, H^{max}) is $(50, 150)$m.

- The path loss from the BS to the PUs is as $\beta_{0,k}^{atg} = 148.1 + 37.6 \log_{10} R$ [dB], R in km.

- The number of UAVs is provided as $M = \{4, 8\}$. The number of PUs is set to $K_P = \{10, 20, 30, 60\}$ while the number of SUs in each group is set to $K_m = \{20, 30\}$. The maximum transmit power is set to 40W for the BS [94] and 5W for UAVs.

- The tolerance and maximum number of iterations for convergence of algorithms are $\varepsilon = 10^{-3}$ and $I_{max} = 10$.

- The carrier frequency is $f_c = 2$ GHz, bandwidth $B = 10$ MHz, white power spectral density is $\sigma^2 = -130$ dBm/Hz [87]. The QoS thresholds are set to $\bar{r}_{m,0} = 40$ Mbps and $\bar{r}_{0,k} = 1$ Mbps.

The parameters of the channel model are set as in [84, 87, 93].

3.6.2 Numerical results

The numerical results are conducted from our proposed approaches, i.e., MaxPRI in (3.22) and MaxSEC in (3.23) and the two conventional methods to guarantee the QoS fairness among the primary and secondary networks. More particularly, four different cases are generated from the following algorithms:

- Primary network throughput maximisation (MaxPRI): maximising the primary network's throughput as in (3.22).

- Secondary network throughput maximisation (MaxSEC): maximising the throughput of secondary network as in (3.23).

- Maximisation of minimum primary network throughput(MaxMinPRI): maximising the worst-case PU throughput, i.e., $\max_{\boldsymbol{p}_0,\boldsymbol{p}_M,(m,k)} \min_{k\in\mathcal{K}_P} R_{0,k}(\boldsymbol{p}_0,\boldsymbol{p}_M)$, under the same constraints as Problem I-A. Here, the worst-case PU throughput is defined as the average throughput (in nats) of the PU with the lowest throughput in the primary network.

- Maximisation of minimum secondary network throughput (MaxMinSEC): maximising the worst-case UAV throughput, i.e., $\max_{\boldsymbol{p}_0,\boldsymbol{p}_M,(m,k)} \min_{m\in\mathcal{M}} R_{m,0}(\boldsymbol{p}_M)$, under the same constraints as Problem II-A. Here, the worst-case UAV throughput is defined as the average throughput (in nats) of the UAV with the lowest throughput in the secondary network.

For the sake of fairness, in all the four algorithms, we evaluate the average total throughput (in nats) of all the PUs and UAVs in the system, i.e., $R_{pri}(\boldsymbol{p}_0,\boldsymbol{p}_M) + R_{sec}(\boldsymbol{p}_M)$. In each figure, four different curves are generated as follows:

- MaxPRI: the total throughput of both primary and second networks are plotted where we only optimise the throughput of the **primary network** as in (3.22) and while set the throughput of the secondary network not to fall below its QoS constraint.

- MaxSEC: the total throughput of both primary and second networks are plotted where we only optimise the throughput of the **secondary network** as in (3.23) while set the throughput of the primary network not to fall

below its QoS constraint. In addition, the maximum tolerable interference impinged on the PUs is also satisfied as in (3.11).

- MaxMinPRI: the total throughput of both the primary and second networks are plotted where we only maximise the worst-case PU throughput.
- MaxMinSEC: the total throughput of both the primary and second networks are plotted where we only maximise the worst-case UAV throughput.

3.6.2.1 Convergence of the proposed algorithms

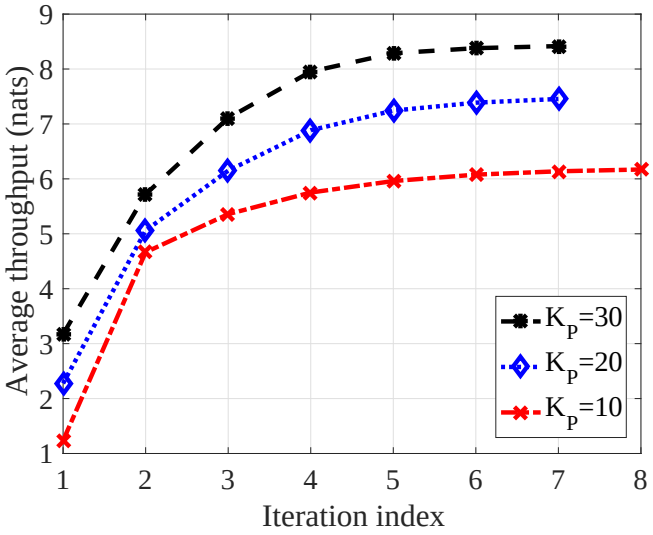

Figure 3.2: The convergence of Algorithm 1 for solving Problem I-C (MaxPRI) at $M = 4$, $K_m = 20$, $P_m = 35$ dBm.

Figure 3.2 illustrates the convergence of Algorithm 1 for solving Problem I-C (MaxRatePri) at $M = 4$, $K_m = 20$, $P_m = 35$ dBm. It is observed that after a few iterations, the objective function (3.24a) converges to its maximum value.

3.6.2.2 Optimal total throughput versus power of UAVs

In Figure 3.3, we show the average total network throughput as a function of the UAV's power (P_m) for the proposed throughput maximisation problems. As expected, the total network throughput with MaxPRI outperforms the others, demonstrating the efficiency of the power allocation with primary network throughput maximisation. Moreover, while MaxPRI and MaxSEC maximise the sum of network throughput, MaxMinPRI and MaxMinSEC only optimise either the PU or UAV with the worst throughput. Therefore, MaxPRI and MaxSEC provide a better total throughput than MaxMinPRI and MaxMinSEC. In addition, although there is a big gap in network throughput between MaxPRI and MaxMinPRI, the gap is not wide between MaxMinPRI, MaxSEC and MaxMinSEC. This indicates that maximising the worst-case UAV throughput is not costly.

For the considered schemes taking into account the secondary network throughput maximisation, the total network throughput increases with the power of UAVs until a threshold (e.g., approximately $P_m = 25$ dBm and $P_m = 20$ dBm in the cases of $M = 4$, $K_m = 20$ and $M = 8$, $K_m = 30$, respectively). The higher the number of UAVs, the lower the P_m threshold above which the network throughput does not increase anymore. This is because the inter-cell interference caused by the UAVs increases significantly with a large number of UAVs. Moreover, the total network throughput with MaxMinSEC suffers a slight degradation when the UAV power increases. This can be explained as follows: when there is an increase in UAV power, the inter-cell interference becomes larger. MaxMinSEC only aims to maximise the worst-case UAV throughput while it has to guarantee the QoS threshold for all the users, resulting in the total network throughput

being reduced by a small amount.

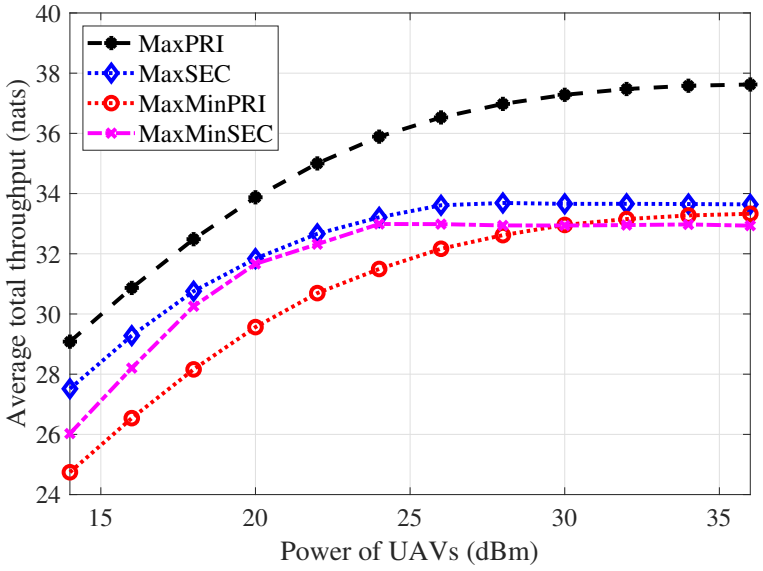

(a) $M = 4$, $K_m = 20$

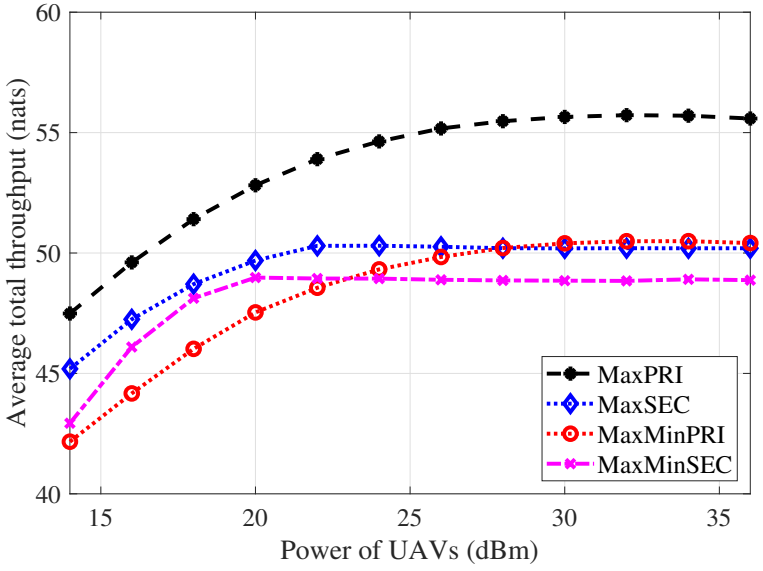

(b) $M = 8$, $K_m = 30$

Figure 3.3: Average total network throughput versus the power of UAVs (P_m) with $K_p = 60$.

3.6.2.3 Optimal throughput versus number of primary users

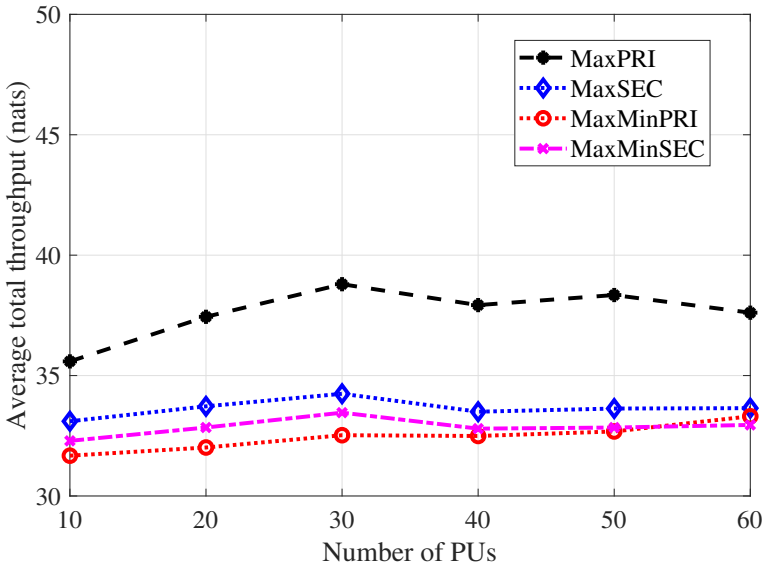

(a) $M = 4$, $K_m = 20$

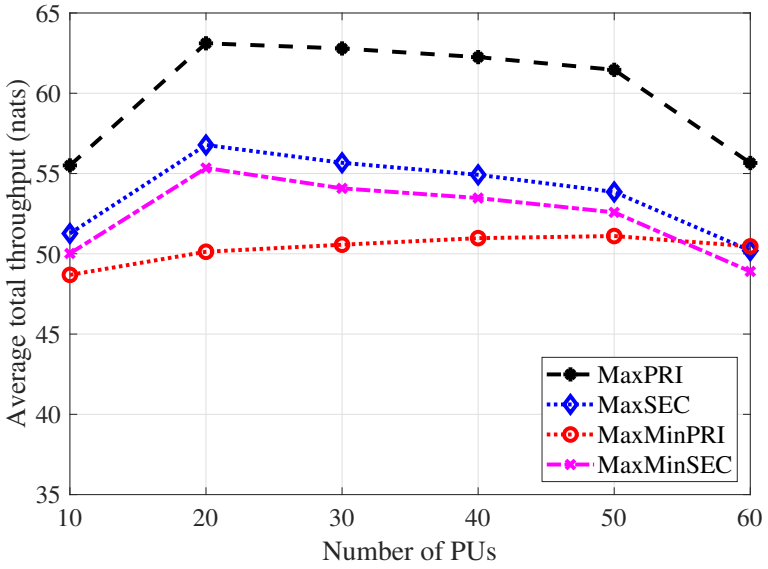

(b) $M = 8$, $K_m = 30$

Figure 3.4: Average total network throughput versus number of PUs (K_p) with $P_m = 35$ dBm.

Figure 3.4 plots the average total throughput versus different number of PUs in the primary network considering different number of UAVs. We can observe from the figure that the average total network throughput goes up when the number of PUs is sufficiently small e.g., $K_P \leq 30$. However, the total throughput would reduce with larger number of PUs due to the co-tier interference in the primary network. As expected, given a particular UAV power, more UAVs are associated with higher the average total throughput of the network.

3.6.2.4 The worst-case UAV and primary user throughput

Figure 3.5 denotes the worst-case UAV throughput versus a range of UAV power at $M = 8$, $K_m = 30$, $K_p = 60$ for different power allocation schemes. We can see that by maximising the throughput of the UAV with the worst performance, MaxMinSEC outperforms the other schemes in terms of the worst-case UAV throughput. On the other hand, MaxSEC obtains lowest performance due to the fact that it only focuses on maximising the total throughput of the secondary network. Moreover, as mentioned above, the worst-case UAV throughput is limited by the inter-cell interference when the power of the UAVs, P_m, is large enough, especially in the case of MaxSEC.

In Figure 3.6, we evaluate the worst-case PU throughput for a range of different number of PUs. MaxMinPRI provides the highest worst-case PU throughput in comparison to the others because its objective function is to maximise throughput of the worst-case PU. Moreover, the larger the number of PUs, the higher the co-tier interference which reduces the PU throughput.

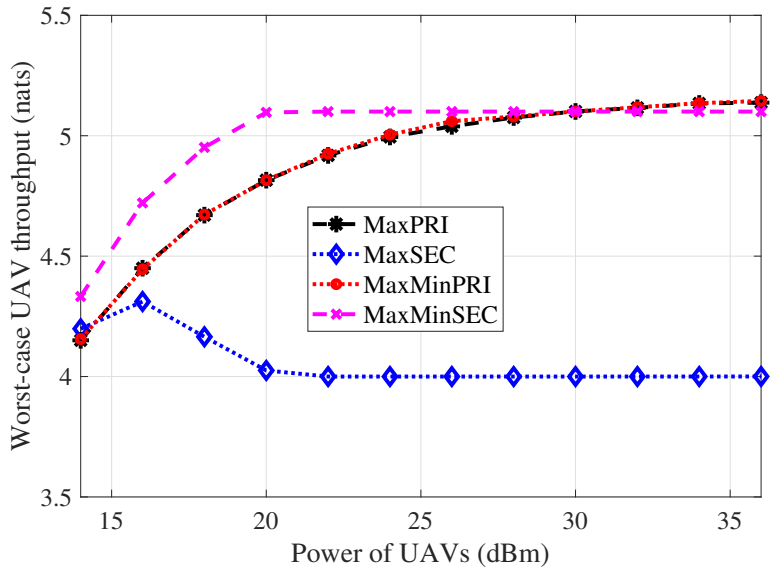

Figure 3.5: Worst-case UAV throughput versus UAV power at $M = 8$, $K_m = 30$, $K_p = 60$.

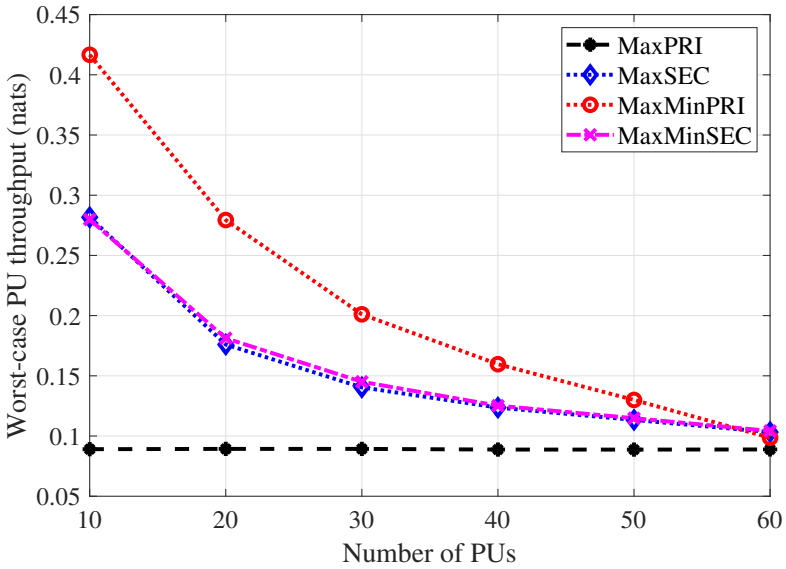

Figure 3.6: Worst-case PU throughput versus the number of PUs at $M = 8$, $K_m = 30$, $P_m = 35$ dBm.

3.6.2.5 Average execution time for solving optimisation problems

In Table 3.1, we provide the average execution time for solving the UAV deployment problem via two proposed methods, i.e., conventional UAV deployment (Conv_Dep) and deep learning UAV deployment (DNN_Dep) schemes. The accuracy metric describes how close the average optimal values achieved in DNN_Dep is to those achieved in Conv_Dep. The figures demonstrate the potential of learning-based optimisation algorithm by using the DNN model. As seen from Table 3.1, our proposed learning-aided UAV deployment procedure exhibits a low complexity and high accuracy, even upon dealing with large-scale scenarios.

Table 3.1: Execution time (s) of our UAV deployment algorithm both under conventional optimisation (Conv_Dep) and learning-aided optimisation using DNN model (DNN_Dep).

$\{M, K_P, K_m\}$	Conv_Dep	DNN_Dep	Accuracy (%)
$\{2, 5, 10\}$	0.15s	0.027s	93.02
$\{4, 10, 20\}$	0.80s	0.028s	92.37
$\{8, 20, 30\}$	4.27s	0.028s	90.82

As shown in Table 3.2, the average execution time for solving optimisation problems under sum rate maximisation and maximin worst-case rate in both primary and secondary networks is provided. All simulation results are consumed within milliseconds for up to 100 devices considered in the system.

3.7 Conclusions

In this chapter, a spectrum-sharing UAV communication scheme was conceived for establishing network coverage for mission-critical services, e.g., in the event of a natural disaster recovery. We proposed a novel learning-aided optimisation

Table 3.2: Execution time (ms) of the proposed optimisation algorithms for optimising network throughput.

$\{M, K_m, K_P\}$	MaxPRI	MaxSEC	MaxMinPRI	MaxMinSEC
$\{4, 20, 10\}$	115	125	75	100
$\{4, 20, 30\}$	260	280	135	220
$\{4, 20, 60\}$	600	670	340	460
$\{8, 30, 10\}$	115	120	100	120
$\{8, 30, 30\}$	280	280	180	250
$\{8, 30, 60\}$	630	750	450	660

scheme for optimal radio resource allocation of the considered networks under the stringent constraint of maximum tolerable interference. By employing the deep learning approach, the UAVs deployment, i.e., the number of UAVs to serve the secondary users, can be quickly established. We then developed the real-time optimisation algorithms to optimise the throughput for both primary and secondary networks. Our low-complexity algorithms lend themselves to real-time deployment in the context of cognitive radio networks relying on UAVs. The numerical results demonstrated that our UAV deployment can be promptly optimised in a large-scale scenario. The proposed schemes revealed a compelling use case of real-time optimisation in wireless communication systems to cope with the lack of network coverage after a disaster. Through the numerical results, we have demonstrated the feasibility of the proposed real-time optimisation which is computationally applicable with just a small amount of time needed for solving it on the millisecond time-scale.

Chapter 4

UAV-aided aerial reconfigurable intelligent surface communications with massive MIMO system

To capture the advantages of UAVs and reconfigurable intelligent surface (RIS) technologies, we propose the use of multiple passive aerial RISs in a massive multiple-input multiple-output (MIMO) network.[6] Each aerial RIS is comprised of a RIS panel attached to a UAV, the intention being to support in extending network coverage from the massive MIMO base station. Compared with stationary RISs, our proposed aerial RISs (termed as UAV-RISs) have the ability to reach more users thanks to the line-of-sight links. Our aim is to maximise the total network throughput by finding the optimal power control coefficients

[6]This chapter is published as [J2] and based on [C2] in the Author's publication list.

at the base station and the phase shifts of the multiple RISs used in the system. This is jointly solved subject to the power consumption constraints, UAV-RIS deployment, and quality-of-service required at the users. We apply zero-forcing precoding for the beamforming design at the base station, and develop an iterative algorithm based on first-order approximation, block coordinate descent, and alternating optimisation technique. Numerical results demonstrate that our proposed method exhibits low computational-complexity and outperforms benchmark schemes in terms of the total network throughput achieved and improvement for the users with worst-case throughput.

4.1 Introduction

In this chapter, we propose an aerial RIS communication scheme where each UAV is equipped with a RIS panel for network coverage extension. Compared with the previous work (e.g., [49–52, 95–97]) in which the RIS panel is installed in a fixed location such as a building facade, the considered scheme is more flexible and more users can be reachable thanks to the UAVs' agility. In addition, we use multiple aerial RISs in our scheme - this is a research gap that has not been sufficiently addressed in the literature.

Different from the aforementioned studies, in this chapter, we propose the use of multiple UAV-RIS set-up for extending network coverage from the massive MIMO base station. Then, we formulate and solve a practical optimisation framework to maximise the total network throughput by jointly optimising the power allocation coefficients and the phase shifts of RIS panels under stringent QoS and power constraints.

In particular, the contributions of this chapter are summarised as follows:

- First, we propose a novel UAV-RIS assisted communication scheme for network coverage extension in a massive MIMO system. We consider a more complex yet practical setting with RIS-equipped UAVs acting as passive reflectors. We focus on the problem of maximising the total network throughput by jointly optimising the power coefficients of the massive MIMO BS (MBS) and the phase shifts of the multiple UAV-RISs deployed to support the network. In addition, we adopt zero-forcing precoding in designing the beamforming matrix to overcome the intra-cluster and inter-cluster interference imposed on the intended user equipments (UEs).

- Second, the optimisation problem is highly non-convex. To deal with this, we decompose the original problem into two sub-problems: (i) a sub-problem of UAV-RIS deployment, and (ii) a sub-problem of joint MBS transmit power and RIS phase shift optimisation. For the former, we propose a procedure based on the K-means clustering to dispatch the UAV-RISs at the beginning. For the latter problem, which is non-convex, we firstly solve the problem separately with respect to each of the two variables, namely the MBS transmit power and RIS phase shift, by proposing two algorithms based on first-order approximation and BCD, respectively. Once the approaches to solving these two optimisation sub-problems are identified, we propose an iterative algorithm in which the MBS power allocation is optimised iteratively with the RIS phase shifts in an alternating fashion, until convergence is reached. It should be noted that although the BCD method has been frequently employed in the literature (e.g. [44]), this chapter con-

siders a more complex setting where multiple UAV-RISs are involved.

- Lastly, we demonstrate the effectiveness of our proposed resource allocation and phase shift optimisation scheme in supporting the aerial RIS-assisted massive MIMO network. Simulation results also reveal the significant gain of the proposed scheme over baseline ones in terms of total network throughput achieved. Concurrently, it is suggested that the users with worst-case throughput can also benefit from our proposed scheme. To be more specific, our scheme outperforms all baseline schemes in terms of providing a better throughput, which is improved by more than 10% in some cases.

The remainder of this chapter is organised as follows. In Section 4.2, we introduce the UAV-RIS communication model as well as the transmission and beamforming scheme. Section 4.3 describes the problem formulation, along with our approach to solving it. Two sub-problems resulting directly from the original problem are solved in the subsequent sections, i.e., the UAV deployment problem (Section 4.4) and the joint power allocation and RIS phase shifts optimisation (Section 4.5). Simulation results are presented in Section 4.6, followed by concluding remarks in Section 4.7.

Notations: Matrices and vectors are denoted by boldface upper and lowercase letters, respectively. The transpose and conjugate transpose operation of a matrix are respectively represented by the superscript T and H. $\mathbb{C}^{M\times N}$ denotes the set of $M \times N$ complex-valued matrices. For a matrix $\mathbf{S}$, $\mathbf{S} \succeq \mathbf{0}$ indicates that $\mathbf{S}$ is positive semi-definite, while rank($\mathbf{S}$) and $tr(\mathbf{S})$ stand for its rank and trace, respectively. $\boldsymbol{I}_K$ denotes an identity matrix with size $K \times K$. A Gaussian random scalar x with 0 mean and covariance σ_x^2 is denoted by $x \sim \mathcal{CN}(0, \sigma_x^2)$.

4.2 Aerial RIS (UAV-RIS) system model

4.2.1 System model

We consider the downlink in a massive MIMO communication network as illustrated in Figure 4.1. Due to severe shadowing and blocking effect, many ground users experience low signal-quality from the MBS that is equipped with a large L-antenna array. A set of $\mathcal{K} = \{1, ..., K\}$ single-antenna user equipments (UEs) are randomly distributed in the deployment area and grouped into M clusters. Then, multiple UAVs, each of which carries a RIS panel with N discrete elements, are deployed to help extend the signal coverage to the ground UEs i.e., network coverage extension, by reflecting the signal from the MBS. To support the M clusters of UEs, we use M UAVs from the set of $\mathcal{M} = \{1, ..., M\}$ to connect the UEs to the MBS where the m-th cluster can only serve a finite number of UEs, $\mathcal{K}_m = \{1, ..., K_m\}$ for $m \in \mathcal{M}$. The (m, k)-th UE denotes the k-th user in the m-th cluster.

It is noted that the jittering effect in UAV platforms caused by UAV jitter could severely reduce the quality of wireless channel in high carrier frequencies [98]. However, there are only a few studies investigating the impact of UAV jittering but mostly at millimetre frequency band (30-300 GHz), e.g., [99, 100]. Therefore, in this chapter, by considering a carrier frequency at 1-2 GHz band, we simply assume that the jittering effect is very small and negligible.

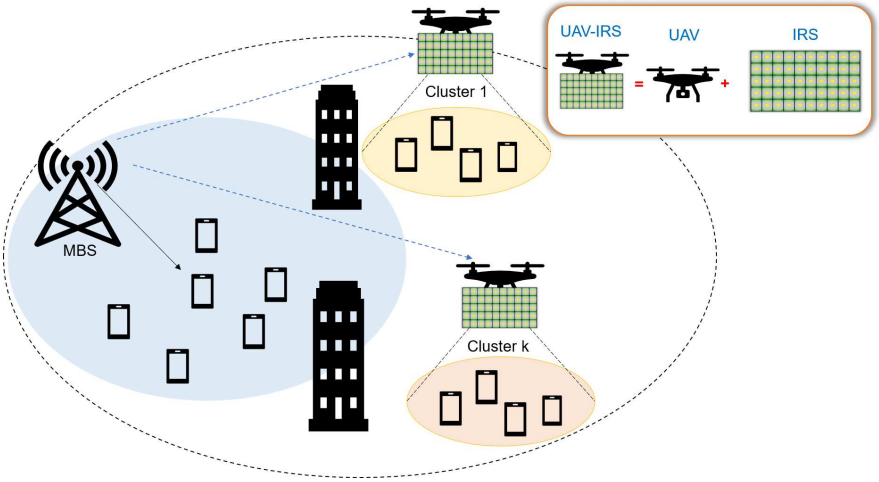

Figure 4.1: A system model of UAV-RIS communication.

4.2.2 Aerial RIS-assisted communication models

Without loss of generality, let us define the locations of the MBS, the UAV-RISs and all the UEs as (x_0, y_0, H_0), (x_m, y_m, H_m), $m \in \mathcal{M}$ and $(x_k, y_k, 0)$, $k \in \mathcal{K}$, respectively, where H_0 is the antenna height of the MBS and H_m is the m-th UAV-RIS's altitude. These location data are identified via the Global Positioning System and stored at the fog nodes near the MBS.

The links between the MBS and the UAV-RISs can be considered as air-to-air communication links, characterised by LoS propagation and three-dimensional UAV-enabled communication. Consequently, the path loss of the link between the MBS and the m-th UAV-RIS follows the free-space path loss model as [42,84]:

$$\beta_{0,m} = \beta_0 R_{0,m}^{-2}, \ m = 1 : M, \tag{4.1}$$

in which β_0 is the channel's power gain at a reference distance d_0; and $R_{0,m} = \sqrt{d_{0,m}^2 + (H_0 - H_m)^2}$ is the distance between the MBS and the m-th UAV-RIS

with $d_{0,m} = \sqrt{(x_0 - x_m)^2 + (y_0 - y_m)^2}$.

By contrast, the air-to-ground channels between the UAV-IRSs and the distributed UEs are more complex due to the effects of propagation blockage including shadowing, which can result in non-light-of-sight (NLoS) channels. Hence, the path loss of the link between the m-th UAV-RIS and the (m,k)-th UE can be formulated as [7]

$$\beta_{m,k} = PL_{m,k} + \eta^{LoS} P_{m,k}^{LoS} + \eta^{NLoS} P_{m,k}^{NLoS}, \tag{4.2}$$

where η^{LoS} and η^{NLoS} are respectively the average additional losses for LoS and NLoS. The distance path loss is expressed as

$$PL_{m,k} = 10 \log(\frac{4\pi f_c R_{m,k}}{c})^{\alpha}, \tag{4.3}$$

where f_c is the carrier frequency (Hz), c is the speed of light (m/s), and $\alpha \geq 2$ is the path loss exponent. The distance $R_{m,k}$ between the m-th UAV-RIS and the (m,k)-th UE is $R_{m,k} = \sqrt{d_{m,k}^2 + H_m^2}$, with $d_{m,k} = \sqrt{(x_m - x_k)^2 + (y_m - y_k)^2}$. $P_{m,k}^{LoS}$ and $P_{m,k}^{NLoS}$ are the probability of LoS and NLoS, respectively, given by [85].

On the other hand, the small-scale fading coefficients for the channels from the MBS to the m-th UAV-RIS and the m-th UAV-RIS to the (m,k)-th UE, denoted by $\mathbf{h}_{0,m} \in \mathbb{C}^{N \times L}$ and $\mathbf{h}_{m,k}^H \in \mathbb{C}^{1 \times N}$, respectively, are assumed as independent and identically distributed random variables with zero mean and unit variance, where the superscript H represents the conjugate transpose operation.

Furthermore, let $\mathbf{H}_{0,m} \in \mathbb{C}^{N \times L}$ and $\mathbf{H}_{m,k}^H \in \mathbb{C}^{1 \times N}$ denote the channel matrix from the MBS to the m-th UAV-RIS and the m-th UAV-RIS to the (m,k)-th UE

in the m-th cluster, respectively. Hence, the cascaded channel matrix of the link from the MBS to the (m,k)-th UE via the m-th UAV-RIS, $\mathbf{G}_{m,k} \in \mathbb{C}^{1\times L}$, can be shown as [96]

$$\mathbf{G}_{m,k} = \mathbf{H}_{m,k}^{H} \mathbf{\Phi}_m \mathbf{H}_{0,m}, \tag{4.4}$$

where $\mathbf{H}_{0,m} = \sqrt{\beta_{0,m}}\mathbf{h}_{0,m}$ and $\mathbf{H}_{m,k}^{H} = \sqrt{\beta_{m,k}}\mathbf{h}_{m,k}^{H}$. $\mathbf{\Phi}_m = diag[\phi_{1m}, \phi_{2m}, ..., \phi_{Nm}]$ is the phase shift matrix at the m-th UAV-RIS, where $\phi_{nm} = \alpha_{nm} e^{j\theta_{nm}}$ with $\alpha_{nm} \in [0,1]$ and $\theta_{nm} \in [0, 2\pi]$ $(\forall n = 1:N,\ m \in \mathcal{M})$ denoting the reflection amplitude and phase shift of the n-th reflecting element, respectively. It is reasonable to assume $\alpha_{nm} = 1$ since each reflecting element can only change the phase of reflected signals but not the amplitude [101].

4.2.3 Transmission and beamforming scheme

As shown in Figure 4.1, the MBS transmits the signal to its UEs via the reflection from the RIS panels deployed on the UAVs. The received signal at the (m,k)-th UE in the m-th cluster is given as

$$\begin{aligned} y_{m,k} = & \underbrace{\sqrt{P_0}\mathbf{G}_{m,k}\boldsymbol{f}_{m,k}s_{m,k}}_{\text{desired signal}} + \underbrace{\sum_{l=1,l\neq k}^{K_m} \sqrt{P_0}\mathbf{G}_{m,k}\boldsymbol{f}_{m,l}s_{m,l}}_{\text{intra-cluster interference}} \\ & + \underbrace{\sum_{m'=1,m'\neq m}^{M} \sum_{l=1}^{K_{m'}} \sqrt{P_0}\mathbf{G}_{m,k}\boldsymbol{f}_{m',l}s_{m',l}}_{\text{inter-cluster interference}} + n_k, \end{aligned} \tag{4.5}$$

where P_0 is the transmit power of the MBS; $\boldsymbol{f}_{m,k} \in \mathbb{C}^{L\times 1}$ is the transmit beamforming vector of the MBS; $s_{m,k}$ is information transmitted by the MBS intended

for the (m,k)-th UE, with $|s_{m,k}|^2 \leq 1$; $n_k \sim \mathcal{CN}(0,\sigma_k^2)$ is the additive white Gaussian noise at the (m,k)-th UE.

To eliminate the interference in (4.5), we apply zero-forcing as follows. Define $\mathbf{G}_m = \left[\mathbf{G}_{m,1},\ldots,\mathbf{G}_{m,K_m}\right] \in \mathbb{C}^{K_m \times L}$ $(m \in \mathcal{M})$ as the channel matrix of the link from the MBS to the K_m UEs within cluster m via the m-th UAV-RIS. Thus, the channel matrix from the MBS to all the UEs via their respective UAV-RIS can be represented by $\mathbf{G} = [\mathbf{G}_1, \mathbf{G}_2, \ldots, \mathbf{G}_M] \in \mathbb{C}^{K \times L}$, with $K << L$ and large L. Accordingly, the square matrix $\boldsymbol{G}\boldsymbol{G}^H \in \mathbb{C}^{K \times K}$ of much smaller size is very well-conditioned, whose eigenvalue distribution becomes more deterministic as L increases [102, 103]. Based on the favourable propagation property in massive MIMO systems, we develop the beamforming vector $\boldsymbol{f}_{m,k}$ by applying zero forcing as follows.

Firstly, the precoding matrix is given by

$$\bar{\boldsymbol{F}}_0 = \left[\bar{\boldsymbol{f}}_1, ..., \bar{\boldsymbol{f}}_M\right] = \boldsymbol{G}^H(\boldsymbol{G}\boldsymbol{G}^H)^{-1}, \tag{4.6}$$

where $\bar{\boldsymbol{f}}_m = \left[\bar{\boldsymbol{f}}_{m,1}, ..., \bar{\boldsymbol{f}}_{m,K_m}\right] \in \mathbb{C}^{L \times K_m}$, in which $\bar{\boldsymbol{f}}_{m,k} \in \mathbb{C}^{L \times 1}$, $m \in \mathcal{M},\ k \in \mathcal{K}_m$. We then normalise $\tilde{\boldsymbol{f}}_{m,k} = \bar{\boldsymbol{f}}_{m,k}/\|\bar{\boldsymbol{f}}_{m,k}\|$ and calculate $\boldsymbol{f}_{m,k}$ in the class of

$$\boldsymbol{f}_{m,k} = \sqrt{p_{m,k}}\tilde{\boldsymbol{f}}_{m,k},\ m \in \mathcal{M},\ k \in \mathcal{K}_m, \tag{4.7}$$

where $p_{m,k}$ is power control coefficient of the MBS with respect to the (m,k)-th UE.

Hence, (4.5) becomes

$$y_{m,k} = \underbrace{\sqrt{P_0}\sqrt{p_{m,k}}\mathbf{G}_{m,k}\tilde{\boldsymbol{f}}_{m,k}s_{m,k}}_{\text{desired signal}} + n_k, \tag{4.8}$$

where the multiple user interference in (4.5) has been cancelled.

Let $\boldsymbol{p}_{0,m} = [p_{m,k}]_{k=1}^{K_m}$ denote the power control coefficients associated with the K_m UEs within cluster m and $\boldsymbol{p}_0 = [\boldsymbol{p}_{0,m}]_{m=1}^{M}$ denote those associated with all the UEs within all the clusters. In addition, let $\boldsymbol{\Phi}_M = [\boldsymbol{\Phi}_m]_{m=1}^{M}$ be the phase shifts of the RISs. Then, the information throughput (in nats) of the (m,k)-th UE can be expressed as

$$R_{m,k}\left(p_{m,k}, \boldsymbol{\Phi}_m\right) = \log_2\left(1 + \frac{P_0 p_{m,k}\left|\mathbf{G}_{m,k}\tilde{\boldsymbol{f}}_{m,k}\right|^2}{\sigma_k^2}\right). \tag{4.9}$$

Hence, the total throughput of all the UEs in the network can be given by

$$R_{total}\left(\boldsymbol{p}_0, \boldsymbol{\Phi}_M\right) = \sum_{m=1}^{M}\sum_{k=1}^{K_m} R_{m,k}\left(p_{m,k}, \boldsymbol{\Phi}_m\right). \tag{4.10}$$

4.3 Problem statement and methodology

In this chapter, we aim to maximise the total network throughput in (4.10) by jointly optimising the power control coefficients at the MBS ($\boldsymbol{p}_0$) and the phase shifts of the M RISs ($\boldsymbol{\Phi}_M$), subject to the power consumption constraints and

the QoS requirements. Accordingly, the optimisation problem is formulated as

$$\textsf{Problem I}: \quad \max_{\boldsymbol{p}_0, \boldsymbol{\Phi}_M} \; R_{total}\left(\boldsymbol{p}_0, \Phi_M\right) \tag{4.11a}$$

$$\text{s.t.} \quad \sum_{m=1}^{M} \sum_{k=1}^{K_m} p_{m,k} \leq 1, \; P_0 \leq P_0^{\max}, m \in \mathcal{M}, \tag{4.11b}$$

$$R_{m,k}\left(p_{m,k}, \boldsymbol{\Phi}_m\right) \geq \bar{r}_{m,k}, \; m \in \mathcal{M}, \; k \in \mathcal{K}_m, \tag{4.11c}$$

$$0 \leq \theta_{nm} \leq 2\pi, \forall n = 1, 2, ..., N, \; m \in \mathcal{M}, \tag{4.11d}$$

$$(m, k) \in \mathcal{K}_m, \; m \in \mathcal{M}, \; k \in \mathcal{K}_m, \tag{4.11e}$$

where the constraint (4.11b) represents the power requirements at the MBS with $P_0^{\max}$ denoting the maximum transmit power of the MBS. The constraint (4.11c) formulates the QoS requirement at the (m, k)-th UE, with $\bar{r}_{m,k}$ being the minimum data throughput required at the UE. The constraint (4.11d) sets the phase shift range of the n-th reflecting elements of the m-th RIS carried by the m-th UAV. The constraint (4.11e) corresponds to the deployment of the UAV-RISs at the beginning.

It can be observed that problem (4.11) is non-convex due to the non-convexity of (i) the objective function (4.11a) and constraint (4.11c) with respect to $\boldsymbol{p}_0$ and $\boldsymbol{\Phi}_M$, and (ii) the constraint (4.11e). In addition, when the number of UAVs (M) and UEs (K) in the deployment area and the number of RIS reflecting elements (N) increase in a large-scale scenario, this problem becomes very complex. In the next two sections, the original problem (4.11) is decomposed into two sub-problems: (i) the user association scheme with UAV clustering will be exploited that will satisfy the constraint (4.11e) under the deployment of UAVs by the constrained K-means clustering procedure, and (ii) the power control coefficients

of the MBS and phase shifts of the RISs will be optimally assigned for maximising the network throughput given QoS requirements.

4.4 Optimisation approach for UAV-RIS deployment

In this section, we will solve the optimisation problem of UAV-RIS deployment as a user association scheme under the constraints of UAV deployment range. First of all, let us introduce a binary variable $u_{m,k}$ to represent whether a UAV-RIS m serves a UE k:

$$u_{m,k} = \begin{cases} 1, & \text{UAV m serves user k} \\ 0, & \text{otherwise.} \end{cases} \tag{4.12}$$

We further define a circular disc of radius D_{cov} as the coverage region of a UAV-RIS. The relation between the altitude of a UAV-RIS m and its coverage is then expressed as:

$$H_m = D_{m,cov} \tan(\omega), \ \forall m \in \mathcal{M}, \tag{4.13}$$

where ω is set to 42.44° [87]. Therefore, a UE can be served by a UAV-RIS in its coverage area $(m,k) \in \mathcal{K}_m$ if the Euclidean distance between the UAV-RIS and the UE is less than the coverage distance $D_{m,cov}$, which is formulated as

$$d_{m,k} \leq D_{m,cov}^{max} \ , k \in \mathcal{K}_m, \tag{4.14}$$

where $D_{m,cov}^{max} = H_m^{max} / \tan(\omega)$.

Let $\boldsymbol{q}_m = [x_m, y_m, H_m^{max}]^T$ denote the three-dimensional location of the m-th UAV-RIS, λ_m denote a specific value corresponding to the maximum network coverage area of the m-th UAV (i.e., $\lambda_m > (D_{m,cov}^{max})^2$), and (x_{min}, x_{max}) and (y_{min}, y_{max}) denote the horizontal and vertical ranges of the UAVs, respectively. The UAV deployment optimisation problem is formulated as

$$\textsf{Problem II}: \max_{\boldsymbol{q}_m, u_{m,k}} \sum_{m=1}^{M} \sum_{k=1}^{K_m} u_{m,k} \tag{4.15a}$$

$$\text{s.t.} d_{m,k}^2 \leq (D_{m,cov}^{max})^2 + \lambda_m (1 - u_{m,k}), \tag{4.15b}$$

$$\boldsymbol{q}_m \in [\boldsymbol{q}_m^{\mathsf{min}}, \boldsymbol{q}_m^{max}], \tag{4.15c}$$

$$u_{m,k} \in \{0, 1\}, \ m \in \mathcal{M}, \ k \in \mathcal{K}_m. \tag{4.15d}$$

Note that problem (4.15) is a mixed-integer (binary) quadratic programming, which is a non-convex problem. Here, adopting the similar approach of the work in [104, 105], the deployment of UAV-RISs in (4.15) can be processed by a constrained K-means algorithm as follows. First of all, we calculate the distance between all K UEs to M UAVs and then assign appropriate UEs into the clusters of (m, k) that has the smallest distance. We then adjust the UAV's altitude to satisfy the QoS constraint of (4.11c). Finally, the position of the m-th UAV is updated by averaging all locations of UEs which belong to the cluster (m, k). The algorithm repeatedly executes the above steps until the cluster members do not change or the procedure reaches the maximum value of iteration index.

4.5 Maximising network throughput via joint power allocation and phase shift optimisation

In this section, the network throughput maximisation problem is solved by searching for the optimal resource allocation strategy of the MBS and phase shift of the RIS reflecting elements, in the absence of UAV-RIS deployment constraint (4.11e). To this end, we first propose solutions for optimising $\boldsymbol{p}_0$ and $\boldsymbol{\Phi}_M$ separately, then design an iterative algorithm that jointly optimises the power control coefficients and the phase shifts by involving the alternating update of the two sub-problems until convergence.

4.5.1 Power control coefficients optimisation

For any given phase shift of the RIS reflecting elements ($\boldsymbol{\Phi}_M$), problem (4.11) can be rewritten as

$$\text{Problem III} - \text{A}: \quad \max_{\boldsymbol{p}_0} R_{total}\left(\boldsymbol{p}_0\right) \tag{4.16a}$$

$$\text{s.t.} \quad (4.11\text{b}), \tag{4.16b}$$

$$R_{m,k}\left(p_{m,k}\right) \geq \bar{r}_{m,k},\ m \in \mathcal{M},\ k \in \mathcal{K}_m. \tag{4.16c}$$

The problem (4.16) is the maximisation of a concave function under convex constraints, yet it is still difficult to compute because of the logarithmic function (4.16a). To solve (4.16), we apply an efficient approximation approach and several logarithm inequalities in [93] (see Appendix B for detailed proof). Hence,

at the κth iteration, problem (4.16) is equivalent to the following problem to generate feasible points:

$$\max_{\boldsymbol{p}_0} \hat{R}_{total}^{(\kappa)}(\boldsymbol{p}_0) \tag{4.17a}$$

$$\text{s.t.} \quad (4.11b), \tag{4.17b}$$

$$P_0 p_{m,k} \left|\mathbf{G}_{m,k}\tilde{\boldsymbol{f}}_{m,k}\right|^2 \geq \left(2^{\bar{r}_{m,k}} - 1\right)\sigma_k^2,\ m \in \mathcal{M},\ k \in \mathcal{K}_m, \tag{4.17c}$$

where the form of $\hat{R}_{m,k}^{(\kappa)}(\boldsymbol{p}_0)$ and $\hat{R}_{total}^{(\kappa)}(\boldsymbol{p}_0)$ are defined in (B.5) and (B.6), respectively. Based on [106], the computational complexity of (4.17) is

$$\mathcal{O}(\bar{n}^2\bar{m}^{2.5} + \bar{m}^{2.5}), \tag{4.18}$$

where $\bar{n} = MK$ is the number of decision variables and $\bar{m} = M(K+1)$ is the number of constraints.

As a result, problem (4.17) can be efficiently solved by using optimisation tools, e.g., CVX [107]. In Algorithm 2, we propose a power allocation procedure for solving problem (4.17).

Algorithm 2 Power allocation procedure for solving problem (4.17).

Input:

Set $\kappa = 0$, $\boldsymbol{\Phi}_M$, and initial point $\boldsymbol{p}_0^{(0)}$.

Set tolerance $\varepsilon = 10^{-3}$, maximum iterations $I_{max} = 20$ to stop the algorithm.

Repeat

Solve problem (4.17) for the feasible solution $(\boldsymbol{p}_0^{(\kappa+1)})$.

Set $\kappa = \kappa + 1$.

Until Convergence or $\kappa > I_{max}$.

Output: Optimal power control coefficients $(\boldsymbol{p}_0^*)$

4.5.2 RIS phase shift optimisation

For any given power control coefficients $\boldsymbol{p}_0$, problem (4.11) can be rewritten as

$$\mathsf{Problem\ III-B}: \quad \max_{\boldsymbol{\Phi}_M} R_{total}\left(\boldsymbol{\Phi}_M\right) \tag{4.19a}$$

$$\text{s.t.} \quad (4.11c), (4.11d). \tag{4.19b}$$

For a given transmit beamforming vector $(\boldsymbol{f}_{m,k},\ \forall n = 1, 2, ..., N,\ m \in \mathcal{M})$, we search for the feasible phase shifts of the RISs. Let $\boldsymbol{\nu}_m = [\nu_m^1, ..., \nu_m^N]^H$ in which $\nu_m^n = e^{j\theta_{nm}}$ $(\forall n = 1, 2, ..., N)$. Then the constraint (4.11d) is equivalent to the unit-modulus constraint, i.e., $|\nu_m^n|^2 = 1$ [27].

Furthermore, we apply the change of variables as follows.

Let $\boldsymbol{\chi}_{m,k} = diag(\mathbf{H}_{m,k}^H)\mathbf{H}_{0,m}\boldsymbol{f}_{m,k}$, then $\mathbf{H}_{m,k}^H\boldsymbol{\Phi}_m\mathbf{H}_{0,m}\boldsymbol{f}_{m,k} = \boldsymbol{\nu}_m^H\boldsymbol{\chi}_{m,k}$. Hence,

problem (4.19) is equivalently rewritten as

$$\max_{\boldsymbol{\nu}_m,\ m\in\mathcal{M}} \sum_{m=1}^{M}\sum_{k=1}^{K_m} \log_2\left(1+a_k\boldsymbol{\nu}_m^H\boldsymbol{\chi}_{m,k}\boldsymbol{\chi}_{m,k}^H\nu_m\right) \tag{4.20a}$$

$$\text{s.t.} \quad \boldsymbol{\nu}_m^H\boldsymbol{\chi}_{m,k}\boldsymbol{\chi}_{m,k}^H\boldsymbol{\nu}_m \geq \left(2^{\bar{r}_{m,k}}-1\right)/a_k,\ m\in\mathcal{M},\ k\in\mathcal{K}_m, \tag{4.20b}$$

$$|\nu_m^n|^2=1, \forall n=1,2,...,N,\ m\in\mathcal{M}, \tag{4.20c}$$

where $a_k = P_0 p_{m,k}/\sigma_k^2$. However, the problem (4.20) is a non-convex quadratically constrained quadratic programming (QCQP) problem. Therefore, we exploit the following transformation. Let $\mathbf{X}_{m,k} = \boldsymbol{\chi}_{m,k}\boldsymbol{\chi}_{m,k}^H$ and $\boldsymbol{\nu}_m^H\mathbf{X}_{m,k}\boldsymbol{\nu}_m = tr\left(\mathbf{X}_{m,k}\boldsymbol{\nu}_m\boldsymbol{\nu}_m^H\right) = tr\left(\mathbf{X}_{m,k}\mathbf{V}_m\right)$, where $\mathbf{V}_m = \boldsymbol{\nu}_m\boldsymbol{\nu}_m^H$ must satisfy $\mathbf{V}_m \succeq \mathbf{0}$ and rank($\mathbf{V}_m$)=1. Note that the rank-one constraint can be relaxed due to the non-convex property of the unit-modulus constraint (4.20c) [27,108]. Hence, problem (4.20) is transformed into the following problem:

$$\max_{\nu_m,\ m\in\mathcal{M}} \sum_{m=1}^{M}\sum_{k=1}^{K_m} \log_2\left(1+a_k tr\left(\mathbf{X}_{m,k}\mathbf{V}_m\right)\right) \tag{4.21a}$$

$$\text{s.t.} \quad tr\left(\mathbf{X}_{m,k}\mathbf{V}_m\right) \geq \left(2^{\bar{r}_{m,k}}-1\right)/a_k,\ m\in\mathcal{M},\ k\in\mathcal{K}_m, \tag{4.21b}$$

$$\mathbf{V}_{m(n,n)}=1, \forall n=1,2,...,N,\ m\in\mathcal{M}, \tag{4.21c}$$

$$\mathbf{V}_m \succeq \mathbf{0}. \tag{4.21d}$$

As observed, problem (4.21) is a convex semi-definite program (SDP) [27,28], which can be efficiently solved by existing convex optimisation solvers e.g., CVX. The computational complexity of (4.21) is based on (4.18) with $\bar{n} = MK$ and $\bar{m} = M(N+K)$.

In Algorithm 3, we propose a BCD-based procedure for solving problem (4.21).

Specifically, the procedure is implemented for each UAV-RIS so that the phase shifts of N elements at the m-th UAV-RIS are identified. Then, the BCD procedure terminates with the convergence of the optimal phase shifts of all the RIS elements.

Algorithm 3 : BCD-based phase shift searching procedure for solving problem (4.21).

Input:

Set $\kappa = 0$, $\boldsymbol{p}_0$, and initial point $\boldsymbol{f}_{m,k}^{(0)}$.

Set tolerance $\varepsilon = 10^{-3}$, maximum iterations $I_{max} = 20$ to stop the algorithm.

Repeat

for $m = 1$ to M do

Solve problem (4.21) for the feasible solution ($\boldsymbol{\Phi}_M^{(\kappa+1)}$).

Update $\boldsymbol{f}_{m,k}^{(\kappa+1)}$.

end for

Set $\kappa = \kappa + 1$.

Until Convergence or $\kappa > I_{max}$.

Output: Optimal phase shift ($\boldsymbol{\Phi}_M^*$)

We note that the solution to problem (4.21) may not meet the rank-one constraint that has been relaxed. In this case, the Gaussian randomisation method can be used to find the near-optimal solution [27, 64].

4.5.3 Iterative optimisation algorithm

In Section 4.5.1 and 4.5.2, the original problem (4.11) has been transformed into two independent convex sub-problems (4.16) and (4.19) (having solved the UAV-

RISs deployment (constraint (4.11e)) in the previous section). Subsequently, we propose an iterative optimisation algorithm, summarised as in Algorithm 4, to jointly solve the MBS optimal power allocation and phase shifts of the RIS reflecting elements. Accordingly, we solve problem (4.16) and (4.19) alternatively, having the solution in each iteration as the initial point in the next iteration.

Algorithm 4 : Iterative optimisation algorithm for jointly solving problem (4.11).

Input:

Set $j = 0$, initial $\boldsymbol{p}_0^{(0)}$ and $\boldsymbol{\Phi}_M^{(0)}$.

Tolerance $\varepsilon = 10^{-3}$, maximum iterations $I_{max} = 20$ to stop the algorithm.

Repeat

For $\boldsymbol{\Phi}_M^{(j)}$, run Algorithm 2 to solve the optimal power control coefficients $\boldsymbol{p}_0^{(j+1)}$.

For $\boldsymbol{p}_0^{(j+1)}$, run Algorithm 3 to solve the optimal phase shifts of the RIS reflecting elements $\boldsymbol{\Phi}_M^{(j+1)}$.

Set $j = j + 1$.

Until Convergence or $j > I_{max}$.

Output: $(\boldsymbol{p}_0^*, \boldsymbol{\Phi}_M^*)$

4.6 Simulation results

In this section, simulation results in Matlab are provided to demonstrate the performance of the proposed algorithms.

4.6.1 Simulation setting

The platform for simulation includes a PC with AMD Ryzen 7 2700X, CPU 3.7GHz and 32GB memory.

The system parameters for our simulations are set as follows. A circle with a radius of 500 m with the MBS at its centre, is considered. The entire deployment area is extended from the MBS coverage area with a radius of up to 2000 m. The location of the MBS is assumed at $(0, 0, 30)$, while the UEs are randomly distributed in the deployment area. The number of UEs is $K = \{30, 50\}$ and the number of UAVs is $M = \{8, 12\}$ [104]. The number of elements of each RIS panel is set to $N = \{40, 80, 120, 160, 200\}$ [27]. The altitude range of the UAVs (H^{min}, H^{max}) is $(50, 150)$ m [87]. The QoS thresholds are set to $\bar{r}_{m,k} = 1$ bps/Hz. The white noise power spectral density is $\sigma^2 = -130$ dBm/Hz. The parameters of the channel model follow the simulation settings in [87, 93].

4.6.2 Numerical results

In order to evaluate the proposed method OPW-OPH, which solves the problem in (4.11), we perform simulations and compare the results based on OPW-OPH against those of three other baseline methods. In particular, we investigate the following cases:

- OPW-OPH: maximising the total network throughput considering optimal transmit power of the MBS and optimal phase shifts of the RIS reflecting elements.

- OPW-RANDPH: maximising the total network throughput considering optimal transmit power of the MBS and random phase shifts of the RIS re-

flecting elements.

- EPW-OPH: maximising the total network throughput considering equal transmit power of the MBS and optimal phase shifts of the RIS reflecting elements while the total power of the MBS is equally allocated to the M clusters.

- EPW-RANDPH: maximising the total network throughput considering equal transmit power of the MBS and random phase shifts of the RIS reflecting elements.

4.6.2.1 Convergence of the proposed algorithms

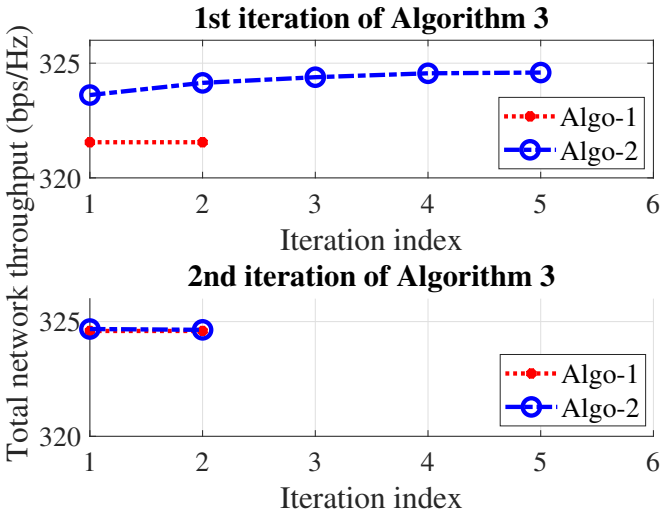

Figure 4.2: The convergence of the proposed algorithms for solving problem (4.11) (OPW-OPH) at $K = 30$, $M = 8$, $N = 80$, $P_0 = 40$ dBm.

Figure 4.2 illustrates the convergence of Algorithms $1-3$ for solving problem (4.11) (OPW-OPH), with $K = 30$, $M = 8$, $N = 100$, $P_0 = 40$ dBm. It is observed that at the first iteration of Algorithm 3, the inner algorithms (Algorithms 1 and

2) converge after a few iterations while only 2 iterations are needed according to the second iteration of Algorithm 3 to reach the final convergence.

4.6.2.2 Optimal network throughput versus maximum transmit power of the MBS

Figure 4.3 shows the total network throughput maximised with respect to the MBS power allocation and RIS phase shifts, $R_{total}\left(\boldsymbol{p}_0^*, \boldsymbol{\Phi}_M^*\right)$, as a function of maximum transmit power of the MBS for different numbers of UAVs (M) and UEs (K). As observed from the figure, the higher the maximum transmit power of the MBS, the better the total network throughput. This is due to the fact that when zero forcing is used at the MBS, it has the tendency to allocate the entire power budget to the UEs in order to maximise the throughput. More importantly, as expected, the total network throughput based on OPW-OPH outperforms the baseline methods, which indicates the efficiency of the joint power allocation and RIS phase shifts optimisation provided by the proposed algorithms.

Specifically, our proposed method can obtain a throughput of up to 10.5 bps/Hz and 13.8 bps/Hz higher than that in the EPW-RANDPH method for $K = 30$, $M = 8$ (Figure 4.3a) and $K = 50$, $M = 12$ (Figure 4.3b), respectively. The gap widens with the number of UEs in the deployment area. Furthermore, given a particular N, e.g., $N = 80$, and at a larger K and M (Figure 4.3b), when only either power allocation optimisation or RIS phase shifts optimisation is exploited, i.e., either OPW-RANDPH or EPW-OPH, the improvement over EPW-RANDPH in terms of network throughput become less significant when compared to that achieved in OPW-OPH.

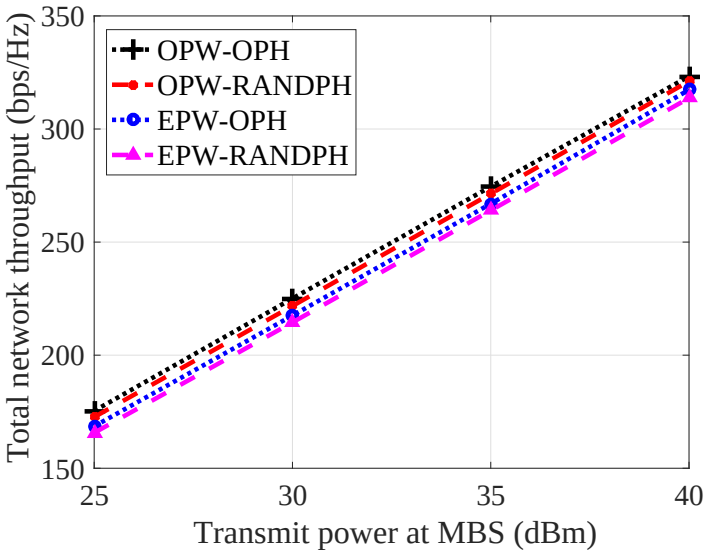

(a) $K = 30$, $M = 8$, $N = 80$.

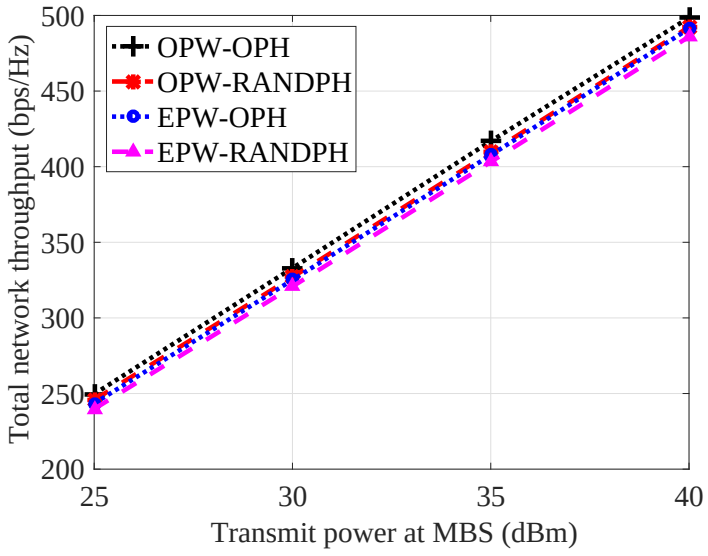

(b) $K = 50$, $M = 12$, $N = 80$.

Figure 4.3: Total network throughput, $R_{total}\left(\boldsymbol{p}_0^*, \boldsymbol{\Phi}_M^*\right)$ for different numbers of UAVs (M) and UEs (K).

4.6.2.3 Optimal network throughput versus the number of RIS reflecting elements

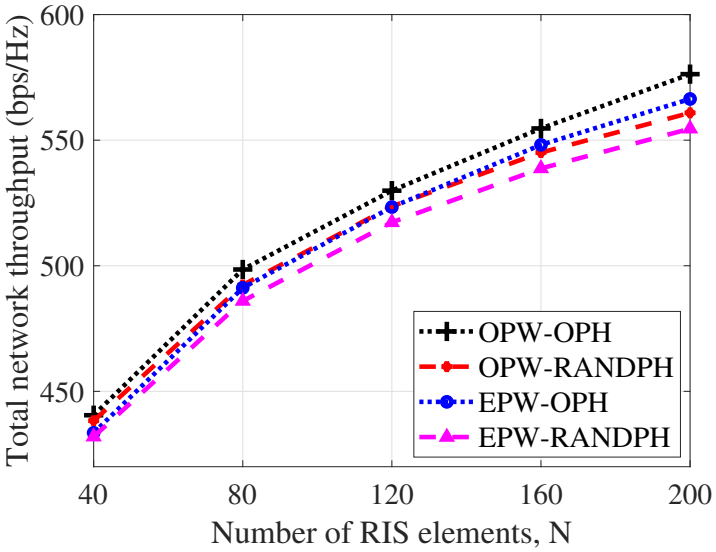

Figure 4.4: Total network throughput, $R_{total}\left(\boldsymbol{p}_0^*, \boldsymbol{\Phi}_M^*\right)$, versus different numbers of RIS reflecting elements (N), at $K = 50$, $M = 12$, $P_0 = 40$ dBm.

Figure 4.4 plots the total network throughput against different numbers of RIS reflecting elements at $K = 50$, $M = 12$, $P_0 = 40$ dBm. The figure indicates an increase of the total network throughput with the number of RIS reflecting elements (N). It is interesting to see that the total network throughput obtained with OPW-OPH is notably improved for large N. Moreover, for sufficiently large N, the performance of EPW-OPH significantly outperforms that of the OPW-RANDPH method. This confirms the advantages of the RIS phase shift optimisation on network throughput. Table 4.2 shows the throughput improvement (in bps/Hz) provided by OPW-OPH as compared to the conventional methods for a range of N. The throughput could be improved by up to 15.41 bps/Hz, 9.88 bps/Hz, and 21.73 bps/Hz compared to OPOW-RANDPH, EPOW-OPH, and

EPOW-RANDPH, respectively, at $N = 200$, and even much higher gain can be attained when a larger number of RIS reflecting elements are used.

Table 4.1: Improvement of total network throughput (in bps/Hz) with OPW-OPH when compared to the other methods for different N with $K = 50$, $M = 12$, $P_0 = 40$ dBm.

OPW-OPH versus	N				
	40	80	120	160	200
OPOW-RANDPH	2.20	6.18	6.23	8.44	15.41
EPOW-OPH	7.01	7.23	7.53	8.16	9.88
EPOW-RANDPH	8.55	12.55	12.61	14.75	21.73

Table 4.2: Improvement of total network throughput (in %) with OPW-OPH when compared to the other methods for different N with $K = 50$, $M = 12$, $P_0 = 40$ dBm.

OPW-OPH versus	N				
	40	80	120	160	200
OPOW-RANDPH	0.5	1.25	1.19	1.55	2.75
EPOW-OPH	1.61	1.47	1.25	0.98	1.74
EPOW-RANDPH	1.98	2.58	2.44	2.74	3.92

4.6.2.4 Worst-case user equipment's throughput

In addition to evaluating the total network throughput, we also consider the worst-case UE throughput where the worst-case UE is defined as the UE that obtains the lowest throughput amongst the K UEs in the deployment area. Figure 4.5 depicts the worst-case UE throughput according to optimised power allocation and RIS phase shifts versus a range of RIS elements. As noticed from the figure, the worst-case UE throughput also benefits from the increase of RIS elements. Hence, the proposed method (OPW-OPH) also provides the worst-case UE with a considerably better throughput than the conventional methods.

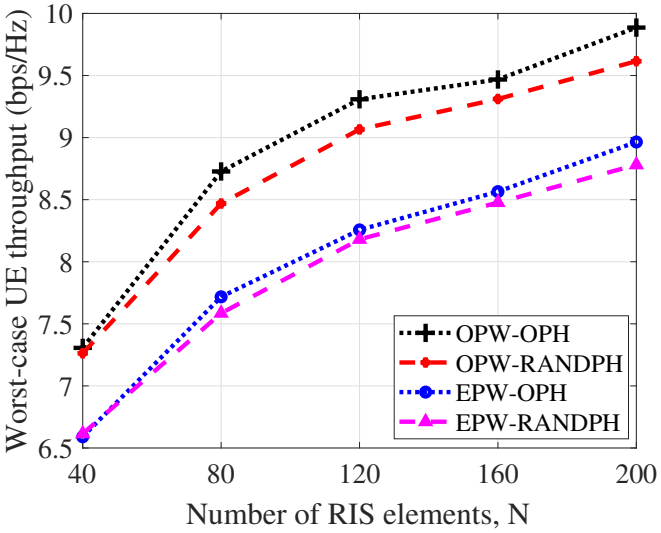

Figure 4.5: Worst-case UE throughput according to optimised power allocation and RIS phase shifts versus different numbers of RIS elements (N), at $K = 50$, $M = 12$, $P_0 = 44$ dBm.

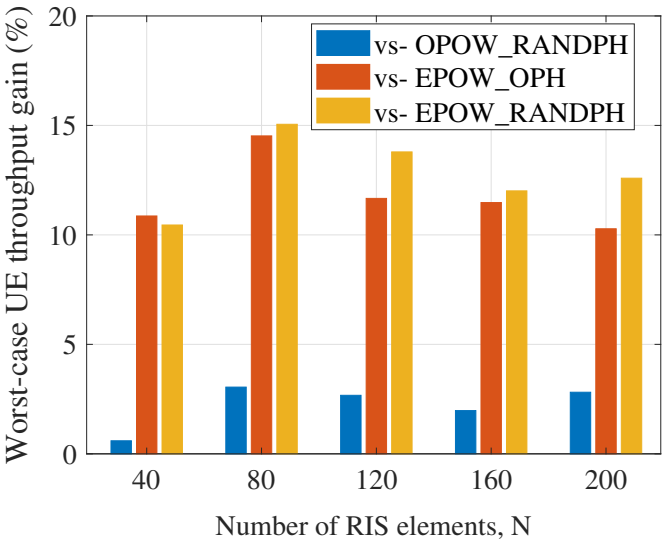

Figure 4.6: Worst-case UE throughput gain (%) obtained based on OPW-OPH versus the other methods for different numbers of RIS elements (N), at $K = 50$, $M = 12$, $P_0 = 40$ dBm.

As depicted in Figure 4.6, the gain in the worst-case UE throughput based

on OPW-OPH could be more than 10% when compared to EPOW-OPH and EPOW-RANDPH, but is smaller when compared to OPOW-RANDPH, for the considered range of N. This indicates the positive impact of optimal power allocation on the worst-case UE throughput.

4.7 Conclusion

We have proposed an optimisation approach of low complexity for extending network coverage in a massive MIMO communication network. By integrating RISs and UAVs, our method takes advantages of both the UAVs' flexibility and RIS's configurability. The numerical results demonstrated that the use of RISs and UAVs could offer better total network throughput and simultaneously provide users who suffer worst-case throughput with an improvement of more than 10%. The proposed scheme is suitable for urban areas or in events where blockages or obstructions prevent users from having a LoS connection.

Some challenging issues remain open and deserve future investigation such as the impact of RIS channel estimation and UAV jitter, i.e., the fast variation of UAV communication channels caused by either the unintended high-frequency change of UAV altitude or the high-frequency vibration from the UAV rotors [99], on the system performance.

Chapter 5

Real-time optimised clustering and caching for 6G satellite-UAV-terrestrial networks

In this chapter,[7] we consider an Internet-of-Things network supported by several satellites and multiple cache-assisted UAVs. Due to the long-distance transmission and detrimental effects from the transmission environment, the latency can be very high, especially in the presence of backhaul congestion. Therefore, we formulate an optimisation problem with the aim of minimising the total network latency. To reduce the complexity of the original problem, it is divided into three sub-problems, namely, the sub-problem of clustering the ground users associated with the UAVs, cache placement in the UAVs (to support the network in avoiding

[7]This chapter is published as [J1] and based on [C1] in the Author's publication list.

backhaul congestion), and power allocation for the satellites and UAVs. We propose a distributed optimisation method consisting of: a non-cooperative game, designed to obtain the solution to the clustering problem; a genetic algorithm, which is powerful in the scenario of many variables, employed to obtain the optimal solution to the high-complexity caching problem; and a quick estimation technique, used for power allocation. Additionally, a centralised optimisation method is presented as a benchmark. Simulation results show that although the distributed method leads to network latency of approximately 30% higher than the centralised method, it takes significantly less time to execute and is suitable for systems requiring strict real-time computing constraints. Furthermore, the numerical results prove the efficiency of our methods compared with other conventional ones.

5.1 Introduction

In this chapter, optimisation techniques are proposed to solve the latency-related problem in satellite-UAV-terrestrial networks (SUTNs). This mix-integer programming problem with many variables poses challenges in obtaining the solution in real-time scenarios. To tackle this issue, depending on the characteristics of variables in the aggregated problem, we divide the initial problem into three sub-problems of lower complexity, namely clustering, cache placements and power allocation (PA). Game theory (GT) is used for solving the clustering problem to guarantee fairness between the users. A genetic algorithm (GA), which is inspired by genetics mechanisms to tackle problems having extraordinarily complex functions, is used for obtaining the solution to the cache placement. In terms of power

allocation, we quickly estimate the transmit power of the satellites and UAVs, taking into consideration the channel gain and the number of requests, instead of operating computing-intensive optimisation algorithms.

The key contributions of this chapter are summarised as follows:

- A model of SUTNs where several satellites and multiple cache-assisted UAVs cooperate to serve numerous ground users (GUs) is designed. The UAVs are able to exchange their pre-stored data in order to quickly serve the GUs if the required files already exist at the clusters of UAVs. This takes advantage of the high-quality channels and short transmission distance between the UAVs, with the aim to reduce latency.

- An optimisation problem is formulated with the objective of minimising the total latency for all the GUs. In order to reduce its complexity, this problem is decomposed into three sub-problems: clustering, cache placement, and PA for the satellites and UAVs. Instead of solving the extremely high-complexity initial problem, three sub-problems of low complexity are treated as independent problems and solved efficiently.

- In particular, a distributed method is proposed. A non-cooperative game is designed to find the equilibrium as a solution to the clustering sub-problem, while cache placement with a huge number of variables is solved by an evolutionary algorithm, i.e., GA. The PA sub-problem is solved by using a quick estimation technique. The overall optimisation of minimising the total network latency is then readily solved in a distributed manner by combining these three algorithms.

- To evaluate the efficiency of the distributed method, we propose a centralised optimisation method as one of the benchmark schemes. The centralised method also adopts the non-cooperative game and evolution algorithm to solve the two respective sub-problems. The difference from the distributed method is that the PA sub-problem is solved centrally in the centralised method.

- The simulation results show that the proposed distributed method outperforms the other methods in minimising the network latency. It only yields higher network latency than the centralised optimisation by an acceptable amount, yet its processing time is much lower, making it capable of supporting SUTNs in large-scale scenarios with real-time requirements. Moreover, inter-UAV communication is also proven to contribute to reducing the network latency.

5.2 System model and transmission scheme

5.2.1 System model

In this work, we consider the downlink transmission of a SUTN consisting of several LEO satellites, a large number of UAVs, and a massive number of GUs, as presented in Fig. 5.1. Each of the S satellites is equipped with N-radiation elements to generate at most N_B spot beams to the UAVs ($N_B < N$), and the set of satellites is denoted by $\mathcal{S} = \{1, ..., S\}$. The set of U cache-enabled UAVs, which are integrated with a memory to store common files (i.e, popular contents), is represented by $\mathcal{U} = \{1, ..., U\}$. After user association, these UAVs

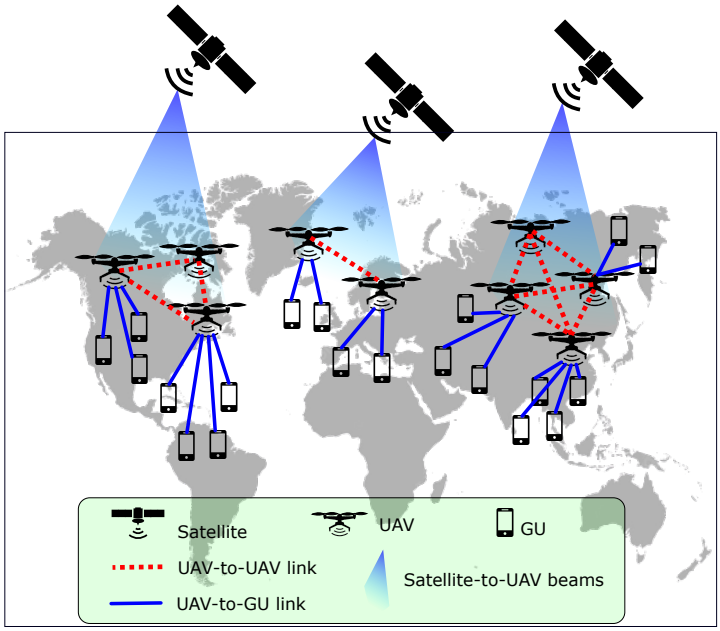

Figure 5.1: A typical SUTN.

form S clusters where they can exchange the pre-stored contents. Additionally, one GU is connected to one UAV only, while one UAV can serve multiple GUs. As shown in Fig. 5.1, each satellite serves a cluster of UAVs, and each UAV serves a cluster of GUs. Each single-antenna UAV is used as a flying relay station to serve its GUs in three cases as follows:

- If the required file is available in the cache of this UAV, the file will be directly transmitted to the target GU.
- If the required file is not available in the cache of this UAV but in the cache of another UAV within the same cluster instead, the file will be transmitted to the primary UAV and forwarded to the target GU.
- If no UAV in the same UAV cluster as this UAV has the required file in store, then one of the satellites will transmit the file to this UAV, which

then forwards it to the target GU.

A UAV u which connects directly to the GU k is defined as the primary UAV to this user. The other UAVs within the same UAV cluster as UAV u are referred to as the secondary UAVs to GU k. The decode-and-forward relaying technique is used at the UAVs in this chapter. The set of K GUs, each of which has one omni-directional antenna, is denoted by $\mathcal{K} = \{1, ..., K\}$.

A three-dimensional coordinate system with the base at the centre of the considered area on the ground is used for determining the locations of the satellites $\boldsymbol{q}_s = [x_s, y_s, z_s]$, UAVs $\boldsymbol{q}_u = [x_u, y_u, z_u]$, and GUs $\boldsymbol{q}_k = [x_k, y_k, 0]$.

5.2.2 Channel model

5.2.2.1 Satellite-to-UAV channel

The shadowed-Rician fading (SRF) model is appropriate to describe the channels between the LEO satellites and UAVs [81], [109]. Therefore, the channel vector from the s-th satellite to the u-th UAV is expressed as

$$\boldsymbol{h}_{s,u} = [h_i]_i^T, \ i = 1 : N, \tag{5.1}$$

where $h_i = \sqrt{g_i d_{s,u}^{-\alpha^{(1)}}}$ is the channel gain from the antenna i of the s-th satellite to the antenna of the u-th UAV, $d_{s,u}$ is the distance between the satellite and the UAV, $\alpha^{(1)}$ is the path loss exponent from the satellite to the UAV, $g_i^{(su)} \sim \text{SR}(\omega_i, \delta_i, \varepsilon_i)$ is the SRF component with the average power of direct signal ω_i, the half average power of the scatter portion δ_i, and the Nakagami-m fading component ε_i for the NLoS part of the signals.

5.2.2.2 UAV-to-UAV channel

Because of the rare appearance of obstacles, the line-of-sight (LoS) components outweigh the non-line-of-sight (NLoS) ones in UAV communications. Therefore, the free-space path loss model is used for modelling the UAV-to-UAV channels [109]. The channel gain from a secondary UAV u' to a primary UAV u is defined as

$$h_{u',u} = g_{u',u}\sqrt{h_0 d_{u',u}^{-\alpha^{(2)}}}, \tag{5.2}$$

where h_0 denotes the power gain at the reference distance d_0, $d_{u',u}$ is the distance between the two UAVs, while $\alpha^{(2)}$ is the free-space path loss exponent, and $g_{u',u}$ represents the small-scale fading component with zero-mean and unit variance.

5.2.2.3 UAV-to-ground user channel

According to the air-to-ground channel models in [84], [110], the channel gain $h_{u,k}$ between UAV u and GU k is defined as

$$h_{u,k} = g_{u,k}\left(\frac{4\pi f_c d_{u,k}}{c}\right)^{-\frac{\alpha^{(3)}}{2}} 10^{-\frac{\eta^{\mathrm{LoS}}P_{u,k}^{\mathrm{LoS}} + \eta^{\mathrm{NLoS}}P_{u,k}^{\mathrm{NLoS}}}{20}}, \tag{5.3}$$

where f_c is the carrier frequency, $d_{u,k}$ is the distance between the UAV and the GU, c is the speed of light, $\alpha^{(3)}$ is the path loss exponent from the UAV to the GU, $g_{u,k}^{(uk)}$ is the small-scale fading component of the channel of the link between the UAV and the GU, η^{LoS} and η^{NLoS} are respectively the weighted constant parameter of LoS and NLoS components. $P_{u,k}^{\mathrm{NLoS}} = 1 - P_{u,k}^{\mathrm{LoS}}$ is the probability of NLoS, in which $P_{u,k}^{\mathrm{LoS}}$ is the probability of LoS component.

5.2.3 Caching scheme

We assume that all the GUs request at most in total F files with the same size of Q bits, and the set of files is denoted by $\mathcal{F} = \{1, ..., F\}$ [19]. The satellites can access all the files from the cloud and forward them to the UAVs. It is clear that each UAV cannot pre-store all the contents, and only carries at most M files ($M \ll F$).

Let $\boldsymbol{\beta}_u = \{\beta_f^{(u)}, \forall f \in \mathcal{F}\}$ be the vector of cache placement, where the binary indicator of cache placement for file f is defined as $\beta_f^{(u)} \in \{0, 1\}$. Due to the limitation of the UAVs' storage, we have the constraint of cache storage at UAV u as $\sum_{f \in \mathcal{F}} \beta_f^{(u)} \leq M$ [19].

In this chapter, the popularity of the contents changes quickly over time, resulting in the need to frequently update the cached files at the UAVs. For instance, the data about sports events, news, and promotion requires to be updated quickly. Additionally, we assume that the popularity features of all the files are the same, in other words, the probability of any file f in the set of files $\mathcal{F}$ being requested by GU k is equal to those of the others.

5.2.4 Transmission scheme

Multiple-antenna technology can support SUTNs in easing the effect of long-distance transmission. In this chapter, we assume that massive multiple-input multiple-output (mMIMO) technology is used at the satellites.

Let $\boldsymbol{v}_{s,u} \in \mathbb{C}^{N \times 1}$ be the precoding vector at satellite s serving UAV u. The signal received at UAV u from satellite s is affected by a few types of interference: interference from the links of satellite s serving its cluster of UAVs $\mathcal{U}_s$ (cross-talk),

interference from other satellites, and interference from UAV-to-UAV communication. In this chapter, we assume that the frequency used for UAV-to-UAV communications is distinct, and thus, there is no interference from the communication between the UAVs to the satellite-UAV links. As such, the data rate from satellite s to UAV u can be calculated as:

$$R_{s,u} = B \log_2 \left(1 + \frac{|\boldsymbol{h}_{s,u}^T \boldsymbol{v}_{s,u}|^2 p_{s,u}}{I_{s,u}^{\text{cross-talk}} + I_{s,u}^{\text{others}} + \sigma_u^2} \right), \tag{5.4}$$

where $p_{s,u}$ is the transmit power of satellite s for serving UAV u, $I_{s,u}^{\text{cross-talk}} = \sum_{u' \in \mathcal{U}_s \setminus u} |\boldsymbol{h}_{s,u}^T \boldsymbol{v}_{s,u'}|^2 p_{s,u'}$ is the cross-talk interference from satellite s serving the other UAVs within the same cluster, and $\mathcal{U}_s$ is the set of the UAVs served by satellite s. In addition, $I_{s,u}^{\text{others}} = \sum_{s' \in \mathcal{S} \setminus s} \sum_{u' \in \mathcal{U}_{s'}} |\boldsymbol{h}_{s',u}^T \boldsymbol{v}_{s',u'}|^2 p_{s',u'}$ is the interference from the other satellites that is imposed on UAV u, and σ_u^2 represents the noise power received at UAV u.

To guarantee the unit length of the beamformer, we use maximal ratio transmission beamformer $\boldsymbol{v}_{s,u} = \boldsymbol{h}_{s,u}^* / ||\boldsymbol{h}_{s,u}||$, which is the division of the complex conjugate of the channel gain vector from satellite s to UAV u and the L2 norm of this vector [110]. With the massive number of antennas at the satellites, the beams toward the target UAV are narrow, with the major energy focusing on these UAVs. In other words, the energy of the beams toward the non-target UAVs is much lower, thus we can neglect inter-satellite interference (i.e. $I_{s,u}^{\text{others}} = 0$) in (5.4).

The data rate from a secondary UAV u' to a primary UAV u is expressed as

$$R_{u',u} = B \log_2 \left(1 + \frac{|h_{u',u}|^2 p_{u',u}}{\sum_{u'' \in \mathcal{U} \setminus u'} |h_{u'',u}|^2 p_{u'',u} + \sigma_u^2} \right). \tag{5.5}$$

Because of the distinct frequency used in UAV-to-UAV communication, the signal received at the primary UAV from the secondary UAV is only affected by the interference from communication between other UAVs. Therefore, we only take this interference into account in (5.5).

Considering the signal from UAV u to GU k, it is subjected to interference from satellite communication, UAV-to-UAV communication (inter-UAV communication), and communication from UAV u to other GUs within the same user cluster (intra-UAV interference). The first two types of interference can be ignored for the following reasons. First of all, to be able to receive directly signals from a satellite, users would need to be equipped with high-gain receivers, which leads to extremely high energy consumption. However, in this chapter, we aim to design networks to serve IoT devices that have a very low receiver gain and energy capacity. Thus, the interference from the satellites to the GUs can be ignored. Secondly, the inter-UAV interference is neglected in (5.6) since the UAV-to-UAV communication, having distinct frequency, does not impact UAV-GU links. Furthermore, the distances from the UAVs, except for UAV u, to GU k are usually long. As such, along with lower transmit power, the power of inter-UAV interference can drop, even lower than the figure for noise.

The data rate from UAV u to GU k is thus expressed as

$$R_{u,k} = B \log_2 \left(1 + \frac{|h_{u,k}|^2 p_{u,k}}{\sum_{k' \in \mathcal{K}_u \setminus k} |h_{u,k}|^2 p_{u,k'} + \sigma_k^2} \right), \tag{5.6}$$

where $\mathcal{K}_u$ is the set of GUs served by UAV u, and σ_k^2 represents the power of noise received at GU k. For dealing with intra-UAV interference, we apply NOMA technology at the links between the UAVs and GUs.

5.3 Problem formulation

In this section, we formulate an optimisation problem for latency minimisation. In future networks, 6G for example, latency plays an ever-important role since many real-time and interactive applications require strict deadlines. Despite long-distance transmission, the high latency of satellite communication can be eased with the aid of UAVs. This leads to SUTNs' potential to be employed widely, especially when serving users who request real-time transmission.

With the aim of latency minimisation, the association between UAVs and GUs is essential. If a user's requested file is available at its primary UAV, this UAV can directly transmit the file to the GU, leading to much lower latency compared to the other cases. Let $\boldsymbol{A} = \{a_{u,k}, \forall u \in \mathcal{U}, \forall k \in \mathcal{K}\}$ be the matrix of association between the UAVs and GUs, with each element being defined as

$$a_{u,k} = \begin{cases} 1, & \text{if the } u\text{-th UAV is the primary UAV of GU } k, \\ 0, & \text{otherwise.} \end{cases}$$

We assume that files arriving from the satellite/secondary UAVs to the primary UAV are directly sent to the GUs without incurring in any queuing delays. In terms of cache placement, depending on whether the requested file f is pre-stored at the UAVs, three cases of the latency for GU k associated with UAV u for the journey from requesting to completely receiving file f are as follows:

- Case 1: File f is available at the primary UAV u of GU k. The latency for GU k is the sum of requesting time, responding time from the UAV, and

transmission time, and can be formulated as

$$t_{k,f,u}^{(pri)} = \frac{2d_{u,k}}{c} + \frac{Q}{R_{u,k}}. \tag{5.7}$$

- Case 2: File f is available at a secondary UAV u' of GU k that is in the same UAV cluster $\mathcal{U}_s$ as UAV u. The latency for GU k is the sum of requesting time and responding time from GU k to the primary UAV u and from the primary UAV u to the secondary UAV u', and transmission times. This latency can be expressed as

$$t_{k,f,u'}^{(sec)} = \frac{2(d_{u',u} + d_{u,k})}{c} + \frac{N_{u',u}Q}{R_{u',u}} + \frac{Q}{R_{u,k}}, \tag{5.8}$$

  where $N_{u',u}$ is the number of files requested concurrently by UAV u to the secondary UAV u'. When $N_{u',u} > 1$, i.e., more than one GUs served by UAV u requires files that are not in UAV u's cache, the data rate must be divided by $N_{u',u}$ to indicate the transfer of only one file required by GU k.

- Case 3: File f is not saved at any UAV in the UAV cluster $\mathcal{U}_s$. The latency for GU k is the sum of requesting time and responding time from GU k to primary UAV u, from primary UAV u to satellite s, and transmission times. In this case, the latency can be formulated as

$$t_{k,f,s}^{(sat)} = \frac{2(d_{s,u} + d_{u,k})}{c} + \frac{N_{s,u}Q}{R_{s,u}} + \frac{Q}{R_{u,k}}, \tag{5.9}$$

  where $N_{s,u}$ represents the number of files simultaneously requested by UAV u to satellite s.

In all three cases, we assume that the size of the management frames or packets to request information is very small and negligible in comparison with the Q bits size of a file, and all the files are transmitted without any bit error. The latency for completely receiving file f requested by GU k which is served by the UAVs connecting to satellite s is defined as

$$\begin{aligned} t_k(\boldsymbol{A},\boldsymbol{\beta},\boldsymbol{P}) = \sum\nolimits_{u\in\mathcal{U}_s} a_{u,k}\Bigg(&\beta_f^{(u)} t_{k,f,u}^{(pri)} \\ &+ \left(1-\beta_f^{(u)}\right) \min_{u'\in\mathcal{U}_s \& \beta_f^{(u')}=1} \left\{\beta_f^{(u')} t_{k,f,u'}^{(sec)}\right\} \\ &+ \left(1-\beta_f^{(u)}\right)\left(1-\max_{u'\in\mathcal{U}_s}\beta_f^{(u')}\right) t_{k,f,s}^{(sat)}\Bigg), \end{aligned} \tag{5.10}$$

where $\boldsymbol{\beta} = \{\boldsymbol{\beta}_u, \forall u \in \mathcal{U}\}$ is the set of all vectors of cache placement, and $\boldsymbol{P} = \{\boldsymbol{P}^{(SAT)}, \boldsymbol{P}^{(UAV)}\}$ is the set of all powers allocated to the satellites and UAVs.

The optimisation problem of minimising the latency for all the GUs is expressed as

$$\min_{\boldsymbol{A},\boldsymbol{\beta},\boldsymbol{P}} \quad \sum\nolimits_{k=1}^{K} t_k(\boldsymbol{A},\boldsymbol{\beta},\boldsymbol{P}) \tag{5.11a}$$

$$\text{s.t} \quad \sum\nolimits_{u\in\mathcal{U}_s} P_{s,u} \le P_s^{(\max)}, \forall s \in \mathcal{S}, \tag{5.11b}$$

$$P_{s,u} \ge 0, \forall s, u, \tag{5.11c}$$

$$\sum\nolimits_{k\in\mathcal{K}_u} P_{u,k} + \sum\nolimits_{u'\in\mathcal{U}_s\setminus u} P_{u,u'} \le P_u^{(\max)}, \forall u \in \mathcal{U}, \tag{5.11d}$$

$$P_{u,k} \ge 0, P_{u,u'} \ge 0, \forall u, k, u', \tag{5.11e}$$

$$\beta_f^{(u)} \in \{0,1\}, \forall u, f, \tag{5.11f}$$

$$\sum\nolimits_{f\in\mathcal{F}} \beta_f^{(u)} \le M, \forall u \in \mathcal{U}, \tag{5.11g}$$

$$a_{u,k} \in \{0,1\}, \forall u, k, \tag{5.11h}$$

$$\sum\nolimits_{u\in\mathcal{U}} a_{u,k} = 1, \forall k \in \mathcal{K}, \tag{5.11i}$$

$$\sum\nolimits_{k\in\mathcal{K}} a_{u,k} \leq N_U, \forall u \in \mathcal{U}, \tag{5.11j}$$

where $P_s^{(\max)}$ and $P_u^{(\max)}$ denote the maximum transmit power of each satellite and each UAV, respectively. N_U is the maximum number of GUs that one UAV can serve. Constraints (5.11b) and (5.11c) show the limitation in the transmit power of each satellite. Similarly, (5.11d) and (5.11e) indicate that each UAV can serve its GUs and the other UAVs in its clusters with the power in the range from 0 to $P_u^{(\max)}$. (5.11f) describes the possible values of cache placement variables while the limitation in cache storage is given in (5.11g). Moreover, (5.11h) describes the possible values of GU clustering variables, and (5.11i) indicates that each GU connects to one UAV only. Finally, (5.11j) sets a limit on the number of GUs served by one UAV in order to avoid overloading. Overall, the problem (5.11) is a mixed-integer programming with the objective function being the combination of fractions of monomial functions and logarithms, maximisation and minimisation functions. Therefore, solving directly this problem is highly complex, especially in large-scale systems.

5.4 Distributed optimisation method

In this section, we propose the combination of three algorithms to cooperatively solve the problem (5.11). To reduce the complexity of the initial problem, we decompose it into three sub-problems according to three variable blocks, namely, clustering, cache placement, and PA. First, a non-cooperative game is designed to represent the clustering problem, and an iterative algorithm is proposed to

find the equilibrium of the game. Then, the GA which is a global search algorithm is used to choose the optimal cache placement. Finally, depending on the characteristic of IoT networks, the quick PA method is used to quickly estimate the transmit power for satellites and UAVs.

5.4.1 Ground users clustering based on game theory

The proposed SUTN is a large-scale model with many GUs playing the same important role. Therefore, to cluster the GUs in real time, using a non-cooperative game in this case is justified and essential. Firstly, given the others' actions, each player in the non-cooperative game chooses their best action, resulting in an improvement of their reward (objective) independently. Secondly, the non-cooperative game is a distributed tool where the best responses of players can be solved simultaneously in multiple processors. Additionally, the players' choice of actions in the non-cooperative game can perfectly model the users' choice of clusters in the clustering problem. In terms of flexibility, GT can be used in a range of problems, e.g. multi-player problems, with the utility functions modified easily depending on the objectives to be optimised.

To begin with, we assume that the values of the cache placement variables in matrix $\boldsymbol{\beta}$, and the valued of the allocated power in matrix $\boldsymbol{P}$ are fixed. The optimisation problem in (5.11) can be rewritten as

$$\min_{\boldsymbol{A}} \quad \sum\nolimits_{k=1}^{K} t_k(\boldsymbol{A}) \tag{5.12}$$

$$\text{s.t.} \quad (5.11h), (5.11i), (5.11j). \tag{5.13}$$

To solve optimisation problem (5.12), we design a non-cooperative game as

$$G_{\text{clustering}} = \left\langle \mathcal{K}, \boldsymbol{A}, ut_k(\boldsymbol{a}_k, \boldsymbol{A}_{-k}) \right\rangle, \tag{5.14}$$

where $\mathcal{K}$ is the set of players (i.e., the set of GUs), and $\boldsymbol{A}$ denotes the action of players and is expressed as the matrix of association between the UAVs and GUs. The utility function for each GU k is represented by $ut_k(\boldsymbol{a}_k, \boldsymbol{A}_{-k})$, in which $\boldsymbol{a}_k$ is the k-th column of $\boldsymbol{A}$ and denotes the action of GU k, and $\boldsymbol{A}_{-k}$ is the matrix $\boldsymbol{A}$ without the k-th column and represents the actions of the other GUs except GU k. To transform the optimisation problem (5.12) into a non-cooperative game, $G_{\text{clustering}}$ has to consider all the constraints of (5.12), and thus the utility function is defined as

$$ut_k(\boldsymbol{a}_k, \boldsymbol{A}_{-k}) = \begin{cases} \infty, \text{ if the constraints of (5.12) are broken,} \\ t_k(\boldsymbol{a}_k, \boldsymbol{A}_{-k}), \text{ otherwise.} \end{cases}$$

With any given matrix $\boldsymbol{A}_{-k}$, the set of GU k's best responses, denoted by $\boldsymbol{BR}(\boldsymbol{A}_{-k})$, consists of vectors $\boldsymbol{a}_k^*$ such that

$$ut_k(\boldsymbol{a}_k^*, \boldsymbol{A}_{-k}) \leq ut_k(\boldsymbol{a}_k, \boldsymbol{A}_{-k}), \forall \boldsymbol{a}_k. \tag{5.15}$$

The best response of GU k is the vector $\boldsymbol{a}_k^*$ which gets the lowest latency according to (5.15). The solving method is described in Algorithm 5. The solution of this non-cooperative game is where all the rational players (GUs) reach the stable convergence which is usually referred to as the Nash equilibrium. In this equilibrium, no GU has an incentive to choose another cluster since the current

one is where they can obtain the lowest value of utility function with the given clusters of the other GUs.

Algorithm 5 GT-based clustering for solving problem (5.12)

1: **Input:** $\boldsymbol{\beta}, \boldsymbol{P}$, and create a feasible matrix $\boldsymbol{A}^{(0)}$, $i = 0$
2: **Repeat** Set $i = i + 1$
3: **for** $k \in \mathcal{K}$
4: Find the best response $\boldsymbol{a}_k^*$ with fixed values $\boldsymbol{a}_{-k}$
5: Update $\boldsymbol{A}^{(i)}$ by replacing column k with $\boldsymbol{a}_k^*$
6: **Stop** $\boldsymbol{A}^{(i)} = \boldsymbol{A}^{(i-1)}$
7: **Output:** $\boldsymbol{A}^{(optimal)}$

5.4.2 Cache placement using genetic algorithm

By fixing the solutions for the stages of clustering and PA, the optimisation problem (5.11) becomes

$$\min_{\boldsymbol{\beta}} \quad T(\boldsymbol{\beta}) = \sum\nolimits_{k=1}^{K} t_k(\boldsymbol{\beta}) \tag{5.16}$$

$$\text{s.t.} \quad (5.11f), (5.11g). \tag{5.17}$$

Problem (5.16) is a combinatorial optimisation problem. If traditional methods are used, the number of feasible solutions can be equal to $U \sum_{m=0}^{M} \left({}^{F}C_m\right)$, where ${}^{F}C_m = F!/(m!(F-m)!)$ is the number of m-combinations of a set consisting of F elements. When the number of possible files is huge in a large-scale integrated satellite and terrestrial network with the presence of many UAVs, searching for the optimal solution of cache placement is extremely complex, or

even impossible in real time.

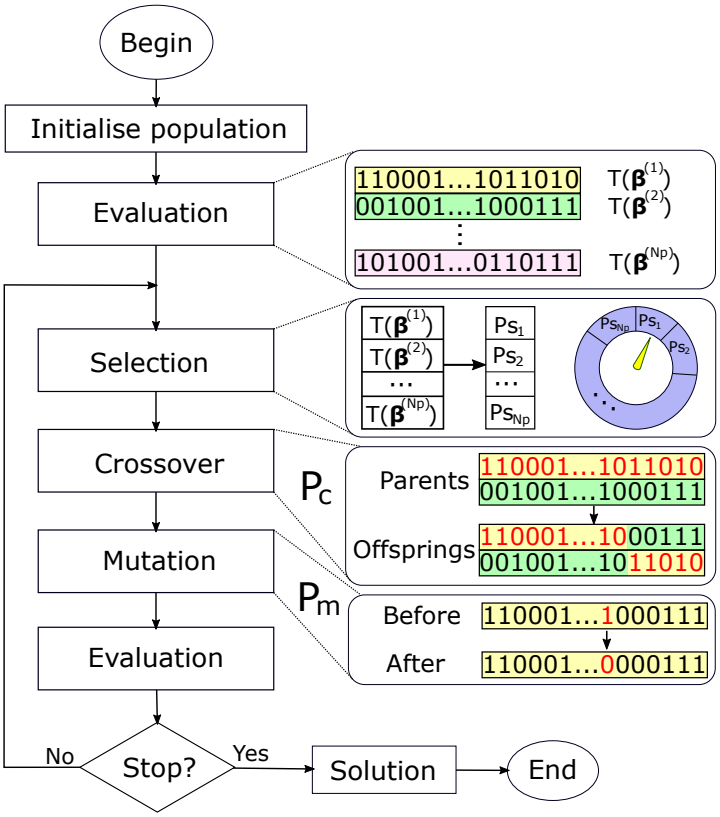

Figure 5.2: The proposed genetic algorithm.

Genetic algorithms, which are a class of evolutionary algorithms in artificial intelligence, are widely used and proven efficient in solving difficult problems, especially combinatorial problems with numerous variables. Additionally, a GA can be applied to solve problems without the demand for calculating the derivative of functions. This is an outstanding benefit since in many optimisation problems, the objective functions and constraints are extraordinarily complex, or even indeterminable. In the optimisation problem (5.16), the objective function includes linear functions, both minimisation and maximisation problems. In addition, the GA is a global search algorithm with evaluation and evolution that can be op-

erated concurrently, resulting in faster convergence. Due to the aforementioned positives, we propose the use of a GA for solving the cache placement problem (5.16).

Since there is no inter-UAV interference, optimising the cache placement for each cluster of UAVs served by each satellite can be done by parallel threads. The proposed algorithm is given as the diagram shown in Fig. 5.2. First of all, we initialise a feasible population, the first generation, of N_P chromosomes with each chromosome being equivalent to a matrix $\boldsymbol{\beta}$ of cache placement at all the UAVs. Then, in each iteration of the GA, there are four operations to get a better population which always consists of at least one chromosome being better than the best one of the previous population.

- Evaluation: The algorithm evaluates the values of $T(\boldsymbol{\beta}^{(n)}), n = 1 : N$ for all chromosomes. The matrix consisting of all these values is called fitness matrix and denoted by $\boldsymbol{T}$.

- Selection: In this step, we select the chromosomes to be parents in the next step. First, the chromosomes that do not meet constraints (5.11f) and (5.11g) are eliminated from the population. After that, we build a roulette wheel where all the remaining chromosomes are placed, each chromosome will occupy a sector that corresponds to its probability of being selected. The probability that a parent (chromosome) n is selected depends on its fitness value, and is calculated as

$$Ps_n = \frac{\max(\boldsymbol{T}) - T(\boldsymbol{\beta}^{(n)})}{\sum_{n=1}^{N_p} \left(\max(\boldsymbol{T}) - T(\boldsymbol{\beta}^{(n)})\right)}. \tag{5.18}$$

  The chromosomes having higher fitness value will be selected more times

into the next step.

- Crossover: With the probability P_c that crossover happens at each parent, one cut point in the chromosome of a UAV is chosen randomly and those of the others have the same location. From these points, the remaining part of the chromosomes of two parents in each UAV will be exchanged with each other, and new chromosomes are their offspring.

- Mutation: The probability that one chromosome has a mutation is P_m. The number of flipping bits if the mutation happens is equal to $U \times M \times P_m$. The locations of these bits are randomly chosen, and the value of a bit is flipped if it is chosen.

In the GA, the best chromosome in a generation is always retained in the next generation by copying precisely this chromosome of a parent to a child. In this way, the algorithm guarantees that the next generation always has at least one better chromosome than all those in the previous population, resulting in the monotonicity of the best value throughout the whole evolutionary process. The GA is presented in Algorithm 6.

With a high number of chromosomes, the GA will have a higher chance to find the optimal solution, but the complexity of evaluating will be higher as a result. There is a trade-off between the two parameters P_c (crossover) and P_m (mutation). If P_c is low and P_m is high, the GA can get the current local optimal solution more quickly. In contrast, if P_c is high and P_m is low, the GA can have more chance to get another better optimal solution, but in the worst case, it may get stuck in the local optima. Therefore, selecting these parameters appropriately is important and depends on the problem.

Algorithm 6 The proposed genetic algorithm

1: **Input:** $\boldsymbol{A}, \boldsymbol{P}$, and create a feasible population $\boldsymbol{Po}^{(0)} = \{\boldsymbol{\beta}^{(n)}, n = \overline{1, N_p}\}$, $i = 0$

2: Evaluate population $\boldsymbol{Po}^{(0)}$

3: **Repeat** Set $i = i + 1$

4: Select parents from population $\boldsymbol{Po}^{(i-1)}$

5: Crossover parents with the probability of P_c to create population $\boldsymbol{Po}^{(i)}$

6: Mutate offsprings with the probability of P_m

7: Evaluate population $\boldsymbol{Po}^{(i)}$

8: **Stop** $|\max(\boldsymbol{T}(\boldsymbol{Po}^{(i)})) - \max(\boldsymbol{T}(\boldsymbol{Po}^{(i-1)}))| < \varepsilon_{GA}$

9: **Output:** $\boldsymbol{\beta}^{(optimal)}$

5.4.3 Quick power allocation for satellites and UAVs

In terms of IoT devices that transmit and receive signals at very low power, it is not desirable to operate optimisation methods of high accuracy but with high computing requirement. Indeed, saving a small amount of transmission energy while requiring high computing capacity would be inefficient. In this sub-section, we use an acceptable approach to quickly estimate the transmit power of the satellites and UAVs.

The power of satellite s allocated to serve UAV $u \in \mathcal{U}_s$ is defined as

$$p_{s,u} = \frac{P_s^{(\max)}}{\sum_{u' \in \mathcal{U}_s} N_{s,u'} / |\boldsymbol{h}_{s,u'}^T \boldsymbol{v}_{s,u'}|^2} \frac{N_{s,u}}{|\boldsymbol{h}_{s,u}^T \boldsymbol{v}_{s,u}|^2}. \tag{5.19}$$

In (5.19), the dot product of the transpose of the channel and precoding vector describes the quality of the channel. Therefore, these values are used for power

division with the total power of $P_s^{(\max)}$. If a channel is good, the power distributed to this channel will be lower in order to increase the data rate of the others. Additionally, more power is allocated to the UAV requesting a higher number of files. Thus, for fairness in PA, we add the number of files concurrently requested from UAV u to satellite s, $N_{s,u}$, as the weighted parameter, together with the quality of the channel.

Similarly, the power for the UAVs is allocated with two distinct parts, $\theta P_u^{(\max)}$ for inter-UAV communications and $(1-\theta)P_u^{(\max)}$ for UAV-GU communications where $\theta = \overline{0,1}$. More specifically, the power values of UAV u which are allocated to communicate with UAV u' and GU k are respectively expressed as follows

$$p_{u,u'} = \frac{\theta P_u^{(\max)}}{\sum_{u' \in \mathcal{U}_s} N_{u,u'}/|h_{u,u'}|^2} \frac{N_{u,u'}}{|h_{u,u'}|^2}, \tag{5.20}$$

$$p_{u,k} = \frac{(1-\theta) P_u^{(\max)}}{\sum_{k' \in \mathcal{K}_u} N_{u,k'}/|h_{u,k'}|^2} \frac{N_{u,k}}{|h_{u,k}|^2}, \tag{5.21}$$

where $\mathcal{K}_u$ is the set of GUs served by UAV u, and $N_{u,k}$ is the number of files concurently requested by GU k to UAV u.

The PA algorithm for satellites and UAVs is shown in Algorithm 7. When the values of $\boldsymbol{A}$ and $\boldsymbol{\beta}$ change, i.e., some GU is served by a new UAV and the caching placement is changed, we have to reallocate power for these changed connections to avoid dividing by zero in (5.10). Consequently, Algorithm 7 is used in line 4 of Algorithm 5, line 2 and line 7 of Algorithm 6, where there are changes in the values of user association $\boldsymbol{A}$ and cache placement $\boldsymbol{\beta}$. In the remainder of this chapter, GT and GA in the distributed method are denoted by GTD and GAD, respectively.

Algorithm 7 Quick power allocation

1: **Input:** $\boldsymbol{A}, \boldsymbol{\beta}$, and create feasible matrices of power allocated for satellites $\boldsymbol{P}^{(SAT)}$ and UAVs $\boldsymbol{P}^{(UAV)}$

2: Use (5.19) to update all elements in $\boldsymbol{P}^{(SAT)}$

3: Use (5.20) and (5.21) to update all elements in $\boldsymbol{P}^{(UAV)}$

4: **Output:** $\boldsymbol{P}^{(SAT)}$ and $\boldsymbol{P}^{(UAV)}$

5.5 Centralised optimisation method

In this section, a partially centralised optimisation method as a benchmark for solving problem (5.11) is proposed. Similarly as in the distributed method, the initial optimisation problem (5.11) is also divided into three sub-problems: clustering, cache placement, and PA. The non-cooperative game (GT) is used for assigning handover between the UAVs and GUs, and the GA is used for determining caching files at the UAVs. However, for the remaining PA sub-problem, the centralised approach converts it into a convex optimisation problem of low complexity to be solved centrally, as opposed to the quick estimation technique in the distributed method.

According to [111], for all $x > 0, y > 0$, and $\bar{x}, \bar{y}$ respectively in the feasible sets of x and y, using first-order condition, it is clear that:

$$\log_2(1 + x/y) \geq \bar{a} - \bar{b}/x - \bar{c}y, \tag{5.22}$$

where $\bar{a} = \log_2(1 + \bar{x}/\bar{y}) + 2\bar{x}/\left(\ln(2)(\bar{x} + \bar{y})\right) > 0$,
$\bar{b} = \bar{x}^2/\left(\ln(2)(\bar{x} + \bar{y})\right) > 0$, $\bar{c} = \bar{x}/\left(\ln(2)(\bar{x} + \bar{y})\bar{y}\right) > 0$.

Let $x_{s,u} = |\boldsymbol{h}_{s,u}^T \boldsymbol{v}_{s,u}|^2 p_{s,u}$, $y_{s,u} = I_{s,u}^{\text{cross-talk}} + \sigma_u^2$,
$\bar{x}_{s,u} = |\boldsymbol{h}_{s,u}^T \boldsymbol{v}_{s,u}|^2 p_{s,u}^{(\kappa)}$, $\bar{y}_{s,u} = I_{s,u}^{\text{cross-talk}}(\boldsymbol{P}^{(\kappa)}) + \sigma_u^2$,
$x_{u',u} = |h_{u',u}|^2 p_{u',u}$, $y_{u',u} = \sum_{u'' \in \mathcal{U} \setminus u'} |h_{u'',u}|^2 p_{u'',u} + \sigma_u^2$,
$\bar{x}_{u',u} = |h_{u',u}|^2 p_{u',u}^{(\kappa)}$, $\bar{y}_{u',u} = \sum_{u'' \in \mathcal{U} \setminus u'} |h_{u'',u}|^2 p_{u'',u}^{(\kappa)} + \sigma_u^2$,
$x_{u,k} = |h_{u,k}|^2 p_{u,k}$, $y_{u,k} = \sum_{k' \in \mathcal{K}_u \setminus k} |h_{u,k}|^2 p_{u,k'} + \sigma_k^2$,
$\bar{x}_{u,k} = |h_{u,k}|^2 p_{u,k}^{(\kappa)}$, $\bar{y}_{u,k} = \sum_{k' \in \mathcal{K}_u \setminus k} |h_{u,k}|^2 p_{u,k'}^{(\kappa)} + \sigma_k^2$.

By substituting these values for $x, y, \bar{x}, \bar{y}$ in (5.22), we obtain three inequalities as follows

$$R_{s,u} \geq \tilde{R}_{s,u}^{(\kappa)} \triangleq B(\bar{a}_{s,u} - \bar{b}_{s,u}/x_{s,u} - \bar{c}_{s,u} y_{s,u}), \tag{5.23}$$

$$R_{u',u} \geq \tilde{R}_{u',u}^{(\kappa)} \triangleq B(\bar{a}_{u',u} - \bar{b}_{u',u}/x_{u',u} - \bar{c}_{u',u} y_{u',u}), \tag{5.24}$$

$$R_{u,k} \geq \tilde{R}_{u,k}^{(\kappa)} \triangleq B(\bar{a}_{u,k} - \bar{b}_{u,k}/x_{u,k} - \bar{c}_{u,k} y_{u,k}). \tag{5.25}$$

Then, by substituting $\tilde{R}_{s,u}^{(\kappa)}, \tilde{R}_{u',u}^{(\kappa)}$, and $\tilde{R}_{u,k}^{(\kappa)}$ for $R_{s,u}, R_{u',u}$, and $R_{u,k}$ in (5.10) respectively, the upper-bound function $\tilde{t}_k(\boldsymbol{P}, \boldsymbol{P}^{(\kappa)})$ of the latency for GU k is expressed as

$$\begin{aligned}\tilde{t}_k(\boldsymbol{P}, \boldsymbol{P}^{(\kappa)}) = \sum_{u \in \mathcal{U}_s} a_{u,k} \Bigg(& \beta_f^{(u)} \tilde{t}_{k,f,u}^{(pri)} + \left(1 - \beta_f^{(u)}\right) \beta_f^{(u')} \tilde{t}_{k,f,u'}^{(sec)} \\ & + \left(1 - \beta_f^{(u)}\right) \left(1 - \max_{u' \in \mathcal{U}_s} \beta_f^{(u')}\right) \tilde{t}_{k,f,s}^{(sat)} \Bigg),\end{aligned} \tag{5.26}$$

where $\tilde{t}_{k,f,u}^{(pri)} = 2d_{u,k}/c + Q/\tilde{R}_{u,k}^{(\kappa)}$,
$\tilde{t}_{k,f,u'}^{(sec)} = 2(d_{u,u'} + d_{u,k})/c + N_{u',u} Q/\tilde{R}_{u',u}^{(\kappa)} + Q/\tilde{R}_{u,k}^{(\kappa)}$,
$\tilde{t}_{k,f,s}^{(sat)} = 2(d_{s,u} + d_{u,k})/c + N_{s,u} Q/\tilde{R}_{s,u}^{(\kappa)} + Q/\tilde{R}_{u,k}^{(\kappa)}$,

To reduce the complexity of the optimisation problem, we set

$u' = \text{argmax}_{u' \in \mathcal{U}_s \& \beta_f^{(u')} = 1} h_{u',u}$.

Additionally, this inequality holds true $t_k(\boldsymbol{P}) \leq \tilde{t}_k(\boldsymbol{P}, \boldsymbol{P}^{(\kappa)})$. With the upper bound of the objective function (5.11a), at the loop κ, the optimisation problem (5.11) for PA can be rewritten as

$$\min_{\boldsymbol{P}} \quad T_{total}(\boldsymbol{P}, \boldsymbol{P}^{(\kappa)}) = \sum\nolimits_{k=1}^{K} \tilde{t}_k(\boldsymbol{P}, \boldsymbol{P}^{(\kappa)}) \tag{5.27a}$$

$$\text{s.t.}(5.11b), (5.11c), (5.11d), (5.11e) \tag{5.27b}$$

It can be seen that optimisation problem (5.27) is a convex problem, so it can be solved efficiently by CVXPY [88].

The centralised optimisation method for solving problem (5.11) is described in Algorithm 8. At the iteration κ, the solution of (5.27) is denoted by $\boldsymbol{P}^{(\kappa)}$. Therefore, at the iteration $\kappa + 1$, we have $T_{total}(\boldsymbol{P}^{(\kappa+1)}, \boldsymbol{P}^{(\kappa)}) \leq T_{total}(\boldsymbol{P}^{(\kappa)}, \boldsymbol{P}^{(\kappa)})$, where $\boldsymbol{P}^{(\kappa+1)}$ is the solution of (5.27) with the objective function $T_{total}(\boldsymbol{P}, \boldsymbol{P}^{(\kappa)})$. In other words, the convergence of centralised PA is guaranteed thanks to the decreasing monotonic value of the objective function.

In Algorithm 5 and Algorithm 6, to find the best response or to evaluate different populations, we have to re-allocate power to satellites and UAVs which have changes in serving GUs. In this centralised optimisation method, the GT and GA in Algorithm 8 uses optimisation problem (5.27) for computing the value of the utility function of each GU and cache placement of each UAV. To distinguish from the distributed method, in what follows, we use GTC and GAC for the ones in the centralised method.

Algorithm 8 Centralised method for solving optimisation problem (5.11)

Initialise: Create $\boldsymbol{A}^{(0)}, \boldsymbol{\beta}^{(0)}$, $i = 0$
Repeat Set $i = i + 1$
  Execute Algorithm 5 using optimal PA
  $\boldsymbol{A}^{(i)} = \boldsymbol{A}^{(optimal)}$
  Execute Algorithm 6 using optimal PA
  $\boldsymbol{\beta}^{(i)} = \boldsymbol{\beta}^{(optimal)}$
  Initialise $\boldsymbol{P}^{(0)}$, $\boldsymbol{P}^{(-1)} = \boldsymbol{P}^{(0)}$, $\kappa = 0$, $T_{total}^{old} = +Inf$
  While $|T_{total}(\boldsymbol{P}^{(\kappa)}, \boldsymbol{P}^{(\kappa-1)}) - T_{total}^{old}| \leq \epsilon$
    $T_{total}^{old} = T_{total}(\boldsymbol{P}^{(\kappa)}, \boldsymbol{P}^{(\kappa-1)})$
    $\boldsymbol{P}^{(\kappa+1)} = \boldsymbol{P}^{*}$ where $\boldsymbol{P}^{*}$ is the solution of (5.27)
    $\kappa = \kappa + 1$
  $\boldsymbol{P}^{(i)} = \boldsymbol{P}^{(\kappa)}$
Stop Convergence or $i = i_{\max}$

5.6 Simulation results

5.6.1 Simulation setting

In this section, simulation results are provided to evaluate the performance of the proposed methods in a SUTN. The considered area of 10×10 km is divided into 4 equal distinct areas, each with a satellite at its centre, i.e. $\boldsymbol{q}_1 = (2.5, 2.5, z_1)$, $\boldsymbol{q}_2 = (7.5, 2.5, z_2)$, $\boldsymbol{q}_3 = (7.5, 7.5, z_3)$, and $\boldsymbol{q}_4 = (2.5, 7.5, z_4)$. The UAVs and GUs are randomly located in these areas according to the uniform distribution. The parameters used to build the channels as well as simulation scenarios are given

in Table 5.1. We used Python to generate simulation results with a PC having the processor Intel Core i5-10400, CPU @2.9 GHz and 8 GB RAM memory.

Table 5.1: Simulation parameters

Parameter	Numerical value
Carrier frequency, f_c	20 GHz
Bandwidth, B	100 MHz
Satellites' altitude, z_s	780 km
Radiation feeds and beams, (N, N_B)	(100, 25)
Maximum transmit power per SAT, $P_m^{(\max)}$	50 dBm
SRF model, $(\omega_i, \delta_i, \varepsilon_i)$	$(0.0005, 0.063, 2)$ [81]
UAVs' altitude, z_u	500 m
Maximum transmit power per UAV, $P_u^{(\max)}$	37 dBm (5W)
Parameters of LoS and NLoS, $(\eta^{\text{LoS}}, \eta^{\text{NLoS}})$	(1, 20) dBm [109]
Constants in UAV-to-GU channel, (a, b)	(9.61, 0.16) [109]
Path loss exponents, $\alpha^{(1)}$=$\alpha^{(2)}$=$\alpha^{(3)}$	2
Noise power, $\sigma_u^2 = \sigma_k^2$	$-174 + 10 \log B$ dBm
Number of possible files, F	30 files
UAV's cache size, M	5 files
One file size, Q	1 kilobit

5.6.2 Numerical results

5.6.2.1 Convergence speed of the genetic algorithm for cache placement

To begin with, we evaluate the convergence speed of the GA in a SUTN consisting of 4 satellites, 16 UAVs and 160 GUs. Six combinations of N_P, P_c and P_m are used as scenarios for comparison, where $N_P = \{20, 40\}$, $P_c = \{0.7, 0.8, 0.9\}$ corresponding to $P_m = 1 - P_c = \{0.3, 0.2, 0.1\}$. Fig. 5.3 describes the differences

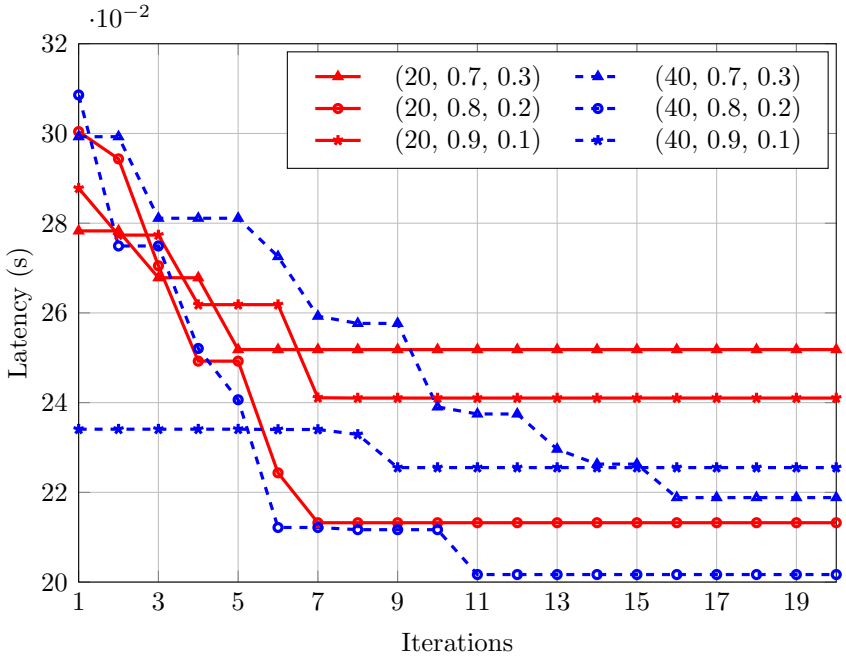

Figure 5.3: Convergence speed of the GA at different (N_P, P_c, P_m).

in the convergence speed of the GA employed in a cluster of UAVs with several combinations of (N_P, P_c, P_m). Overall, the GA converges after 11 iterations in most scenarios. Specially, in the case of $(20, 0.8, 0.2)$, it takes only 7 iterations to converge while 11 iterations are required in the case of $(40, 0.8, 0.2)$.

Compared with the scenarios using $N_P = 20$, the ones with $N_P = 40$ yield lower latency at their convergence points regardless of the values of P_c and P_m. However, the latter take considerably more time to evaluate the chromosomes than those of $N_P = 20$ while the latency improves by just a small amount, i.e., 5.42% in the case of $P_c = 0.8, P_m = 0.2$. On the other hand, the scenarios with $P_c = 0.8, P_m = 0.2$ lead to the lowest latency for all users at the convergence points. Consequently, the combination of $N_P = 20, P_c = 0.8, P_m = 0.2$ works best in the six considered cases and thus are used in the following simulations.

5.6.2.2 Convergence speed of the game theory-based clustering method

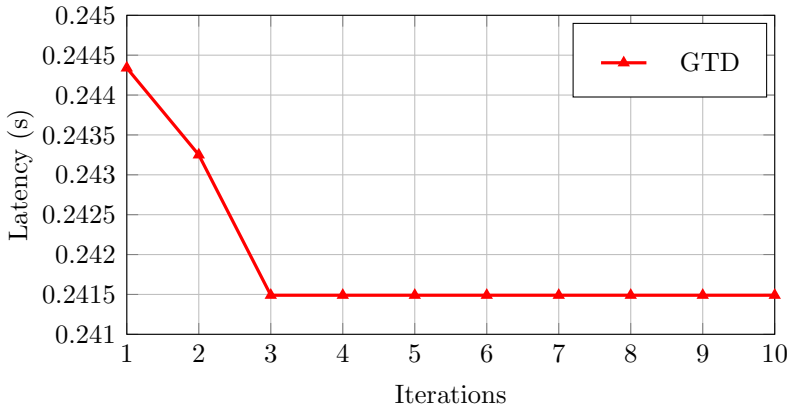

(a) Convergence speed of the GT using quick power allocation (GTD).

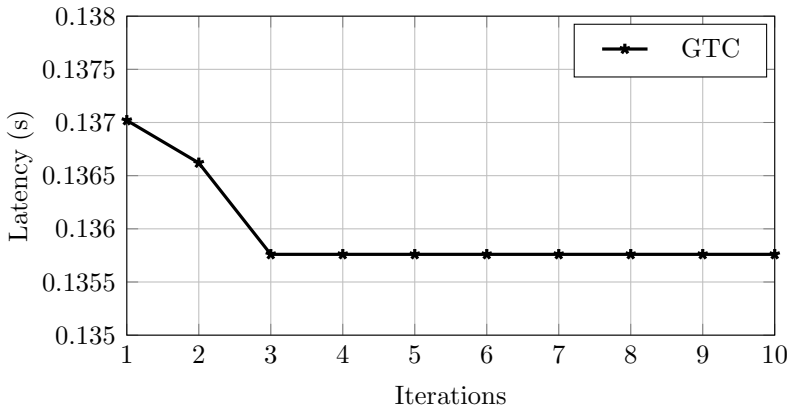

(b) Convergence speed of the GT using optimal power allocation (GTC).

Figure 5.4: Convergence of the GT using different power allocation methods.

To evaluate the convergence of the GT-based method, a typical SUTN which consists of 4 satellites, 16 UAVs, and 80 GUs is used in this simulation. The results in Fig. 5.4 show the convergence speed of two GT algorithms using quick or optimal PA, i.e. GTD and GTC in 10 iterations. Each iteration is completed if all the players (GUs) update their best responses. In both cases, the algorithms converge at the lowest points after three iterations. With GTD, the value at

the convergence point is equal to 98.83% of the value after one loop, while this number with GTC is 99.08%. This means that the GT-based method nearly converges after only one iteration.

5.6.2.3 Power allocation between inter-UAV communications and UAV-ground user communications

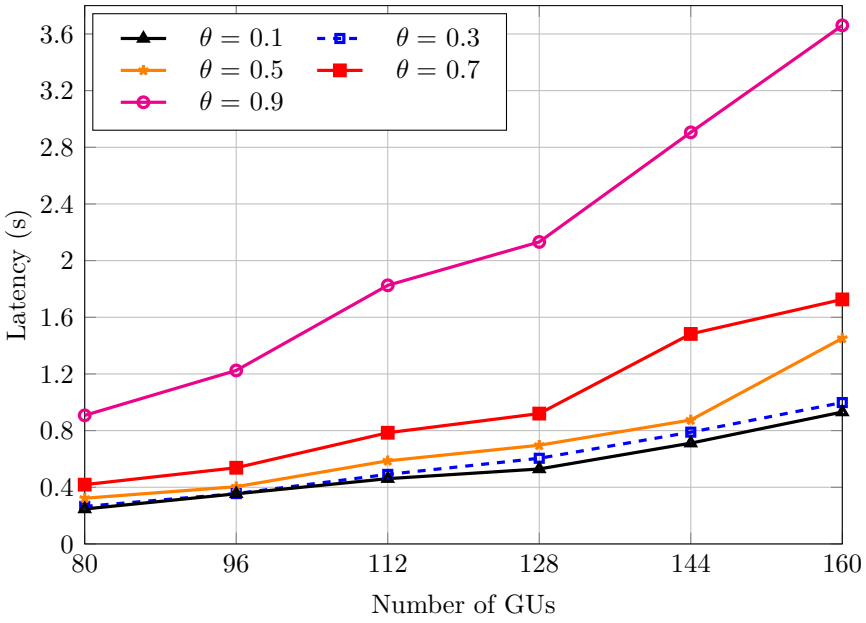

Figure 5.5: Network latency against the amount of power allocated to inter-UAV communications and UAV-GU communications.

In this sub-section, the value θ for dividing the maximum power of the UAVs between the two kinds of communications (i.e. inter-UAV and UAV-GU) is analysed. The considered SUTN consists of 4 satellites and 16 UAVs with the different numbers of GUs ranging from 80 to 160. In Fig. 5.5, the result shows that when $\theta = 0.1$, the latency is lowest among the five cases with 0.247 s at $K = 80$ and 0.931 s at $K = 160$. In other words, serving GUs is fastest if 10% of the

maximum power of a UAV is allocated to inter-UAV communications and the remaining amount is used for UAV-GU communications. Therefore, we use $\theta = 0.1$ in the remaining simulations. Clearly, in the case that the channels between the UAVs are affected by harmful environmental factors, the value of θ can be increased to tackle this issue to guarantee the balance between the two kinds of communications.

5.6.2.4 Comparison in latency

The acronyms of amalgamations of algorithms are given in Table 5.2. There are three important methods:

1. GTGA is the distributed optimisation method (our proposed method).
2. GTGAPA denotes the centralised optimisation method.
3. GTGA-NoU represents the distributed optimisation method without inter-UAV communications.

Additionally, random clustering means that the GUs in the area of one satellite connect randomly to the UAVs served by that satellite; nearest clustering is the method where each GU is served by its nearest UAV; and random cache placement refers to when the files are pre-stored randomly.

Table 5.2: ID of strategies for comparison.

ID	Clustering	Cache placement	Power allocation
GTGA	GTD	GAD	Quick PA
GTRP	GTA	Random	Quick PA
GTGAPA	GTC	GAC	Optimal PA
GTGA-NoU	GTD	GAD	Quick PA without inter-UAV communication
RCGA	Random clustering	GAD	Quick PA
RCRP	Random clustering	Random	Quick PA
NCGA	Nearest clustering	GAD	Quick PA
NCRP	Nearest clustering	Random	Quick PA

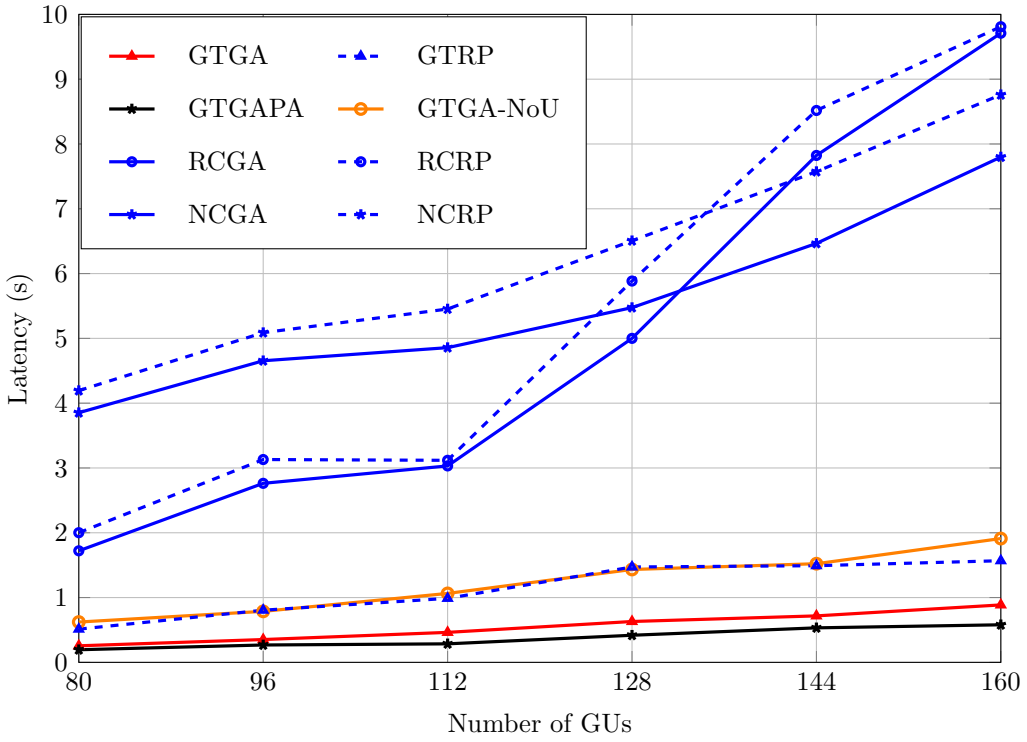

Figure 5.6: The latency of our method GTGA and other traditional ones with the different numbers of GUs.

The comparison in the total latency of our method against those of other traditional methods is shown in Fig. 5.6 when the number of GUs increases from 80 to 160 and the numbers of satellites and UAVs are fixed at 4 and 16, respectively. In terms of latency, the performance of GTGA, GTRP, GTGAPA, and GTGA-NoU outperform the others. Therefore, GT helps to improve considerably the latency for SUTNs compared to random clustering and nearest clustering. The latency of the centralised method GTGAPA is lower than that of the distributed method GTGA by approximately 30% on average. On the other hand, the latency of GTGA-NoU is much higher by the range from 0.37 s to 1.02 s than the one of GTGA. This shows that using inter-UAV communications for exchanging the files significantly reduces the latency compared to the transmission without this type of connection.

5.6.2.5 Execution time

The execution time of GT-based clustering algorithms, GA-based cache placement algorithms and optimal PA are given in Table 5.3 with different sizes of networks, $(U, K) = \{(8, 40), (16, 80), (24, 120), (32, 160), (40, 200)\}$. It is clear that the execution time of GTC and GAC using optimal PA are much higher than those of their counterparts GTD and GAD. The reason is that optimal PA, which requires high computing time from 1.8 s to 9.35 s, is operated many times in GTC and GAC to find the best responses and evaluate populations. Meanwhile, even when the number of UAVs equals 40 and the number of GUs is 200, the execution time of the two algorithms GTD and GAD is still lower than 760 ms because of the insignificant execution time of quick PA. Therefore, the GTD and GAD algorithms have the ability to be applied efficiently in large-scale systems

which require real-time computing, especially in IoT networks with a massive number of users.

Table 5.3: Average execution time of GT and GA with different numbers of UAVs and GUs

Number of UAVs	8	16	24	32	40
Number of GUs	40	80	120	160	200
GTD (s)	0.003	0.023	0.073	0.164	0.318
GAD (s)	0.029	0.112	0.291	0.466	0.759
GTC (s)	51.6	333	1016	2177.6	3548.4
GAC (s)	133.2	273.4	339.7	398.9	444.2
Optimal PA (s)	1.8	3.19	4.79	7.77	9.35

To summarise the results, Table 5.4 provides the evaluation of the proposed methods in terms of "real-time" processing and "latency" for all the users. There are three levels of priority: $\star$, $\star\star$ and $\star\star\star$ denote low priority, average priority, and high priority, respectively. Moreover, "applicability" describes how effectively each method can be used in real systems. The methods that have low priority in any criterion should not be used in practice. In Table 5.4, it can be seen that the proposed method GTGA has the best performance when considering the two criteria of transmission latency and execution time simultaneously.

Table 5.4: Evaluation of the efficiency of methods

Method	Latency	Real-time	**Applicability**
GTGA	$\star\star\star$	$\star\star\star$	$\star\star\star$
GTRP	$\star\star$	$\star\star\star$	$\star\star$
GTGAPA	$\star\star\star$	$\star$	$\star$
GTGA-NoU	$\star\star$	$\star\star\star$	$\star\star$
RCGA	$\star$	$\star\star\star$	$\star$
RCRP	$\star$	$\star\star\star$	$\star$
NCGA	$\star$	$\star\star\star$	$\star$
NCRP	$\star$	$\star\star\star$	$\star$

5.7 Conclusions

This chapter has investigated SUTNs and the problem of latency minimisation consisting of three sub-problems: clustering, cache placement, and PA. In the scenario of highly dense satellite-UAV-user IoT networks, by employing GT and GA respectively for clustering and cache placement, the initial combinatorial optimisation problem is solved efficiently, resulting in the proposed distributed approach outperforming many other benchmarks. Additionally, the study in this chapter has shown the importance of inter-UAV communications in the system model through the much lower latency of the proposed method GTGA compared to the case of no connection between the UAVs. On the other hand, the latency of the distributed method GTGA is higher by around 30% than that of the centralised method GTGAPA. However, in terms of execution time, the distributed method can be applied efficiently in large-scale scenarios which require real-time computing, while the centralised manner is inapplicable due to extremely long processing time.

Chapter 6

Conclusions and future work

6.1 Summary of the thesis

While research on UAVs covers a broad range of topics such as control, power transfer, or security, this thesis has looked at UAV-assisted networks from the communication perspective, giving special consideration to the resource allocation under dynamic environment and stringent constraints.

This thesis has considered UAV-assisted communication in the presence of technologies such as RISs and satellites, and designed resource allocation schemes to maximise network throughput or to minimise latency. The methods employed are based on optimisation, ML and game theory, and have been proven to efficiently provide solutions to complex optimisation problems, and/or to accelerate running time where real-time requirements are involved.

6.1.1 Summary of Chapter 3

Chapter 3 investigated power allocation in a spectrum sharing UAV-assisted CRN to tackle the lack of network coverage in the aftermath of a disaster. The UAVs connected to a BS would form a secondary network that gave access to users

in the disaster area. Optimal resource allocation algorithms were proposed to maximise the throughput of the primary/secondary network, subject to the QoS requirement, power budget at the BS and UAVs, and UAV deployment. Optimisation and ML methods were combined to design a DNN that reduced running time in deployment strategies. The worst-case PU throughput and worst-case UAV throughput were also examined. The simulation results showed that the proposed method is suitable for real-time deployment in mission-critical services thanks to its low-complexity and quick solving time. Some implications of the chapter are:

- The number of UAVs used in the secondary networks should be optimised. This is because the average total throughput of the whole network increases with the power of UAVs, yet only to a certain threshold of UAV's power. After this threshold, due to the effect of interference from the UAVs, the total throughput does not increase any more. The threshold becomes lower with a larger number of UAVs.

- In a disaster scenario, it is reasonable to maximise the throughput of the secondary network (MaxSEC) or of the UAV with worst throughput (MaxMinSEC), while guaranteeing the QoS of the primary network and the maximum tolerable interference imposed on the PUs. Again, large power of the UAVs can cause significant interference, limiting the worst-case UAV thoughput.

6.1.2 Summary of Chapter 4

In Chapter 4, many UAVs carrying passive RISs were used to extend network coverage from a massive MIMO base station. The resource allocation problem was formulated as maximising the total network throughput by finding the optimal power control coefficients at the base station and the phase shifts of the multiple RISs used in the system, subject to the power budgets, UAV-RIS deployment, and QoS required at the users. It was shown that the proposed scheme outperformed benchmark schemes in terms of total network throughput. The results in this chapter have some implications:

- The joint optimisation of RIS phase shifts and UAVs is beneficial to the network throughput, especially when the number of UEs is large.
- The worst-case UE throughput in the joint optimisation scheme is higher than in other schemes. The gap widens with a larger number of RIS elements.

6.1.3 Summary of Chapter 5

In Chapter 5, the resource allocation problem involved user clustering, UAV cache placement and satellite/UAV power allocation. A satellite-UAV-terrestrial network with several satellites, multiple cache-assisted UAVs, and numerous ground users (GUs), was investigated. The UAVs were able to pre-store popular files in their cache in order to quickly serve the GUs when requested. An optimisation problem was formulated to minimise the total latency for all the GUs, with respect to UAV-GU association, caching placement at the UAVs, and power allocation at the satellites and UAVs. The initial problem of extremely high complexity was

decomposed into three sub-problems of low complexity and solved efficiently. We used game theory, a genetic algorithm and a quick power allocation technique to solve these sub-problems. The proposed method has been proven to outperform other schemes in terms of minimising the total latency. The chapter has a few implications:

- The proposed scheme based on distributed method leads to significantly lower latency compared to the other methods, and only yields higher latency than the centralised method. However, the proposed scheme solves optimisation problems notably faster. Therefore, the proposed method can be applied efficiently and in large-scale systems, especially in networks with a massive number of users.

- Inter-UAV communication is proven to efficiently reduce network latency compared with the case where the UAVs do not communicate to exchange files in their caches, hence the practicality of having a network/cluster of UAVs. Dividing a UAV's power between inter-UAV communication and UAV-GU communication is important so that the latency for users is as low as possible while ensuring secure communication between the UAVs. When the channels between the UAVs are subjected to noise or interference, extra power can be allocated to inter-UAV communication to compensate.

6.2 Future work

Looking ahead, coming next in the horizon is the sixth generation (6G) of wireless communication technology. 6G communication networks are expected to be able to serve a significantly greater number of users at higher network capacity

and data rate (a target of 1 Terabit/s), with ultra-low latency (less than 1 ms), providing wider coverage and very high reliability (99.99999 %) [112].

This thesis has so far investigated resource allocation for UAV-assisted communication in the presence of enabling technologies that are also relevant to 6G (RIS in Chapter 4), or considered UAV use cases in 6G: when the UAVs are part of non-terrestrial networks to complement terrestrial networks (UAVs extending network coverage in Chapter 3 and UAVs as a layer in between satellites and terrestrial networks in Chapter 5). There are many research problems to be examined that either are developed directly based on this thesis, or relate to aspects of the future 6G communication technologies.

UAV-aided mobile edge servers

New applications are likely to generate multiple computation-intensive tasks while UEs are limited in size, battery, and computing capacity. To tackle this issue, integrating mobile edge computing servers on UAVs offers a suitable approach. When computation tasks are partially offloaded to the UAVs, the UEs can save energy and extend their operation time.

Moreover, due to the massive number of UEs and their diverse requirements with respect to, e.g., data rate, seamless connectivity, and real-time data transmission, the need for ultra-reliable low-latency communication (URLLC)-aided mobile edge servers arises. UAVs as URLLC-aided mobile edge servers will be able to support computing-intensive applications such as autonomous driving, and face or speed recognition. However, offloading in UAV-assisted wireless communication is a mixed-integer non-convex optimisation problem, which is not only complex but also large-scale with numerous users. In this case, a novel mobile edge server technology needs to be developed for modelling the computing

capacity of network elements and, depending on the current status from real-time updating of edge servers and users, to provide optimal offloading decisions. New offloading schemes that can avoid data and computing overhead at the edge servers with poor connections and many requests in queue should be investigated.

Real-time optimisation for resource allocation

The challenges to resource allocation in future networks are characterised by the massive number of devices (up to 100 billion connected devices by 2025, 40% of which are smart devices [113]) generating a massive amount of data, and diverse requirements from a myriad of applications. Optimisation problems in these situations are highly-complex, large-scale in nature and time-consuming, while it is important to obtain the optimal solution in real-time. Real-time optimisation is essential in the sense that it significantly accelerates the processing time while guaranteeing the decisions are optimal.

There will be a massive number of ground users, base stations, and UAVs in the networks. In addition, the ground users may change their positions very quickly. Hence, real-time optimal user clustering schemes are necessary to reduce interference. The problems of user clustering/association are often mixed-integer non-convex problems, now with an even higher numbers of variables and the stringent constraints of a real-time deadline. Newly emerging ML methods in the interplay with optimisation will continue to be very useful in solving such optimisation problems of resource allocation. Federated learning [114] (a distributed ML method that enables local training and thus reducing complexity in the training phase) and meta learning [115] (a method allowing the agents to incorporate their past experience into determining hyper-parameters of a model for a new task) are two examples of the learning algorithms in the upcoming ultra dense

networks.

Other distributed methods will also be employed more in solving resource allocation problems. A multi-game approach [10] is promising in the sense that there are multiple groups of players in the network (users, UAVs, BSs), each group with their own game and reward to optimise.

Quantum machine learning (QML) for resource allocation:
With the aforementioned challenges in UAV-assisted future communication, soon enough the current (classical) computers will be unable to solve optimisation problems within real-time deadlines. Meanwhile, research in quantum computing have undergone some breakthroughs during the recent years. Quantum computing uses quantum bits, which exist in many states at the same time, as the basic unit of information, to compute in parallel - this makes solving optimisation problems using quantum machine learning (QML) exponentially faster than current ML algorithms [116]. QML depends on the properties of superposition and entanglement in quantum mechanics to solve ML problems. There have been studies on QML for wireless communication, for instance, an optimisation algorithm based on quantum neural network to solve the transmitter-user assignment problem in [117], and a quantum-inspired reinforcement learning method to solve the UAVs' trajectory planning [118]. Hence, the potential of QML could ultimately be harnessed for solving optimisation problems of resource allocation in UAV-assisted future networks.

Appendix A

Proof of results in Chapter 3

Approximation approaches and inequalities used to solve the optimisation problems (3.22) and (3.23)

To solve problems (3.22) and (3.23), we exploit the logarithmic inequality of [93,119], which follows from the convexity of the function $f(x,y) = \ln\Big(1+1/xy\Big)$, yielding

$$f(x,y) = \ln(1+\frac{1}{xy}) \geq \hat{f}(x,y), \tag{A.1}$$

where we have

$$\begin{aligned}\hat{f}(x,y) = \ln\Big(1+\frac{1}{\bar{x}\bar{y}}\Big)+\frac{2}{(\bar{x}\bar{y}+1)} \\ - \frac{x}{\bar{x}(\bar{x}\bar{y}+1)} - \frac{y}{\bar{y}(\bar{x}\bar{y}+1)},\end{aligned} \tag{A.2}$$

$\forall x>0, \bar{x}>0, y>0, \bar{y}>0$.

Let i denote the ith iteration and exploit

$$x_1 = \frac{1}{P_0 p_{0,k}|\rho_{0,k,k}|^2}, y_1 = \mathcal{I}_k^{\mathsf{intra}}(\boldsymbol{p}_0) + \sigma_k^2,$$

$$\bar{x}_1 = x_1^{(i)} = \frac{1}{P_0 p_{0,k}^{(i)} |\rho_{0,k,k}|^2}, \bar{y}_1 = y_1^{(i)} = \mathfrak{I}_k^{\mathsf{intra}}(\boldsymbol{p}_0^{(i)}) + \sigma_k^2,$$

for the approximation of the kth PU's throughput in (3.10) as

$$R_{0,k}(\boldsymbol{p}_0, \boldsymbol{p}_M) \geq \hat{R}_{0,k}^{(i)}(\boldsymbol{p}_0, \boldsymbol{p}_M), \forall k \in \mathcal{K}_P \tag{A.3}$$

where

$$\begin{aligned} \hat{R}_{0,k}^{(i)}(\boldsymbol{p}_0, \boldsymbol{p}_M) = & \ln\left(1 + \frac{1}{\bar{x}_1 \bar{y}_1}\right) + \frac{2}{(\bar{x}_1 \bar{y}_1 + 1)} \\ & - \frac{x_1}{\bar{x}_1(\bar{x}_1 \bar{y}_1 + 1)} - \frac{y_1}{\bar{y}_1(\bar{x}_1 \bar{y}_1 + 1)}. \end{aligned} \tag{A.4}$$

Similarly, we can invoke

$$x_2 = \frac{1}{P_m |\rho_{m,0,m}|^2}, y_2 = \mathfrak{I}_m^{\mathsf{MBS}}(\boldsymbol{p}_M) + \sigma_0^2,$$

$$\bar{x}_2 = x_2^{(i)} = \frac{1}{P_m^{(i)} |\rho_{m,0,m}|^2}, \bar{y}_2 = y_2^{(i)} = \mathfrak{I}_m^{\mathsf{BS}}(\boldsymbol{p}_M^{(i)}) + \sigma_0^2,$$

for the approximation of BS's throughput function in (3.14) as

$$R_{m,0}(\boldsymbol{p}_M) \geq \hat{R}_{m,0}^{(i)}(\boldsymbol{p}_M), m \in \mathcal{M} \tag{A.5}$$

where

$$\begin{aligned} \hat{R}_{m,0}^{(i)}(\boldsymbol{p}_M) = & \ln\left(1 + \frac{1}{\bar{x}_2 \bar{y}_2}\right) + \frac{2}{(\bar{x}_2 \bar{y}_2 + 1)} \\ & - \frac{x_2}{\bar{x}_2(\bar{x}_2 \bar{y}_2 + 1)} - \frac{y_2}{\bar{y}_2(\bar{x}_2 \bar{y}_2 + 1)}. \end{aligned} \tag{A.6}$$

Appendix B

Proof of results in Chapter 4

Approximation approaches and inequalities used to solve the optimisation problem in (4.16)

To solve problem (4.16), we follow the approach in [93, 119]. In particular, we consider the function $f(z) = \log_2(1 + \frac{1}{z})$ in $z > 0$, whose convexity can be proven via its Hessian. The following logarithmic inequality thus holds true $\forall z > 0, \bar{z} > 0$ [93]:

$$f(z) = \log_2(1 + \frac{1}{z}) \geq \hat{f}(z), \tag{B.1}$$

where we have

$$\begin{aligned} \hat{f}(z) = & \log_2(1 + \frac{1}{\bar{z}}) + \left(\frac{\partial f(\bar{z})}{\partial z}\right)(z - \bar{z}) \\ = & \log_2\left(1 + \frac{1}{\bar{z}}\right) + \frac{1}{1 + \bar{z}} - \frac{z}{(1 + \bar{z})\bar{z}}, \end{aligned} \tag{B.2}$$

$\forall z > 0, \bar{z} > 0$.

Hence, at the κ-th iteration, we can invoke

$$z = \frac{\sigma_k^2}{P_0 p_{m,k} \left| \mathbf{G}_{m,k} \tilde{\boldsymbol{f}}_{m,k} \right|^2},$$

$$\bar{z} = z^{(\kappa)} = \frac{\sigma_k^2}{P_0 p_{m,k}^{(\kappa)} \left| \mathbf{G}_{m,k} \tilde{\boldsymbol{f}}_{m,k} \right|^2},$$

for the approximation of the (m,k)-th UE's throughput in (4.9) and the total throughput of all the UEs in (4.10) as follows:

$$R_{m,k}\left(p_{m,k}\right) \geq \hat{R}_{m,k}^{(\kappa)}\left(p_{m,k}\right), \ \forall m \in \mathcal{M}, \ \forall k \in \mathcal{K}_m, \tag{B.3}$$

$$R_{total}\left(\boldsymbol{p}_0\right) \geq \hat{R}_{total}^{(\kappa)}\left(\boldsymbol{p}_0\right), \ \forall m \in \mathcal{M}, \ \forall k \in \mathcal{K}_m, \tag{B.4}$$

where

$$\hat{R}_{m,k}^{(\kappa)}\left(p_{m,k}\right) = \log_2\left(1 + \frac{1}{\bar{z}}\right) + \frac{1}{1+\bar{z}} - \frac{z}{(1+\bar{z})\bar{z}}, \tag{B.5}$$

$$\hat{R}_{total}^{(\kappa)}\left(\boldsymbol{p}_0\right) = \sum_{m=1}^{M} \sum_{k=1}^{K_m} \hat{R}_{m,k}^{(\kappa)}\left(p_{m,k}\right). \tag{B.6}$$

References

[1] PricewaterhouseCoopers, "Skies without limits v2.0: The potential to take the UK's economy to new heights," PricewaterhouseCoopers LLP, UK, Tech. Rep., Jul. 2022.

[2] S. Hayat, E. Yanmaz, and R. Muzaffar, "Survey on unmanned aerial vehicle networks for civil applications: A communications viewpoint," *IEEE Commun. Surveys Tuts.*, vol. 18, no. 4, pp. 2624–2661, 2016.

[3] Y. Zeng and R. Zhang, "Energy-efficient UAV communication with trajectory optimization," *IEEE Transactions on Wireless Communications*, vol. 16, no. 6, pp. 3747–3760, 2017.

[4] X. Yuan, Y. Hu, J. Zhang, and A. Schmeink, "Joint user scheduling and UAV trajectory design on completion time minimization for UAV-aided data collection," *IEEE Trans. Wireless Commun.*, vol. 22, no. 6, pp. 3884–3898, 2023.

[5] K. Xiao, K. Feng, A. Dong, and Z. Mei, "Efficient data dissemination strategy for UAV in UAV-assisted VANETs," *IEEE Access*, vol. 11, pp. 40 809–40 819, 2023.

[6] J. Ji, K. Zhu, D. Niyato, and R. Wang, "Joint cache placement, flight trajectory, and transmission power optimization for multi-UAV assisted wireless networks," *IEEE Trans. Wireless Commun.*, vol. 19, no. 8, pp. 5389–5403, 2020.

[7] M. Mozaffari, W. Saad, M. Bennis, and M. Debbah, "Efficient deployment of multiple unmanned aerial vehicles for optimal wireless coverage," *IEEE Commun. Lett.*, vol. 20, pp. 1647–1650, Aug. 2016.

[8] W. Saad, M. Bennis, M. Mozaffari, and X. Lin, *Wireless Communications and Networking for Unmanned Aerial Vehicles.* Cambridge, U.K: Cambridge Univ. Press, 2020.

[9] L. D. Nguyen, A. Kortun, and T. Q. Duong, "An introduction of real-time embedded optimisation programming for UAV systems under disaster communication," *EAI Endorsed Trans. Ind. Netw. Intell. Syst.*, vol. 5, no. 17, pp. 1–8, Dec. 2018.

[10] M. Mozaffari, W. Saad, M. Bennis, Y.-H. Nam, and M. Debbah, "A tutorial on UAVs for wireless networks: Applications, challenges, and open problems," *IEEE Commun. Surveys Tuts.*, vol. 21, no. 3, pp. 2334–2360, 2019.

[11] M. A. Jasim, H. Shakhatreh, N. Siasi, A. H. Sawalmeh, A. Aldalbahi, and A. Al-Fuqaha, "A survey on spectrum management for unmanned aerial vehicles (UAVs)," *IEEE Access*, vol. 10, pp. 11 443–11 499, 2022.

[12] X. Liu, M. Guan, X. Zhang, and H. Ding, "Spectrum sensing optimization in an UAV-based cognitive radio," *IEEE Access*, vol. 6, pp. 44 002–44 009, 2018.

[13] Y. Huang, J. Xu, L. Qiu, and R. Zhang, "Cognitive UAV communication via joint trajectory and power control," in *IEEE SPAWC*, Kalamata, Greece, Jun. 2018, pp. 1–5.

[14] X. Liang, W. Xu, H. Gao, M. Pan, J. Lin, Q. Deng, and P. Zhang, "Throughput optimization for cognitive UAV networks: A three-dimensional-location-aware approach," *IEEE Wirel. Commun. Lett.*, vol. 9, no. 7, pp. 948–952, 2020.

[15] B. Shang, V. Marojevic, Y. Yi, A. S. Abdalla, and L. Liu, "Spectrum sharing for UAV communications: Spatial spectrum sensing and open issues," *IEEE Veh. Technol. Mag.*, vol. 15, no. 2, pp. 104–112, 2020.

[16] Y. Liu, X. Liu, X. Mu, T. Hou, J. Xu, M. Di Renzo, and N. Al-Dhahir, "Reconfigurable intelligent surfaces: Principles and opportunities," *IEEE Commun. Surveys Tuts.*, vol. 23, no. 3, pp. 1546–1577, 2021.

[17] S. Basharat, S. A. Hassan, H. Pervaiz, A. Mahmood, Z. Ding, and M. Gidlund, "Reconfigurable intelligent surfaces: Potentials, applications, and challenges for 6G wireless networks," *IEEE Wireless Commun.*, vol. 28, no. 6, pp. 184–191, 2021.

[18] N. Zhao, F. R. Yu, L. Fan, Y. Chen, J. Tang, A. Nallanathan, and V. C. Leung, "Caching unmanned aerial vehicle-enabled small-cell networks: Em-

ploying energy-efficient methods that store and retrieve popular content," *IEEE Veh. Technol. Mag.*, vol. 14, no. 1, pp. 71–79, 2019.

[19] D.-H. Tran, S. Chatzinotas, and B. Ottersten, "Satellite-and cache-assisted UAV: A joint cache placement, resource allocation, and trajectory optimization for 6G aerial networks," *IEEE Open J. Veh. Technol.*, vol. 3, pp. 40–54, Jan. 2022.

[20] T. Q. Duong, L. D. Nguyen, H. D. Tuan, and L. Hanzo, "Learning-aided realtime performance optimisation of cognitive UAV-assisted disaster communication," in *IEEE GLOBECOM*, Waikoloa, HI, USA, Dec. 2019, pp. 1–6.

[21] L. D. Nguyen, T. Q. Duong, and H. D. Tuan, *Real Time Convex Optimisation for 5G Networks and Beyond*. London, U.K: IET, 2022.

[22] A. O. Hashesh, S. Hashima, R. M. Zaki, M. M. Fouda, K. Hatano, and A. S. T. Eldien, "AI-enabled UAV communications: Challenges and future directions," *IEEE Access*, vol. 10, pp. 92 048–92 066, 2022.

[23] T. Q. Duong, L. D. Nguyen, and L. K. Nguyen, "Practical optimisation of path planning and completion time of data collection for UAV-enabled disaster communications," in *Proc. IEEE IWCMC*, Tangier, Morocco, Jul. 2019, pp. 372–377.

[24] S. Boyd and L. Vandenberghe, *Convex optimization*. Cambridge university press, 2004.

[25] B. G. Lee, D. Park, and H. Seo, *Mathematical Tools for Resource Management*. Wiley-IEEE Press, 2009, pp. 73–106.

[26] Z.-Q. Luo and W. Yu, "An introduction to convex optimization for communications and signal processing," *IEEE Journal on Selected Areas in Communications*, vol. 24, no. 8, pp. 1426–1438, Aug 2006.

[27] Q. Wu and R. Zhang, "Intelligent reflecting surface enhanced wireless network via joint active and passive beamforming," *IEEE Trans. Wireless Commun.*, vol. 18, no. 11, pp. 5394–5409, Nov. 2019.

[28] ——, "Intelligent reflecting surface enhanced wireless network: Joint active and passive beamforming design," in *Proc. IEEE Global Commun. (GLOBECOM)*, Abu Dhabi, U.A.E, Dec. 2018, pp. 1–6.

[29] Z.-q. Luo, W.-k. Ma, A. M.-c. So, Y. Ye, and S. Zhang, "Semidefinite relaxation of quadratic optimization problems," *IEEE Signal Process. Mag.*, vol. 27, no. 3, pp. 20–34, 2010.

[30] L. D. Nguyen, K. K. Nguyen, A. Kortun, and T. Q. Duong, "Realtime deployment and resource allocation for distributed UAV systems," in *Proc. SPAWC*, Cannes, France, Jul. 2019, pp. 1–6.

[31] H. Sun and *et al.*, "Learning to optimize: Training deep neural networks for interference management," *IEEE Trans. Signal Process.*, vol. 66, no. 20, pp. 5438–5453, Oct. 2018.

[32] Y. Shen, Y. Shi, J. Zhang, and K. B. Letaief, "LORM: Learning to optimize for resource management in wireless networks with few training samples," *IEEE Trans. Wireless Commun.*, vol. 19, no. 1, pp. 665–679, Jan. 2020.

[33] S. Sai, A. Garg, K. Jhawar, V. Chamola, and B. Sikdar, "A comprehensive survey on artificial intelligence for unmanned aerial vehicles," *IEEE Open J. Veh. Technol.*, pp. 1–26, Sep. 2023, early access.

[34] A. Hajijamali Arani, M. M. Azari, P. Hu, Y. Zhu, H. Yanikomeroglu, and S. Safavi-Naeini, "Reinforcement learning for energy-efficient trajectory design of UAVs," *IEEE Internet Things J.*, vol. 9, no. 11, pp. 9060–9070, 2022.

[35] X. Zhang, G. Zheng, and S. Lambotharan, "Trajectory design for UAV-assisted emergency communications: A transfer learning approach," in *IEEE GLOBECOM*, 2020, pp. 1–6.

[36] L. Sboui, H. Ghazzai, Z. Rezki, and M. Alouini, "Achievable rates of UAV-relayed cooperative cognitive radio MIMO systems," *IEEE Access*, vol. 5, pp. 5190–5204, 2017.

[37] L. Wang, H. Yang, J. Long, K. Wu, and J. Chen, "Enabling ultra-dense UAV-aided network with overlapped spectrum sharing: Potential and approaches," *IEEE Network*, vol. 32, no. 5, pp. 85–91, Sep. 2018.

[38] L. Sboui, H. Ghazzai, Z. Rezki, and M. Alouini, "Energy-efficient power allocation for UAV cognitive radio systems," in *Proc. IEEE VTC-Fall*, Toronto, ON, Canada, Sep. 2017, pp. 1–5.

[39] Y. Zhou, F. Zhou, H. Zhou, D. W. K. Ng, and R. Q. Hu, "Robust trajectory and transmit power optimization for secure UAV-enabled cognitive radio networks," *IEEE Trans. Commun.*, vol. 68, no. 7, pp. 4022–4034, 2020.

[40] H. T. Nguyen, H. D. Tuan, T. Q. Duong, H. V. Poor, and W. J. Hwang, "Joint D2D assignment, bandwidth and power allocation in cognitive UAV-enabled networks," *IEEE Trans. Cogn. Commun. Netw.*, vol. 6, no. 3, pp. 1084–1095, 2020.

[41] Y. Huang, W. Mei, J. Xu, L. Qiu, and R. Zhang, "Cognitive UAV communication via joint maneuver and power control," *IEEE Trans. Commun.*, vol. 67, no. 11, pp. 7872–7888, 2019.

[42] M. Nguyen, L. D. Nguyen, T. Q. Duong, and H. D. Tuan, "Real-time optimal resource allocation for embedded UAV communication systems," *IEEE Wireless Commun. Lett.*, vol. 8, no. 1, pp. 225–228, Feb. 2019.

[43] H. Hashida, Y. Kawamoto, and N. Kato, "Intelligent reflecting surface placement optimization in air-ground communication networks toward 6G," *IEEE Wireless Commun.*, pp. 146–151, Dec. 2020.

[44] H. Guo, Y.-C. Liang, J. Chen, and E. G. Larsson, "Weighted sum-rate maximization for reconfigurable intelligent surface aided wireless networks," *IEEE Trans. Wireless Commun.*, vol. 19, pp. 3064–3076, May 2020.

[45] D. L. Dampahalage, K. B. S. Manosha, N. Rajatheva, and M. Latva-Aho, "Weighted-sum-rate maximization for an reconfigurable intelligent surface aided vehicular network," *IEEE Open J. Commun. Society*, vol. 2, pp. 687–703, 2021.

[46] T. Zhou, K. Xu, X. Xia, W. Xie, and J. Xu, "Achievable rate optimization for aerial intelligent reflecting surface-aided cell-free massive MIMO system," *IEEE Access*, vol. 9, pp. 3828–3837, 2021.

[47] Y. Liang, L. Xiao, D. Yang, Y. Liu, and T. Zhang, "Joint trajectory and resource optimization for UAV-aided two-way relay networks," *IEEE Trans. Veh. Technol.*, vol. 71, no. 1, pp. 639–652, 2022.

[48] H. Peng, A.-H. Tsai, L.-C. Wang, and Z. Han, "Leopard: Parallel optimal deep echo state network prediction improves service coverage for UAV-assisted outdoor hotspots," *IEEE Commun. Surveys Tuts.*, vol. 8, no. 1, pp. 282–295, 2022.

[49] Z. Wei, Y. Cai, Z. Sun, D. W. K. Ng, J. Yuan, M. Zhou, and L. Sun, "Sum-rate maximization for IRS-assisted UAV OFDMA communication systems," *IEEE Trans. Wireless Commun.*, vol. 20, pp. 2530–2550, Apr. 2021.

[50] X. Liu, Y. Liu, and Y. Chen, "Machine learning empowered trajectory and passive beamforming design in UAV-RIS wireless networks," *IEEE J. Sel. Areas Commun.*, vol. 39, no. 7, pp. 2042 – 2055, Jul. 2021.

[51] S. Li, B. Duo, M. D. Renzo, M. Tao, and X. Yuan, "Robust secure UAV communications with the aid of reconfigurable intelligent surfaces," *IEEE Trans. Wireless Commun.*, vol. 20, pp. 6402–6417, Oct. 2021.

[52] Y. Pan, K. Wang, C. Pan, H. Zhu, and J. Wang, "UAV-assisted and intelligent reflecting surfaces-supported terahertz communications," *IEEE Wireless Commun. Lett.*, vol. 10, pp. 1256–1260, Jun. 2021.

[53] D. Ma, M. Ding, and M. Hassan, "Enhancing cellular communications for UAVs via intelligent reflective surface," in *Proc. IEEE Wireless Commun. Networking Conf. (WCNC)*, virtual conference, May 2020, pp. 1–6.

[54] C. You, Z. Kang, Y. Zeng, and R. Zhang, "Enabling smart reflection in integrated air-ground wireless network: IRS meets UAV," *IEEE Wireless Commun.*, vol. 28, no. 6, pp. 138–144, 2021.

[55] Q. Zhang, W. Saad, and M. Bennis, "Reflections in the sky: Millimeter wave communication with UAV-carried intelligent reflectors," in *Proc. IEEE Global Commun. (GLOBECOM)*, Waikoloa, HI, Dec. 2019, pp. 1–6.

[56] H. Lu, Y. Zeng, S. Jin, and R. Zhang, "Aerial intelligent reflecting surface: Joint placement and passive beamforming design with 3D beam flattening," *IEEE Trans. Wireless Commun.*, vol. 20, pp. 4128 – 4143, Jul. 2021.

[57] Z. Mohamed and S. Aissa, "Leveraging UAVs with intelligent reflecting surfaces for energy-efficient communications with cell-edge users," in *Proc. IEEE Int. Commun. Conf. (ICC) Workshops*, virtual conference, Jun. 2020, pp. 10–15.

[58] H. Long, M. Chen, Z. Yang, Z. Li, B. Wang, X. Yun, and M. Shikh-Bahaei, "Joint trajectory and passive beamforming design for secure UAV networks with RIS," in *Proc. IEEE Global Commun. (GLOBECOM) Workshops*, Taipei, Taiwan, Dec. 2020, pp. 1–6.

[59] T. Shafique, H. Tabassum, and E. Hossain, "Optimization of wireless relaying with flexible UAV-borne reflecting surfaces," *IEEE Trans. Commun.*, vol. 69, pp. 309–325, Jan. 2021.

[60] M. Samir, M. Elhattab, C. Assi, S. Sharafeddine, and A. Ghrayeb, "Optimizing age of information through aerial reconfigurable intelligent surfaces: A deep reinforcement learning approach," *IEEE Trans. Veh. Technol.*, vol. 70, pp. 3978–3983, Apr. 2021.

[61] M. Hua, L. Yang, Q. Wu, C. Pan, C. Li, and A. L. Swindlehurst, "UAV-assisted intelligent reflecting surface symbiotic radio system," *IEEE Trans. Wireless Commun.*, pp. 5769 – 5785, Sep. 2021.

[62] A. Mahmoud, S. Muhaidat, P. Sofotasios, I. Abualhaol, O. A. Dobre, and H. Yanikomeroglu, "Intelligent reflecting surfaces assisted UAV communications for IoT networks: Performance analysis," *IEEE Trans.Green Commun. Netw.*, vol. 5, pp. 1029 – 1040, Sep. 2021.

[63] Y. Li, C. Yin, T. Do-Duy, A. Masaracchia, and T. Q. Duong, "Aerial reconfigurable intelligent surface-enabled URLLC UAV systems," *IEEE Access*, vol. 9, pp. 140 248–140 257, 2021.

[64] A. Khalili, E. M. Monfared, S. Zargari, M. R. Javan, N. Mokari, and E. A. Jorswieck, "Resource management for transmit power minimization in UAV-assisted RIS HetNets supported by dual connectivity," *IEEE Trans. Wireless Commun.*, pp. 1–1, 2021.

[65] S. Alfattani, W. Jaafar, Y. Hmamouche, H. Yanikomeroglu, and A. Yongacoglu, "Link budget analysis for reconfigurable smart surfaces in aerial platforms," *IEEE Open J. Commun. Society*, vol. 2, pp. 1980–1995, 2021.

[66] T. Huang, W. Yang, J. Wu, J. Ma, X. Zhang, and D. Zhang, "A survey on green 6G network: Architecture and technologies," *IEEE Access*, vol. 7, pp. 175 758–175 768, Dec. 2019.

[67] J. Wang, C. Jiang, and L. Kuang, "High-mobility satellite-UAV communications: Challenges, solutions, and future research trends," *IEEE Commun. Mag.*, vol. 60, no. 5, pp. 38–43, May 2022.

[68] A. C. Boley and M. Byers, "Satellite mega-constellations create risks in low earth orbit, the atmosphere and on earth," *Scientific Reports*, vol. 11, no. 1, pp. 1–8, Feb. 2019.

[69] C. Liu, W. Feng, Y. Chen, C.-X. Wang, and N. Ge, "Cell-free satellite-UAV networks for 6G wide-area Internet of Things," *IEEE J. Sel. Areas Commun.*, vol. 39, no. 4, pp. 1116–1131, Apr. 2021.

[70] X. Zhu and C. Jiang, "Integrated satellite-terrestrial networks toward 6G: Architectures, applications, and challenges," *IEEE Internet Things J.*, vol. 9, no. 1, pp. 437–461, 2022.

[71] C. Zhou, W. Wu, H. He, P. Yang, F. Lyu, N. Cheng, and X. Shen, "Delay-aware IoT task scheduling in space-air-ground integrated network," in *Proc. IEEE Global Commun. Conf. (GLOBECOM)*, Hawaii, USA, Dec. 2019, pp. 1–6.

[72] J. Yang, T. Zhang, X. Wu, T. Liang, and Q. Zhang, "Efficient scheduling in space-air-ground-integrated localization networks," *IEEE Internet Things J.*, vol. 9, no. 18, pp. 17 689–17 704, Mar. 2022.

[73] L. D. Nguyen, K. K. Nguyen, A. Kortun, and T. Q. Duong, "Real-time deployment and resource allocation for distributed UAV systems in disaster relief," in *Proc. IEEE 20th Int. Workshop Signal Process. Adv. Wireless Commun. (SPAWC)*, Cannes, France, Jul. 2019, pp. 1–5.

[74] L. D. Nguyen, A. Kortun, and T. Q. Duong, "An introduction of real-time embedded optimisation programming for UAV systems under disaster communication," *EAI Endorsed Trans. Ind. Netw. Intell. Syst.*, vol. 5, no. 17, pp. 1–5, Dec. 2018.

[75] Q. Huang, M. Lin, J.-B. Wang, T. A. Tsiftsis, and J. Wang, "Energy efficient beamforming schemes for satellite-aerial-terrestrial networks," *IEEE Trans. Commun.*, vol. 68, no. 6, pp. 3863–3875, Jun. 2020.

[76] Z. Jia, M. Sheng, J. Li, D. Niyato, and Z. Han, "LEO-satellite-assisted UAV: Joint trajectory and data collection for internet of remote things in 6G aerial access networks," *IEEE Internet Things J.*, vol. 8, no. 12, pp. 9814–9826, Sep. 2020.

[77] Y. Hu, M. Chen, and W. Saad, "Joint access and backhaul resource management in satellite-drone networks: A competitive market approach," *IEEE Trans. Wireless Commun.*, vol. 19, no. 6, pp. 3908–3923, Jun. 2020.

[78] Z. Li, Y. Wang, M. Liu, R. Sun, Y. Chen, J. Yuan, and J. Li, "Energy efficient resource allocation for UAV-assisted space-air-ground Internet of remote things networks," *IEEE Access*, vol. 7, pp. 145 348–145 362, Oct. 2019.

[79] S. Mirbolouk, M. Valizadeh, M. C. Amirani, and S. Ali, "Relay selection and power allocation for energy efficiency maximization in hybrid satellite-UAV networks with CoMP-NOMA transmission," *IEEE Trans. Veh. Technol.*, vol. 71, no. 5, pp. 5087–5100, May 2022.

[80] X. Fang, W. Feng, Y. Wang, Y. Chen, N. Ge, Z. Ding, and H. Zhu, "NOMA-based hybrid satellite-UAV-terrestrial networks for 6G maritime coverage," *IEEE Trans. Wireless Commun.*, vol. 22, no. 1, pp. 138–152, 2023.

[81] Y.-J. Chen, W. Chen, and M.-L. Ku, "Trajectory design and link selection in UAV-assisted hybrid satellite-terrestrial network," *IEEE Commun. Lett.*, vol. 26, no. 7, pp. 1643–1647, Jul. 2022.

[82] S. Gu, X. Sun, Z. Yang, T. Huang, W. Xiang, and K. Yu, "Energy-aware coded caching strategy design with resource optimization for satellite-UAV-vehicle-integrated networks," *IEEE Internet Things J.*, vol. 9, no. 8, pp. 5799–5811, Apr. 2022.

[83] D.-B. Ha, V.-T. Truong, and Y. Lee, "Performance analysis for RF energy harvesting mobile edge computing networks with SIMO/MISO-NOMA schemes," *EAI Endorsed Trans. Ind. Netw. Intell. Syst.*, vol. 8, no. 27, p. e2, Jun. 2021.

[84] R. I. Bor-Yaliniz, A. El-Keyi, and H. Yanikomeroglu, "Efficient 3-D placement of an aerial base station in next generation cellular networks," in *IEEE ICC*, Kuala Lumpur, Malaysia, May 2016, pp. 1–5.

[85] A. Al-Hourani, S. Kandeepan, and S. Lardner, "Optimal LAP altitude for maximum coverage," *IEEE Wirel. Commun. Lett.*, vol. 3, no. 6, pp. 569–572, Dec. 2014.

[86] T. L. Marzetta, E. G. Larsson, H. Yang, and H. Q. Ngo, *Fundamentals of massive MIMO*. Cambridge, U.K: Cambridge Univ. Press, 2016.

[87] M. Alzenad, A. El-Keyi, and H. Yanikomeroglu, "3-D placement of an unmanned aerial vehicle base station for maximum coverage of users with different QoS requirements," *IEEE Wirel. Commun. Lett.*, vol. 7, no. 1, pp. 38–41, Feb. 2018.

[88] S. Diamond and S. Boyd, "CVXPY: A Python-embedded modeling language for convex optimization," *J. Mach. Learn. Res.*, vol. 17, no. 83, pp. 1–5, 2016.

[89] Y. Chen, M. W. Hoffman, S. G. Colmenarejo, M. Denil, T. P. Lillicrap, and N. de Freitas, "Learning to learn for global optimization of black box functions," in *30th Conf. Neur. Inf. Process. Syst.*, Barcelona, Spain, Dec. 2016.

[90] A. Cochocki and R. Unbehauen, *Neural networks for optimization and signal processing*. New York, NY, USA: John Wiley & Sons, Inc., 1993.

[91] I. Goodfellow, Y. Bengio, A. Courville, and Y. Bengio, *Deep learning*. Cambridge, MA, USA: MIT Press, 2016, vol. 1.

[92] L. Deng, D. Yu *et al.*, "Deep learning: methods and applications," *Found. Trends Signal Process.*, vol. 7, no. 3–4, pp. 197–387, 2014.

[93] L. D. Nguyen, H. D. Tuan, T. Q. Duong, O. A. Dobre, and H. V. Poor, "Downlink beamforming for energy-efficient heterogeneous networks with massive MIMO and small cells," *IEEE Trans. Wireless Commun.*, vol. 17, no. 5, pp. 3386–3400, May 2018.

[94] M. Mozaffari, W. Saad, M. Bennis, and M. Debbah, "Optimal transport theory for cell association in uav-enabled cellular networks," *IEEE Commun. Lett.*, vol. 21, no. 9, pp. 2053–2056, 2017.

[95] Z. Chu, P. Xiao, M. Shojafar, D. Mi, J. Mao, and W. Hao, "Intelligent reflecting surface assisted mobile edge computing for Internet of Things," *IEEE Wireless Commun. Lett.*, vol. 10, no. 3, pp. 619–623, Mar. 2021.

[96] Q. Wu and R. Zhang, "Beamforming optimization for wireless network aided by intelligent reflecting surface with discrete phase shifts," *IEEE Trans. Commun.*, vol. 68, no. 3, pp. 1838–1851, Mar. 2020.

[97] P. Wang, J. Fang, X. Yuan, Z. Chen, and H. Li, "Intelligent reflecting surface-assisted millimeter wave communications: Joint active and passive precoding design," *IEEE Trans. Veh. Technol.*, vol. 69, no. 12, pp. 14 960–14 973, Dec. 2020.

[98] M. Banagar, H. S. Dhillon, and A. F. Molisch, "Impact of UAV wobbling on the air-to-ground wireless channel," *IEEE Trans. Veh. Technol.*, vol. 69, no. 11, pp. 14 025–14 030, 2020.

[99] W. Wang and W. Zhang, "Jittering effects analysis and beam training design for UAV millimeter wave communications," *IEEE Trans. Wireless Commun.*, pp. 1–1, 2021.

[100] Z. Xiao, L. Zhu, Y. Liu, P. Yi, R. Zhang, X.-G. Xia, and R. Schober, "A survey on millimeter-wave beamforming enabled UAV communications and networking," *IEEE Commun. Surveys Tuts.*, vol. 24, no. 1, pp. 557–610, 2022.

[101] X. Xie, F. Fang, and Z. Ding, "Joint optimization of beamforming, phase-shifting and power allocation in a multi-cluster IRS-NOMA network," *IEEE Trans. Veh. Technol.*, vol. 70, no. 8, pp. 7705–7717, Aug. 2021.

[102] A. M. Tulino and S. Verdu, *Random Matrix Theory and Wireless Communications.* Delft, The Netherlands: Now Publishers Inc., 2004.

[103] L. D. Nguyen, H. D. Tuan, T. Q. Duong, and H. V. Poor, "Beamforming and power allocation for energy-efficient massive MIMO," in *Proc. Int. Conf. Digital Signal Process. (DSP)*, London, U.K, Aug. 2017, pp. 1–5.

[104] T. Do-Duy, L. D. Nguyen, T. Q. Duong, S. R. Khosravirad, and H. Claussen, "Joint optimisation of real-time deployment and resource allocation for UAV-aided disaster emergency communications," *IEEE J. Sel. Areas Commun.*, vol. 39, no. 11, pp. 3411–3424, 2021.

[105] L. D. Nguyen, K. K. Nguyen, A. Kortun, and T. Q. Duong, "Real-time deployment and resource allocation for distributed UAV systems in disaster relief," in *Proc. IEEE Workshop Signal Process. Advances Wireless Commun. (SPAWC)*, Cannes, France, Jul. 2019, pp. 1–5.

[106] D. Peaucelle, D. Henrion, and Y. Labit, "Users guide for SeDuMi interface 1.03," LAAS-CNRS, Tech. Rep., 2002.

[107] M. Grant and S. Boyd, "CVX: MATLAB software for disciplined convex programming, version 2.1," http://cvxr.com/cvx, Mar. 2014.

[108] H. Yu, H. D. Tuan, A. A. Nasir, T. Q. Duong, and H. V. Poor, "Joint design of reconfigurable intelligent surfaces and transmit beamforming under proper and improper Gaussian signaling," *IEEE J. Sel. Areas Commun.*, vol. 38, no. 11, pp. 2589–2603, Nov. 2020.

[109] T. Q. Duong, L. D. Nguyen, H. D. Tuan, and L. Hanzo, "Learning-aided realtime performance optimisation of cognitive UAV-assisted disaster communication," in *Proc. IEEE Global Commun. Conf. (GLOBECOM)*, Hawaii, USA, Dec. 2019, pp. 1–6.

[110] T. Do-Duy, L. D. Nguyen, T. Q. Duong, S. Khosravirad, and H. Claussen, "Joint optimisation of real-time deployment and resource allocation for UAV-aided disaster emergency communications," *IEEE J. Sel. Areas Commun.*, vol. 39, no. 11, pp. 3411–3424, Nov. 2021.

[111] L. D. Nguyen, H. D. Tuan, T. Q. Duong, H. V. Poor, and L. Hanzo, "Energy-efficient multi-cell massive MIMO subject to minimum user-rate constraints," *IEEE Trans. Commun.*, vol. 69, no. 2, pp. 914–928, Feb. 2021.

[112] W. Saad, M. Bennis, and M. Chen, "A vision of 6G wireless systems: Applications, trends, technologies, and open research problems," *IEEE Network*, vol. 34, no. 3, pp. 134–142, 2020.

[113] Huawei, "Global industry vision 2025: Unfolding the industry blueprint of an intelligent world," Huawei Technologies Co., Ltd., Tech. Rep., 2018.

[114] Y. Shen, Y. Qu, C. Dong, F. Zhou, and Q. Wu, "Joint training and resource allocation optimization for federated learning in UAV swarm," *IEEE Internet Things J.*, vol. 10, no. 3, pp. 2272–2284, 2023.

[115] Z. Lu, X. Wang, and M. C. Gursoy, "Trajectory design for unmanned aerial vehicles via meta-reinforcement learning," in *2023 IEEE INFOCOM Wkshps.*, NY, USA, May 2023, pp. 1–6.

[116] T. Q. Duong, J. A. Ansere, B. Narottama, V. Sharma, O. A. Dobre, and H. Shin, "Quantum-inspired machine learning for 6G: Fundamentals, security, resource allocations, challenges, and future research directions," *IEEE Open J. Veh. Technol.*, vol. 3, pp. 375–387, 2022.

[117] B. Narottama and T. Q. Duong, "Quantum neural networks for optimal resource allocation in cell-free MIMO systems," in *Proc. 2022 IEEE GLOBECOM*, Rio de Janeiro, Brazil, Dec. 2022.

[118] Y. Li, A. H. Aghvami, and D. Dong, "Intelligent trajectory planning in UAV-mounted wireless networks: A quantum-inspired reinforcement learning perspective," *IEEE Wireless Commun. Lett.*, vol. 10, no. 9, pp. 1994–1998, 2021.

[119] L. D. Nguyen, H. D. Tuan, T. Q. Duong, and H. V. Poor, "Multi-user regularized zero-forcing beamforming," *IEEE Trans. Signal Process.*, vol. 67, no. 11, pp. 2839 – 2853, 2019.